DISSERTATION | DOCTORAL THESIS

Titel | Title

NMR Spin Relaxation in Intrinsically Disordered Proteins

verfasst von | submitted by

Dott.ssa Dott.ssa mag. Irene Ceccolini

angestrebter akademischer Grad | in partial fulfilment of the requirements for the degree of

Doktorin der Naturwissenschaften (Dr.rer.nat.)

Wien | Vienna, 2024

Studienkennzahl lt. Studienblatt | Degree programme code as it appears on the student record sheet:	UA 796 605 419
Dissertationsgebiet lt. Studienblatt | Field of study as it appears on the student record sheet:	Chemie
Betreut von | Supervisor:	Univ.-Prof. Dr. Robert Konrat

SUPERVISOR:
Univ.-Prof. Dr. Robert Konrat

LOCATION:
Vienna, Austria

TIME FRAME:
October 2020 - April 2024

Dedicated to my little ones.

Above all, don't fear difficult moments.
The best comes from them.

— Rita Levi-Montalcini

ACKNOWLEDGMENTS

I want to thank the many people who have supported and accompanied me along this journey:

- my supervisor Prof. Robert Konrat; I want to express my deepest gratitude for your unwavering scientific and emotional support throughout these years. Your understanding and encouragement have been invaluable to me. Thank you for the trust and the flexibility you gave me in this last special here. You made everything possible.
- Anna Zawadzka-Kazimierczuk, the best teacher who thought me how to "deal with NMR". Without your guidance, I wouldn't be at this point. I am truly grateful for everything I've leaned from you, for the countless hours we've spent on Zoom, and for your endless support.
- my coauthors Clemens Kauffmann, Julian Holzinger; for their expertise, and help. Thank you for complementing my research.
- Philippe Pelupessy; for being a genuine an amazing scientist who helped me in finding the "accurate" way to do my work.
- my PhD mate Theresa Hoefurtner. I am immensely grateful to have crossed paths with you in my life. Without you, things would not have been the same.
- my sister Clara, my parents, my friends and colleagues at the department: Andreas Beier, Daniel Braun, Sven Bruschweiler, Julian Holzinger, Clemens Kauffmann, Sonja Knödelstorfer, Karin Ledolter, Mario Migotti, Thomas Schwarz; thank you for always being there.
- my family: Salvatore, Ada and the coming one; thank you for being my strength.

PUBLICATIONS

Parts of this thesis have been previously published as scientific articles in peer-reviewed academic journals. These publications are featured as separate chapters, in order of appearance:

[1] C. Kauffmann, I. Ceccolini, G. Kontaxis, and R. Konrat, "Detecting anisotropic segmental dynamics in disordered proteins by cross-correlated spin relaxation," *Magnetic Resonance*, vol. 2, no. 2, pp. 557–569, 2021.

[2] I. Ceccolini, C. Kauffmann, J. Holzinger, R. Konrat, and A. Zawadzka Kazimierczuk, "A set of cross-correlated relaxation experiments to probe the correlation time of two different and complementary spin pairs," *Journal of Magnetic Resonance*, vol. 361, p. 107 661, 2024.

ABSTRACT

Intrinsically disordered proteins (IDPs) represent a class of biologically relevant proteins lacking a defined tertiary structure. Instead, they exist as ensembles of rapidly inter-converting heterogeneous conformations. Currently, nuclear magnetic resonance (NMR) spectroscopy stands as the most powerful tool for studying IDPs in solution, offering unique opportunities for atomic-level structural and dynamic investigations. NMR spin relaxation experiments, in particular, serve as primary sources of protein dynamics.

In folded proteins, relaxation is primarily driven by the rotational diffusion of the entire molecule. Within this context, one 15N-1H spin pair per residue is typically considered sufficient to capture and elucidate protein motions. In this fixed molecular tumbling frame, local variations are often interpreted as minor perturbations of an otherwise rigid molecule, seemingly separating structure and dynamics.

However, in more intricate and flexible systems such as IDPs, this relationship becomes intertwined. For IDPs, where local motions predominantly dictate their dynamic behavior, the commonly used 15N spin relaxation auto-correlated rates may not be able to fully capture the system's dynamics, necessitating the consideration of additional spin pairs for a comprehensive understanding of structural disorder. This thesis investigates a complementary spin pair to the well-studied 15N-1H, employing cross-correlated spin relaxation (CCR). The two contributions presented propose a new way to determine local correlation times and probe segmental anisotropic diffusion in disordered proteins, not only conceptually but also through the development of a novel pulse sequence. By investigating the efficacy of CCR-based methods in characterizing local fast dynamics, this work offers an agnostic method to disentangle geometric from dynamic contributions in the convoluted IDPs relaxation rates.

ZUSAMMENFASSUNG

Intrinsisch ungeordnete Proteine (IDPs) stellen eine Klasse biologisch relevanter Proteine dar, denen eine definierte Tertiärstruktur fehlt. Stattdessen existieren sie als Ensembles von sich schnell verändernden heterogenen Konformationen. Derzeit ist die Kernspinresonanzspektroskopie (NMR) das leistungsfähigste Instrument zur Untersuchung von IDPs in Lösung und bietet einzigartige Möglichkeiten für strukturelle und dynamische Untersuchungen auf atomarer Ebene. Insbesondere NMR-Spinrelaxationsexperimente dienen als primäre Quellen für die Proteindynamik.

In gefalteten Proteinen wird die Relaxation hauptsächlich durch die Rotationsdiffusion des gesamten Moleküls angetrieben. In diesem Zusammenhang wird in der Regel ein 15N-1H-Spinpaar pro Rest als ausreichend angesehen, um Proteinbewegungen zu erfassen und aufzuklären. In diesem festen molekularen Taumelrahmen werden lokale Variationen oft als geringfügige Störungen eines ansonsten starren Moleküls interpretiert, wodurch Struktur und Dynamik scheinbar voneinander getrennt werden.

In komplizierteren und flexibleren Systemen wie IDPs ist diese Beziehung jedoch verwoben. Bei IDPs, deren dynamisches Verhalten in erster Linie von lokalen Bewegungen bestimmt wird, können die üblicherweise verwendeten autokorrelierten 15N-Spinrelaxationsraten die Dynamik des Systems nicht vollständig erfassen, was die Berücksichtigung zusätzlicher Spinpaare für ein umfassendes Verständnis der strukturellen Unordnung erforderlich macht. In dieser Arbeit wird ein komplementäres Spinpaar zu dem gut untersuchten 15N-1H untersucht, das die kreuzkorrelierte Spinrelaxation (CCR) verwendet. In den beiden vorgestellten Beiträgen wird ein neuer Weg zur Bestimmung lokaler Korrelationszeiten und zur Untersuchung segmentaler anisotroper Diffusion in ungeordneten Proteinen vorgeschlagen, und zwar nicht nur konzeptionell, sondern auch durch die Entwicklung einer neuartigen Pulssequenz. Durch die Untersuchung der Wirksamkeit von CCR-basierten Methoden bei der Charakterisierung lokaler schneller Dynamik bietet diese Arbeit eine agnostische Methode, um geometrische von dynamischen Beiträgen in den gefalteten IDPs Relaxationsraten zu entflechten.

CONTENTS

Part I

INTRODUCTION

1 INTRODUCTION

Traditionally, protein function was believed to hinge on a clearly defined 3D structure[1]. Yet, as early as the 1970s, it was found that certain peptide hormones, in their functional states, were either partially or entirely unstructured[2]. The 1990s witnessed a breakthrough with the application of enhanced biochemical methods, revealing a plethora of fully functional proteins, intrinsically disordered under physiological conditions[3]–[5]. Nowadays, it is acknowledged that more than 30% of diverse proteosomes comprise intrinsically disordered proteins (IDPs), lacking a well-defined tertiary structure in their native states[4], [6]–[8]. A folded protein adopts a specific 3D structure defined as a unique set of backbone and side-chain atom positions along with dihedral angles[9], [10]. This structure represents an average, around which small-amplitude fluctuations in positions and angles occur[11]. Its uniqueness comes from the protein energy landscape's topology, that shows a well-defined kinetically-accessible energy minimum[12](Figure 1(a)). In contrast, IDPs exist as highly dynamic conformational ensembles, where atom positions and dihedral angles notably change over time. Their energy landscape is rather flat and rugged, allowing for a broader range of conformations due to numerous temperature-accessible states separated by small-energetic barriers[13]–[15](Figure 1(b)). hese various states may exhibit both lo-

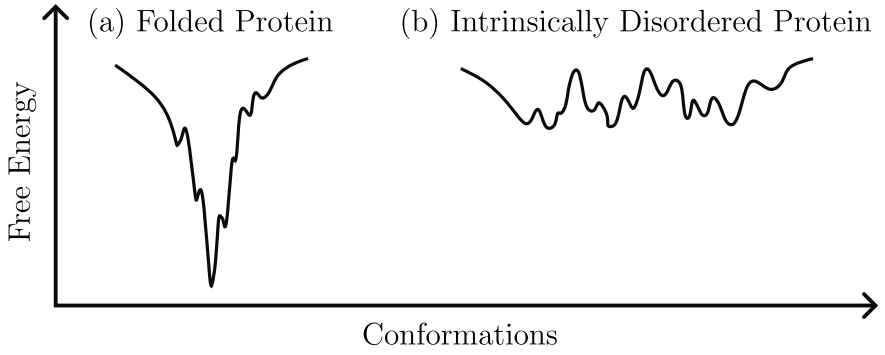

Figure 1: Schematic representation of energy landscapes (folding funnels) for (a) A folded protein and (b) An intrinsically disordered protein (IDP).

cal and global features. Local features influence the interactions with partner proteins and binding to various targets, while global features play a role in regulating accessibility/exposure of motifs and facilitate long-range interactions within the protein[16]–[19]. This departure from the traditional "structure-function paradigm" challenges the notion that a specific structure is a prerequisite for protein function-

ality, emphasizing the functional relevance of disorder in biological processes and human diseases (including cancer, amyloidosis, neurodegenerative diseases, cardiovascular disease, and diabetes)[20].

Due to the lack of well-defined structure in IDPs, high-resolution structures by X-ray crystallography are impossible to obtain. Fortunately, not all biophysical methods are as limited in characterizing IDPs as X-ray crystallography. Indeed residual dipolar couplings (RDCs), electron paramagnetic resonance (EPR) spectroscopy, steady-state fluorescence spectroscopy, circular dichroism (CD), differential scanning calorimetry (DSC), surface plasmon resonance (SPR), electrospray mass spectrometry, Fourier transform infrared (FTIR), Raman spectroscopy, and Raman optical activity can provide useful information on IDPs [4] Among the various biochemical methodologies available, Nuclear Magnetic Resonance (NMR) spectroscopy has been the leading technique that guided to the discovery of a plethora of different IDPs. NMR emerges as the unique technique providing comprehensive structural details of IDPs, thereby facilitating the elucidation of their conformational ensembles[21], [22].

1.1 NMR SPIN RELAXATION IN DISORDERED PROTEINS

Despite the recent emergence of cutting-edge technologies and advancements in the computational field (e.g. cryo-electron microscopy and AlphaFold), solution state NMR continues to be the preferred method for investigating IDPs and protein dynamics in general[23]. Indeed, NMR has a unique capability to access a wide range of dynamic timescales[24], [25] (Figure 2). The sheer power to access this

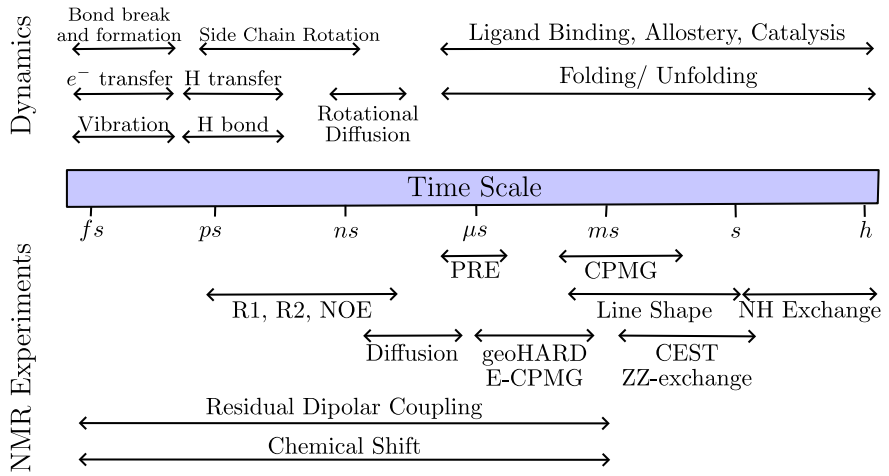

Figure 2: Timescales accessible to solution NMR.The upper part illustrates protein dynamics, while the lower one depicts the NMR techniques to probe these. Figure adapted from [26].

information comes from the fact that NMR spectroscopy can probe different and selective spin pairs in a molecule. In very general terms,

an NMR experiment involves a combination of radio frequency (rf) pulses and periods of free precession[27]. The application of an rf pulse perturbs the thermal equilibrium state that the spin ensemble reaches after being placed in an external magnetic field. By poking the ground state, the Boltzmann distribution population is altered and an excited state is created[28]. Over time, the magnetization irreversibly evolves toward the initial thermal equilibrium, i.e. nuclear spin relaxation[29]. Spin relaxation can either restore magnetization to the ground state (T1 relaxation) or cause dephasing of transverse coherences (T2 relaxation)[29], [30], and is induced by fluctuating fields arising from random overall diffusion of the molecule or internal motions within the molecule.

NMR spin relaxation studies historically centered on folded proteins. The majority of applications of spin relaxation methods in folded proteins probe amide ^{15}N spin [24]. Most commonly, ^{15}N auto-relaxation (R1, R1ρ, R2) or ^{15}N-^{1}H heteronuclear NOE cross-relaxation are used [31]–[36]. The power-fullness of the ^{15}N-^{1}H vector as a probe for dynamics is strictly connected to the nature of folded systems. The adoption of a rigid 3D structure allows us to approximate these proteins as rigid rotors, whose dynamics are mainly dominated by the overall molecular tumbling in solution [37], [38]. Therefore, the ^{15}N relaxation rates of folded proteins have been usually modeled by considering their diffusion in solution as rigid spheres (later, asymmetric top and anti-symmetric top were also considered) [35], [37], [39], [40]. This rationalization was also based on the assumption of statistical independence between slow global motions and fast local motions [37], [41]. When folded proteins are treated as isotropic spheres, a single spin vector is able to successfully capture the shared tumbling frame within the protein's 3D structure. The correlated motions of individual ^{15}N-^{1}H spin vectors offer a comprehensive overview of collective dynamics, reflecting the overall tumbling due to Brownian motion [37], [38], [42].

When considering more flexible and highly dynamic systems such as IDPs it becomes apparent that the approximation of an isotropic sphere does not hold anymore [43]–[47]. The lack of well-defined tertiary structures in IDPs results in distinct spin relaxation modes, reflecting the more isolated and specific motions of the individual peptide planes [43], [48]. Given the inherently local nature of spin relaxation in IDPs, a single ^{15}N nucleus per residue might not suffice anymore to capture the underlying motions. Traditional NMR spin relaxation experiments, in this context, may not provide a comprehensive understanding of IDPs dynamics. Recent MD studies, have provided insights into the contributions of different motional modes to relaxation in IDPs [43], [44], [49]–[51]. These studies apply existing models for folded proteins to disordered systems, and still have the limitation of being case-dependent and cannot be generalized, outlin-

ing the inevitable difficulties that come with extending concepts of folded proteins to IDPs. The interpretation of relaxation studies in IDPs is further complicated by experimental limitations. In particular, extensive conformational exchange leads to inherently averaged data, while significant water exchange introduce an extra relaxation outlet for exchangeable protons (e.g. H^N). To address these limitations, alternative experimental and analytical approaches become essential.

The focus of this doctoral thesis is on tackling these challenges by employing the cross-correlated spin relaxation (CCR) methodology. The next chapter aims to provide a brief introduction to some of the key concepts involved.

2

SPIN RELAXATION THEORY

In this Chapter is given a brief exposition of spin relaxation theory. It's important to note that it isn't exhaustive or comprehensive; rather, the author's aim is to offer a coherent and insightful analysis of spin relaxation fundamental quantity: the time correlation function (TCF).

Various mathematical strategies can be employed to address spin relaxation. However, one of the most straightforward approach are perturbation theories. In the latter, relaxation is treated as a minor perturbation, or noise, in the spin Hamiltonian. Historically, as starting point in the theory's derivation, is considered a small subsystem of a spin system ensemble, while accounting for the influence of the remaining part ("bath" or "lattice") in some effective manner[52]. Relaxation arises from the interaction between the system and the bath. In essence, the dynamics of the bath acts as a "local pulse" that induces relaxation if it matches the system's transition frequency[53].

Among perturbation theories, the Bloch-Wangsness-Redfield relaxation theory (*aka* Redfield relaxation theory)[54]–[57] is the one generally used in NMR spin relaxation as it ultimately provides useful practical applications. Redfield relaxation theory, often referred to as semi-classical relaxation theory, treats the dynamics of the bath as classical, while the spin system is treated quantum mechanically. It is important to note that the theory is formally correct only for an infinite Boltzmann spin temperature. To fix this problem thermal equilibrium is generally introduced *ad hoc*[58], nevertheless only a fully quantum mechanical treatment of the bath resolves this limitation and enables accurate prediction of the system's equilibrium behavior[59], [60].

While more intricate mathematical methods are available (for detailed references, see[52]), in this discussion we will concentrate only on Redfield relaxation theory.

2.1 REDFIELD RELAXATION THEORY

In Redfield relaxation theory, the time evolution of a spin system is described by the Liouville von Neumann (LvN) equation[52]:

$$\begin{aligned} &\frac{d\hat{\rho}(t)}{dt} = -i[\mathcal{H}_0 + \mathcal{H}_1(t)]\hat{\rho}(t), \\ &\mathcal{H}\hat{\rho} = [\hat{H}, \hat{\rho}] = \hat{H}\hat{\rho} - \hat{\rho}\hat{H} \end{aligned} \tag{1}$$

in which $\hat{\rho}$ is the spin density operator, $\mathcal{H}_0$ is the stationary Hamiltonian and $\mathcal{H}_1(t)$ is the stochastic Hamiltonian that couples the spins

to the bath. Eq. (1) can be expressed in the interaction picture (i.e. the rotating frame), to obtain an equation that depends only on the effect of the stochastic perturbation term[52]:

$$\frac{d\langle\hat{\rho}^R(t)\rangle}{dt} = -\left[\int_0^t \langle\mathcal{H}_1^R(t)\mathcal{H}_1^R(t_1)\rangle dt_1\right]\langle\hat{\rho}^R(t)\rangle \tag{2}$$

where the superscript R indicates the rotating frame, the angular brackets denote the ensemble average over all stochastic Hamiltonians, as we deal with a large amount of molecules[61].

The nuclear spin Hamiltonians are Hermitian operators that have the fundamental property to be invariant under the action of the rotational group. Therefore, we can expand the stochastic Hamiltonian $\mathcal{H}_1^R(t)$ in a useful basis of irreducible tensor operators of rank-2[61], [62]:

$$\mathcal{H}_1^R(t) = \sum_u \sum_p \sum_{m=-2}^{2} (-1)^m c_u(t) Y_{-m}^2(\Phi_u(t)) \mathcal{T}_{mp}^{(2)}(u) \tag{3}$$

where the summation over u refers to all the possible interactions, such as dipole-dipole (DD) and chemical shielding anisotropy (CSA) interactions, $c(t)$ is a function of the spatial variables depending on the type of u interaction considered (e.g. the DD internuclear distances r_{IS}^{-3} or chemical shift tensor σ vector components), Y_{-m}^2 are the modified spherical harmonics of order-2, $\Phi_u(t) = \{\theta_u(t), \phi_u(t)\}$ are the polar angles in the laboratory frame, which describe the orientation of the unit spin vector u that points in the principal direction of the interaction[53]. For a DD interaction the unit vector u points along the line between the two nuclei, for a CSA with axially symmetric chemical shift tenors, the unit vector u is collinear with the principal axis of the CSA tensor [53]. $\mathcal{T}_{mp}^{(2)}(u) = [\hat{T}_{mp}^{(2)}(u),]$ where $\hat{T}_{mp}^{(2)}(u)$ are irreducible spherical tensor basis operators of rank-2, constituting of $2 \times 2 + 1$ operators [63], [64], which also depends on the interactions involved in the relaxation process (for DD and CSA interactions they can be found in [61], p.38). The basis operators $\hat{T}_{mp}^{(2)}(u)$, can be freely chosen to be eigenoperators of the static Hamiltonian $\mathcal{H}_0$:

$$\mathcal{H}_0 \hat{T}_{mp}^{(2)}(u) = \omega_p^m \hat{T}_{mp}^{(2)}(u) \tag{4}$$

where the index p is included to distinguish spin operator with same order m but different eigenfrequencies[53].

Inserting Eq. (3) in Eq. (2) yields:

$$\frac{d\langle\hat{\rho}^R(t)\rangle(t)}{dt} = -\sum_{u,v}\sum_{m,m'}\sum_{p,p'}(-1)^{m'} e^{i(\omega_p^m + \omega_{p'}^{m'})t} \mathcal{T}_{m'p'}^{(2)}(u)\mathcal{T}_{mp}^{(2)}(v) \tag{5}$$
$$\times \int_0^\infty \langle c_u(t) c_v(t+\tau) Y_{-m'}^2(\Phi_u(t)) Y_m^{*2}(\Phi_v(t+\tau))\rangle e^{-i\omega_p^m \tau} d\tau$$

where the relationship $(-1)^m Y^2_{-m} = Y^{*2}_m$ has been used. The random processes $Y^2_{-m}(\Phi_u(t))$ are assumed to be statistically independent unless $m' = -m$, consequently the ensemble average vanishes when $m' \neq -m$ [53], [61]. Moreover, in the secular approximation only terms with $\omega^m_p \approx -\omega^{m'}_{p'}$ are retained. Considering these assumptions and transforming back in the laboratory frame yields the master equation:

$$\frac{d\langle\hat{\rho}(t)\rangle(t)}{dt} = -i\mathcal{H}_0\langle\hat{\rho}(t)\rangle + \mathcal{R}\langle\hat{\rho}(t)\rangle \tag{6}$$

where $\mathcal{R}$ is the Redfield relaxation superoperator:

$$\begin{aligned}\mathcal{R} = -\sum_{u,v}\sum_{p,p'}\sum_{m=-2}^{2}(-1)^{-m}\mathcal{T}^{(2)}_{-mp'}(u)\mathcal{T}^{(2)}_{mp}(v) \\ \times\int_0^\infty C^m_{uv}(\tau)e^{-i\omega^m_p\tau}d\tau\end{aligned} \tag{7}$$

in which the p' are chosen to satisfy the secular condition[61]. Note that the upper limit of integration is infinity because it has been assumed that the time t is long enough for the TCF to decay completely to zero by $\tau = t$[62]. When the transitions are degenerate there are additional pathways for relaxation coming from the fact that $\omega_i - \omega_j = 0$[61].

The $C^m_{uv}(\tau)$ is the time correlation function (TCF):

$$C^m_{uv}(\tau) = \langle c_u(t)c_v(t+\tau)Y^2_m(\Phi_u(t))Y^{*2}_m(\Phi_v(t+\tau)\rangle. \tag{8}$$

We can observe that the TCF depends only on the separation of times $\tau = |t-(t+\tau)|$, because the random functions $Y^2_{-m}(\Phi(t))$ are assumed stationary. The TCF's Fourier Transform (FT), namely the spectral density function (SDF), reads:

$$J^m_{uv}(\omega^m_p) = \int_0^\infty C^m_{uv}(\tau)e^{-i\omega^m_p\tau}d\tau. \tag{9}$$

The SDF is a complex valued function, where the imaginary part (generally very small) causes the dynamic frequency shift[65].

To summarize, the derivation of Redfield relaxation theory provides an equation for the evolution of the density operator under the effect of random fluctuations of the bath, in which the separation between the stochastic part (spectral densities) and the spin part (double commutator) provides a rather straightforward way to calculate relaxation rate constants. Indeed, when the density operator in Eq. (6) is expanded in term of the basis operators[53], [61], [66], we obtain the matrix form of the master equation in which the matrix representation of $\mathcal{R}$ (see Eq. (7)) has as elements the actual relaxation rates: a linear combination of the SDF at selected few frequencies[53].

2.2 A TYPE OF TIME CORRELATION FUNCTION

This section analyses the information encoded within the time correlation function (TCF) for a macromolecule diffusing in an isotropic solution. As $Y^2_{-m}(t)$ are stationary random function, the TCF dependence on t can be replaced by an evaluation at 0 without loss of generality[61]:

$$C^m_{uv}(\tau) = \langle c_u(0)c_v(\tau)Y^2_m(\Phi_u(0))Y^{*2}_m(\Phi_v(\tau)\rangle. \tag{10}$$

When dealing with an isotropic solution, it can be shown that the correlation function does not depend on the index m[37], [66], [67]. In this case, from the addition theorem of the spherical harmonics (Eq. (11)) we have[64], [68]:

$$\begin{aligned} P_2(u(0)\cdot v(\tau)) &= \sum_{m'=-2}^{2} Y^2_{m'}(\Phi_u(0))Y^{*2}_{m'}(\Phi_v(\tau)) \\ &= Y^2_m(\Phi_u(0))Y^{*2}_m(\Phi_v(\tau)) \sum_{m'=-2}^{2} 1 \\ &= 5[Y^2_m(\Phi_u(0))Y^{*2}_m(\Phi_v(\tau))]. \end{aligned} \tag{11}$$

Again, u and v describe the orientation in the laboratory frame of the unit spin-vectors (either DD or CSA) involved in the relaxation process, at time 0 and τ. Substituting this relation in Eq. (12) yields[53], [61], [63], [68]:

$$C_{uv}(\tau) = \frac{1}{5}\langle c_u(0)c_v(\tau)P_2(u(0)\cdot v(\tau))\rangle \tag{12}$$

where $P_2(x) = \frac{1}{2}(3x^2 - 1)$ is the second order Legendre polynomial.

Next, for the interactions here considered one can assume that the time-dependent distance fluctuations, represented by $c_u(0)c_v(\tau)$, factorize. Consequently, they can be assimilated with the factor $\frac{1}{5}$ into constant coefficients, for later convenience.

It becomes apparent that the TCF describes the process of temporal decorrelation within a spin ensemble. By depending on the orientation of the spin vectors involved in the relaxation process, it encodes a protein's "structural memory", i.e., the temporal persistence of concerted motions and structural arrangements.

The real component of its FT yields the real term of the spectral density function (see section 2.1), which reads:

$$\begin{aligned} J_{uv}(\omega) &= \int_0^\infty C_{uv}(\tau)\cos(\omega\tau)d\tau \\ &= \int_0^\infty \langle P_2(u(0)\cdot v(\tau))\rangle \cos(\omega\tau)d\tau \end{aligned} \tag{13}$$

2.2.1 *Factorization of Structure and Dynamics: The J(0) term*

Numerous studies have concentrated on isolating the SDF at zero frequency, denoted as $J(0)$, primarily because it is the component most sensitive to the timescales with $t \geq 1$ ns (tumbling). Additionally, isolating $J(0)$ enables a reasonably accurate separation of the structural components from the correlation time. This section will briefly elucidate this concept starting form the TCF (Eq. (12)).

When evaluating the TCF at time zero ($\tau = 0$) we have: $C_{uv}(0) = \langle P_2(u(0) \cdot v(0)) \rangle$. We can distinguish two cases: (i) when $u = v$ (auto-correlated relaxation) we have $C_{uu}(0) = 1$. The correlation function starts at 1 and then decays to zero. At $t = 0$, the u vectors align with themselves. As time progresses and the protein molecules move in solution, the distribution of projection angles between $u(0)$ and $u(t)$ randomizes throughout the ensemble, and C_{uu} decays toward zero.

(ii) When $u \neq v$ (cross-correlated relaxation) the TCF does not start at one anymore, but $C_{uv}(0) = \langle P_2(u(0) \cdot v(0)) \rangle$. Next, if a fixed and relatively small angle between u and v (θ_{uv}) is assumed, $\langle P_2(u(0) \cdot v(0)) \rangle = P_2(\cos \theta_{uv})$. In these cases, it is convenient to normalize the TCF to its initial amplitude:

$$C_{uv}(t) = C_{uv}(0) \frac{C_{uv}(t)}{C_{uv}(0)} = P_2(\cos \theta_{uv}) \frac{C_{uv}(t)}{C_{uv}(0)} \tag{14}$$

to obtain for its SDF counterpart a very useful factorization[69]:

$$J_{uv}(0) = P_2(\cos \theta_{uv}) \int_0^\infty \frac{C_{uv}(t)}{C_{uv}(0)} dt = P_2(\cos \theta_{uv}) \tau_{uv} \tag{15}$$

where the correlation time τ_{uv} is defined in very general terms as the integral of the normalized TCF. For a multi-exponential decay, it corresponds to the average correlation time; for a rigid spherical top, τ equates to the rotational tumbling time. This notation formally separates the static ensemble average $C_{u,v}(0) = P_2(\cos \theta_{uv})$ and its associated correlation time τ_{uv}. It provides a unique agnostic method that does not make any prior assumptions about the nature of the motions, enabling the disentanglement of information encoded in relaxation rates for complex systems such as IDPs.

2.3 SUMMARY OF THE THESIS

This thesis delves into cross-correlated spin relaxation (CCR) within the realm of structural disorder. As discussed by Ferrage et al. "The broad conformational space of IDPs makes the wide variety of cross-correlated relaxation methods developed for folded proteins difficult to interpret in disordered proteins, as the effects of average relative orientations (structure) and correlation times (dynamics) are difficult to deconvolute" ([70], p. 72). The two papers presented here offer a

fresh perspective on this challenge, relying on the factorization of the SDF presented above (see 2.2.1). The first paper proposes a complementary spin pair to the ^{15}N-^{1}H to probe segmental anisotropic diffusion in IDPs, laying the groundwork. The second paper expands upon this idea, and proposes a new pulse sequence for the determination of two different but complementary correlation times in the peptide plane. Together, these contributions investigate the power of CCR-based method to untangle structure and dynamics in IDPs.

Part II

SHOWCASE OF PUBLISHED WORK

The central part of this cumulative thesis consists of two scientific articles, which have been published in peer-reviewed scientific journals. Aside from the continuous page numbering, the original layout design should be considered intellectual property of the respective journals. Supporting figures and tables are also included in the original format. Their respective digital object identifiers (DOIs) are provided together with a short statement of personal contribution at the beginning of each chapter.

3

AN ADDITIONAL SPIN PAIR TO PROBE ANISOTROPIC SEGMENTAL DYNAMICS IN IDPS

C. Kauffmann, I. Ceccolini, G. Kontaxis, and R. Konrat, "Detecting anisotropic segmental dynamics in disordered proteins by cross-correlated spin relaxation," *Magnetic Resonance*, vol. 2, no. 2, pp. 557–569, 2021 [71]

DOI: 10.5194/mr-2-557-2021

PERSONAL CONTRIBUTION

Conceptualization, simulation, visualization.
Shared First Author with C. Kauffmann.

Magn. Reson., 2, 557–569, 2021
https://doi.org/10.5194/mr-2-557-2021

Open Access
MAGNETIC RESONANCE

Detecting anisotropic segmental dynamics in disordered proteins by cross-correlated spin relaxation

Clemens Kauffmann[1,★], **Irene Ceccolini**[1,★], **Georg Kontaxis**[1], **and Robert Konrat**[1]

[1]Department of Structural and Computational Biology, Max Perutz Laboratories, University of Vienna, Campus-Vienna-Biocenter 5, 1030 Vienna, Austria
★These authors contributed equally to this work.

Correspondence: Clemens Kauffmann (clemens.kauffmann@univie.ac.at) and Robert Konrat (robert.konrat@univie.ac.at)

Received: 23 March 2021 – Discussion started: 8 April 2021
Revised: 25 May 2021 – Accepted: 2 June 2021 – Published: 6 July 2021

Abstract. Among the numerous contributions of Geoffrey Bodenhausen to NMR spectroscopy, his developments in the field of spin-relaxation methodology and theory will definitely have a long lasting impact. Starting with his seminal contributions to the excitation of multiple-quantum coherences, he and his group thoroughly investigated the intricate relaxation properties of these "forbidden fruits" and developed experimental techniques to reveal the relevance of previously largely ignored cross-correlated relaxation (CCR) effects, as "the essential is invisible to the eyes". Here we consider CCR within the challenging context of intrinsically disordered proteins (IDPs) and emphasize its potential and relevance for the studies of structural dynamics of IDPs in the future years to come. Conventionally, dynamics of globularly folded proteins are modeled and understood as deviations from otherwise rigid structures tumbling in solution. However, with increasing protein flexibility, as observed for IDPs, this apparent dichotomy between structure and dynamics becomes blurred. Although complex dynamics and ensemble averaging might impair the extraction of mechanistic details even further, spin relaxation uniquely encodes a protein's structural memory. Due to significant methodological developments, such as high-dimensional non-uniform sampling techniques, spin relaxation in IDPs can now be monitored in unprecedented resolution. Not embedded within a rigid globular fold, conventional ^{15}N spin probes might not suffice to capture the inherently local nature of IDP dynamics. To better describe and understand possible segmental motions of IDPs, we propose an experimental approach to detect the signature of anisotropic segmental dynamics by quantifying cross-correlated spin relaxation of individual $^{15}N^{1}H^{N}$ and $^{13}C'^{13}C^{\alpha}$ spin pairs. By adapting Geoffrey Bodenhausen's symmetrical reconversion principle to obtain zero frequency spectral density values, we can define and demonstrate more sensitive means to characterize anisotropic dynamics in IDPs.

1 Introduction

Geoffrey Bodenhausen's 70th anniversary marks an ideal occasion to take a fresh look at some of his numerous contributions to spin-relaxation methodology and theory. By considering his experiments within the challenging context of intrinsically disordered proteins (IDPs), we want to emphasize their potential and relevance in the future years to come. Arguably, this rediscovery might require some collective effort, as current trends appear to point in the opposite direction. As Paul Schanda put it recently: "The popularity of detailed spin-relaxation measurements in liquids, *en vogue* 10 or 20 years ago, is declining; [...] with lengthy measurements it is not easy to gain much more insight than 'loops are more flexible than secondary structures', which often does not answer mechanistic questions." (Schanda, 2019, p. 3–4). While intentionally exaggerated, this statement does point to some of the inherent limitations of relaxation experiments. Owing to their convoluted nature, spin relaxation reports on protein dynamics only in ambiguous terms. A variety of

stochastic processes can lead to time correlation functions (TCFs) of identical shape and form (Richert and Blumen, 1994, p. 1–7). In addition, the TCF is not probed directly, only its spectral density; i.e., its Fourier transform is sampled at a few select frequencies. Thus, with far more detailed structural models at hand, protein dynamics are often understood as mere perturbations of otherwise rigid bodies tumbling in solution (Lipari and Szabo, 1982; Halle and Wennerström, 1981; Clore et al., 1990; Halle, 2009). Relaxation experiments commonly employed to calculate protein structures, such as nuclear Overhauser effects (NOEs) and paramagnetic relaxation enhancements (PREs), are usually modeled without accounting for their dynamic nature (Iwahara et al., 2004; Clore and Iwahara, 2009; Xue et al., 2009; Vögeli, 2014). In a sense, protein dynamics might appear separate from protein structure, at least within the structure–function paradigm.

However, with increasing protein flexibility this apparent dichotomy becomes blurred as structure and dynamics can no longer be considered independent of each other. While complex dynamics and ensemble averaging obfuscate mechanistic details even further, the structural information content of relaxation parameters becomes increasingly apparent. In comparison to simple population-averaged quantities, such as chemical shifts or scalar couplings, spin relaxation uniquely encodes a system's structural memory, i.e., the temporal persistence of concerted motions and structural arrangements. Somewhat counterintuitively, spin-relaxation experiments are among the prime sources of structural information available for disordered systems. However, due to a general lack of analytical descriptions for IDP dynamics (Modig and Poulsen, 2008; Idiyatullin et al., 2001; Bussell and Eliezer, 2001; Kadeřávek et al., 2014; Khan et al., 2015), this notion has been of somewhat academic nature until the recent past. Continuous developments in molecular dynamics (MD) simulation protocols (Piana et al., 2015, 2020; Rauscher et al., 2015; Robustelli et al., 2018; Zerze et al., 2019; Gopal et al., 2021; Shea et al., 2021) demonstrate how this gap can finally be bridged, allowing us to validate, refine and/or analyze dynamic ensemble representations of proteins in solution (Kämpf et al., 2018; Kümmerer et al., 2020; Salvi et al., 2016, 2017). With the necessary timescales becoming increasingly accessible (Stone et al., 2007, 2010; Salomon-Ferrer et al., 2013; Eastman et al., 2017) and the spectral resolution provided by high-dimensional non-uniform sampling experiments to overcome the problem of spectral overlap (Grudziąż et al., 2018), spin relaxation in IDPs can be investigated in unprecedented fashion.

This aspect alone suggests a systematic reassessment and evaluation of less commonly employed experiments. Far more pressing, in our opinion, is the inherently local nature of spin relaxation in IDPs. In contrast to folded proteins, spins in IDPs are not embedded within a fixed molecular tumbling frame. Thus, a single ^{15}N nucleus per residue as a dynamic probe might not suffice to capture the underlying motions in adequate detail. While detecting and quantifying the presence of anisotropy in IDP dynamics might seem like a rather academic endeavor, it represents an important stepping stone towards the structural interpretation of other experiments. As we recently demonstrated, an appropriate estimate for the average correlation time is an important prerequisite for the angular evaluation of cross-correlated relaxation (CCR) of remote spins (Kauffmann et al., 2021).

More immediate in its structural implications would be the presence of diffusion anisotropy, which has been hypothesized to be of substantial size even in highly disordered proteins such as α-synuclein. Specifically, segmental tumbling of α-helical and extended chain conformations has been implied to lead to pronounced diffusion anisotropy effects for intraresidual and sequential ^{1}H$-^1$H NOEs (Ying et al., 2014; Mantsyzov et al., 2014, 2015). At the same time, the 3D GAF model (Bremi and Brüschweiler, 1997; Lienin et al., 1998) has been invoked to further rationalize the presence of anisotropic dynamics on the local scale of the peptide plane. This model has recently been reframed by Salvi et al. (2017) to analyze MD-simulated ^{15}N relaxation of a partially disordered protein. In essence, it was demonstrated that NH^N TCFs are well described by the $C^\alpha C^\alpha$ TCFs of the same peptide plane as long as variations of the flanking dihedral angles and NH^N librations are accounted for. Explicit corrections for possible effects of anisotropic segmental tumbling were not required. However, noticeable deviations could be observed for the transverse ^{15}N relaxation of the slowly moving residual α-helix. Marcellini et al. (2020) have reported pronounced diffusion anisotropy within the α-helical region of an otherwise disordered construct. Flexible residues were affected noticeably less. It was suggested this might be due to their average orientation in the molecular tumbling frame (Marcellini et al., 2020). The SRLS model of Tugarinov et al. (2001) and Meirovitch et al. (2006) also predicts pronounced anisotropy for α-helices and β-sheets. However, loops and terminal chain segments appear isotropic, asserting that proteins with substantial internal mobility are best represented by an isotropic global diffusion tensor (Zerbetto et al., 2011).

Arguably, this somewhat ambiguous body of evidence illustrates the inevitable difficulties that come with extending concepts of folded proteins to IDPs. In fact, many of the above observations might very well be case-dependent. In the present study, we want to approach this question in a more agnostic manner. Are there experimental ways to better detect the signature of anisotropic dynamics in IDPs? At what level of evidence could we evoke the mental image of extended chains and α-helical segments tumbling in solution? The principal difficulty in characterizing these structural elements lies in their translational periodicity. In an α-helix, NH^N vectors are strongly aligned along the main axis, while in an extended chain they are oriented perpendicularly. In order to detect possible orientational biases in their relaxation behavior, additional spin probes with different orientations must be considered. While $C^\alpha H^\alpha$ might be suitable for α-

helices (Barnes et al., 2019), its orientation is too similar to NH^N in the extended chain conformation. Moreover, since it does not share a peptide plane with NH^N, it varies as a function of ϕ and ψ as do the $^1H-^1H$ intraresidual and sequential NOEs. Spin probes within the same peptide plane and thus less ambiguous orientations would certainly be preferable.

For IDPs in particular, Kadeřávek et al. (2014) have shown that the NH^N spectral density is best mapped by a combination of transversal and longitudinal CCR rates, employing Geoffrey Bodenhausen's symmetrical reconversion principle (Pelupessy et al., 2003, 2007). Together with Bodenhausen and coworkers, this concept was later extended to measure the zero frequency spectral density in a single experiment (Kadeřávek et al., 2015). By translating these concepts to the $C'C^\alpha$ spin pair, we want to derive and demonstrate more sensitive means to detect anisotropic segmental dynamics in IDPs.

2 Theory

Our aim is to define an experimental measure for anisotropic segmental dynamics in IDPs. While the measure itself should be general, the considered source of anisotropy will be rather specific. To assess the sensitivity of the proposed protocol, we resort to the simplified image of extended chain and α-helical segments tumbling in solution as previously asserted by Mantsyzov et al. (2014). Before considering experimental aspects, we start by defining the spectral density. Sampled at zero frequency and/or (combinations of) the involved Larmor frequencies, it constitutes the fundamental quantity of all spin-relaxation experiments:

$$J_{\boldsymbol{u},\boldsymbol{v}}(\omega) = \int_0^\infty C_{\boldsymbol{u},\boldsymbol{v}}(t)\cos(\omega t)\,\mathrm{d}t \tag{1}$$

with the time correlation function (TCF),

$$C_{\boldsymbol{u},\boldsymbol{v}}(t) = \langle P_2(\boldsymbol{u}(0)\cdot\boldsymbol{v}(t))\rangle, \tag{2}$$

where $P_2(x) = 1.5x^2 - 0.5$ is the second-order Legendre polynomial, $\boldsymbol{u}$ and $\boldsymbol{v}$ represent either dipolar unit vectors or principal components of chemical shift anisotropy (CSA) tensors. Note that our simplified definition of the TCF implicitly assumes that time-dependent distance fluctuations factorize and can thus be absorbed into constant coefficients. This requirement will be well satisfied for the spins considered henceforth.

For most processes, the TCF can be described as a sum or distribution of exponential decays (Lipari and Szabo, 1982; Idiyatullin et al., 2001; Modig and Poulsen, 2008; Khan et al., 2015):

$$C_{\boldsymbol{u},\boldsymbol{v}}(t) = \sum_{k=0}^{N} a_k e^{-t/\tau_k}. \tag{3}$$

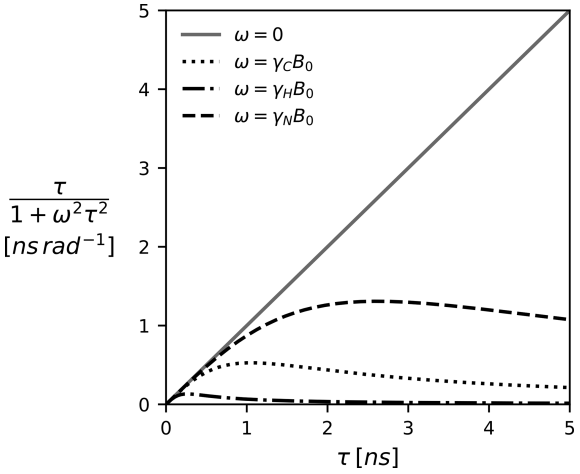

Figure 1. The Lorentzian as a function of the correlation time τ and the (Larmor) frequency. The spectral density $J(\omega)$, which is modeled as a linear combination of Lorentzian functions, can be pictured as a weighted average of all correlation times τ. Since $J(0)$ weights all correlation times equally, it represents the component most sensitive to correlation times > 1 ns. The magnetic field B_0 is 18.8 T (800 MHz proton Larmor frequency).

Evaluating at $t = 0$ yields a type of normalization condition,

$$\sum_{k=0}^{N} a_k = C_{\boldsymbol{u},\boldsymbol{v}}(0) = \langle P_2(\boldsymbol{u}(0)\cdot\boldsymbol{v}(0))\rangle, \tag{4}$$

which equates to 1 for the familiar case of auto-correlation ($\boldsymbol{u} = \boldsymbol{v}$). For cross-correlation ($\boldsymbol{u} \neq \boldsymbol{v}$), Eq. (4) is bounded within $[-0.5, 1]$.

The spectral density of Eq. (3) is a sum of Lorentzian functions

$$J_{\boldsymbol{u},\boldsymbol{v}}(\omega) = \sum_{k=0}^{N} a_k \frac{\tau_k}{1+(\omega\tau_k)^2} \tag{5}$$

Note that, depending on how the TCF and the spectral density are defined, Eq. (5) might come with additional coefficients such as the familiar factor of $\frac{2}{5}$ (Lipari and Szabo, 1982). We prefer the above definitions as they highlight $J_{\boldsymbol{u},\boldsymbol{v}}(\omega)$ as a weighted average. At zero frequency all τ_k's are weighted equally; i.e., $J(0)$ encodes the average correlation time. With increased frequency, the impact of larger τ_k becomes less pronounced. This is illustrated in Fig. 1 for a selection of Larmor frequencies assuming a magnetic field strength of 18.8 T (800 MHz proton Larmor frequency).

Detecting anisotropy amounts to quantifying orientational biases in a_k and τ_k. Similarly to Mantsyzov et al. (2014), we will attribute these biases to relative orientations in idealized extended chain and α-helical segments. These structural elements are well described by an axially symmetric diffusion tensor, which yields the following expression for the spectral

density (Tjandra et al., 1996; Woessner, 1962):

$$J_{\boldsymbol{u},\boldsymbol{v}}(\omega) = \sum_{k=0}^{2} A_k(\boldsymbol{u},\boldsymbol{v}) \frac{\tau_k}{1+(\omega\tau_k)^2}, \tag{6}$$

where

$$\begin{aligned} a_0 &\equiv A_0(\boldsymbol{u},\boldsymbol{v}) = P_2(\theta_{\boldsymbol{u}})P_2(\theta_{\boldsymbol{v}}),\\ a_1 &\equiv A_1(\boldsymbol{u},\boldsymbol{v}) = 0.75\sin(2\theta_{\boldsymbol{u}})\sin(2\theta_{\boldsymbol{v}})\cos(\phi_{\boldsymbol{u}}-\phi_{\boldsymbol{v}}),\\ a_2 &\equiv A_2(\boldsymbol{u},\boldsymbol{v}) = 0.75\sin^2(\theta_{\boldsymbol{u}})\sin^2(\theta_{\boldsymbol{v}})\cos(2\phi_{\boldsymbol{u}}-2\phi_{\boldsymbol{v}}), \end{aligned} \tag{7}$$

and θ and ϕ denote the polar angles in the tumbling frame. The τ_k's correspond to the inverted eigenvalues of the axially symmetric diffusion tensor:

$$\begin{aligned} \tau_k &= \left(6D_\perp + k^2\left(D_\parallel - D_\perp\right)\right)^{-1}\\ &= D_\perp^{-1}\left(6 + k^2\left(\frac{D_\parallel}{D_\perp} - 1\right)\right)^{-1} \end{aligned} \tag{8}$$

with $k = 0, 1, 2$. With $\boldsymbol{u}$ and $\boldsymbol{v}$ alone, Eq. (6) would not allow us to distinguish between size effects in τ_k (i.e., "segment length") and orientational biases in $A_k(\boldsymbol{u},\boldsymbol{v})$ (i.e., "secondary structure"). To quantify the anisotropy ($\frac{D_\parallel}{D_\perp}$) only, we consider another interaction described by a second set of vectors ($\boldsymbol{x}$, $\boldsymbol{y}$) embedded with different orientations in the same tumbling frame and focus our attention on $J(0)$ for three reasons. First and foremost, $J(0)$ is the component most sensitive to the $\tau_k \geq 1$ ns (cf. Fig. 1) commonly associated with tumbling motions (Kämpf et al., 2018). Secondly, the zero frequency does not depend on the type of nuclei involved. Lastly, $J(0)$ allows us to define a convenient ratio,

$$\begin{aligned} \frac{J_{\boldsymbol{u},\boldsymbol{v}}(0)}{J_{\boldsymbol{x},\boldsymbol{y}}(0)} &= \frac{D_\perp^{-1}\sum_{k=0}^{2} A_k(\boldsymbol{u},\boldsymbol{v})(6+k^2(\frac{D_\parallel}{D_\perp}-1))^{-1}}{D_\perp^{-1}\sum_{k=0}^{2} A_k(\boldsymbol{x},\boldsymbol{y})(6+k^2(\frac{D_\parallel}{D_\perp}-1))^{-1}}\\ &= \frac{\sum_{k=0}^{2} A_k(\boldsymbol{u},\boldsymbol{v})(6+k^2(\frac{D_\parallel}{D_\perp}-1))^{-1}}{\sum_{k=0}^{2} A_k(\boldsymbol{x},\boldsymbol{y})(6+k^2(\frac{D_\parallel}{D_\perp}-1))^{-1}} \end{aligned} \tag{9}$$

such that the explicit size dependency cancels out. In general, if ($\boldsymbol{u}$,$\boldsymbol{v}$) and ($\boldsymbol{x}$,$\boldsymbol{y}$) have fixed relative orientations and experience the same dynamics, we obtain the isotropic edge case:

$$\frac{J_{\boldsymbol{u},\boldsymbol{v}}(0)}{J_{\boldsymbol{x},\boldsymbol{y}}(0)} = \frac{P_2(\boldsymbol{u}\cdot\boldsymbol{v})}{P_2(\boldsymbol{x}\cdot\boldsymbol{y})}. \tag{10}$$

Thus, the ratio (Eq. 9) encodes a simple and intuitive relation: isotropic motions tend towards the limit (Eq. 10), while anisotropic motions deviate from it. Importantly, the source of anisotropy is not essential. The invoked model of a tumbling symmetric top, Eq. (6), does not need to apply in any strict sense; rather, it is used to assess the sensitivity of the $J(0)$ ratio (Eq. 9) to its associated features. Presuming that segmental arrangements are sufficiently stable, remnants of Eq. (6) might still be detectable even in the case of pronounced local mobility.

In general, assessing the effects of internal motions on Eq. (6) is not straightforward. Even for folded proteins, the commonly employed model-free (MF) (Lipari and Szabo, 1982) and extended MF (Clore et al., 1990) approaches are not strictly applicable in the case of anisotropic diffusion (Daragan and Mayo, 1999; Halle, 2009). For CCR in particular, the proposed adaptations can become quite intricate (Vögeli, 2010). Geoffrey Bodenhausen and coworkers have investigated this topic in a series of publications (Deschamps and Bodenhausen, 2001; Deschamps, 2002; Vugmeyster et al., 2004; Abergel and Bodenhausen, 2004, 2005; Nodet et al., 2008). Given the toy nature of the considered model, we will assess the presence of fast, isotropic motions as simply as possible by introducing a fourth Lorentzian:

$$\begin{aligned} J_{\boldsymbol{u},\boldsymbol{v}}(\omega) = S^2 &\sum_{k=0}^{2} A_k(\boldsymbol{u},\boldsymbol{v}) \frac{\tau_k}{1+(\omega\tau_k)^2}\\ &+ (1-S^2)P_2(\boldsymbol{u}\cdot\boldsymbol{v})\frac{\tau_3}{1+(\omega\tau_3)^2} \end{aligned} \tag{11}$$

with $\tau_3^{-1} = \tau_{\text{int}}^{-1} + 4D_\perp + 2D_\parallel$, where τ_{int} is the average correlation time of the fast internal motion. The generalized order parameter $S^2 \in [0, 1]$ acts as a weight balancing the contributions of slow anisotropic tumbling and fast isotropic motions. To account for the angular relation between $\boldsymbol{u}$ and $\boldsymbol{v}$, a_3 necessarily corresponds to $P_2(\boldsymbol{u}\cdot\boldsymbol{v})$, which follows intuitively from condition Eq. (4), assuming a fixed angle between $\boldsymbol{u}$ and $\boldsymbol{v}$.

Of course, the additional Lorentzian can be rationalized in terms of established models. As shown in the Appendix, Eq. (11) corresponds to a simplification of the MF-like extension proposed by Ghose et al. (1998), Eq. (A1) and generalized by Vögeli and Yao (2009) and Vögeli (2010). In this model, the generalized order parameters depend on k as well; i.e., the weighting between isotropic and anisotropic contributions can indeed vary between different k's. Using a single order parameter is exact only if the molecule is fully rigid ($S^2 = 1$) or if the dynamics are entirely isotropic ($\frac{D_\parallel}{D_\perp} = 1$ or $S^2 = 0$). In the case of pronounced diffusion anisotropy and intermediate local mobility, Eq. (11) is only an approximate interpolation between these edge cases. Still, it is worth noting that the use of a single order parameter is both a common heuristic to account for the effects of local dynamics on experimental CCR rates (Vögeli and Yao, 2009) and an established approximation for sufficiently small angles between $\boldsymbol{u}$ and $\boldsymbol{v}$ (Tjandra et al., 1996; Kroenke et al., 1998). To keep the amount of parameters manageable, possible differences in local dynamics for different k and/or between ($\boldsymbol{u}$,$\boldsymbol{v}$) and ($\boldsymbol{x}$,$\boldsymbol{y}$) are not reflected in Eq. (11). Systematic differences in local peptide plane dynamics (Chang and Tjandra, 2005; Ferrage et al., 2006; Wang et al., 2006; Salvi et al., 2017) will necessarily result in deviations from the isotropic case,

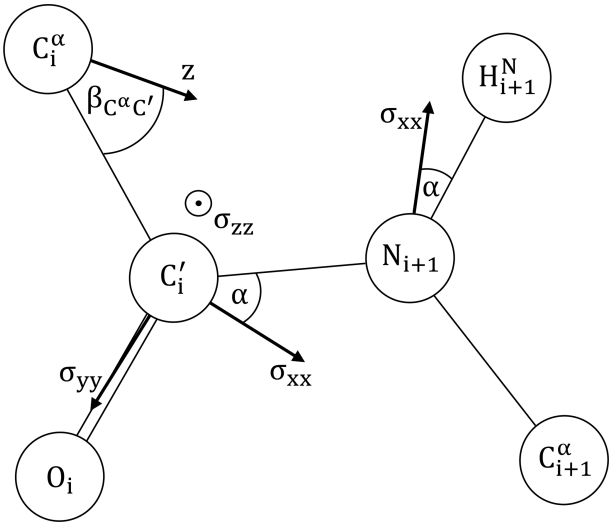

Figure 2. The peptide plane as defined by Corey et al. (1953): $C^\alpha - C' = 1.53$ Å, $C' - O = 1.24$ Å, $C' - N = 1.32$ Å, $N - C^\alpha = 1.47$ Å. $C^\alpha - C' - O = 121°$, $C^\alpha - C' - N = 114°$, $O - C' - N = 125°$, $C' - N - H = 123°$, $C' - N - C^\alpha = 123°$ and $H - N - C^\alpha = 114°$. $N - H = 1.04$ Å is taken from Ottiger and Bax (1998). The ^{15}N and $^{13}C'$ CSA principal components are adapted from Bodenhausen and coworkers (Cisnetti et al., 2004; Loth et al., 2005). ^{15}N: $\Delta_N \approx \sigma_{xx} - \sigma_{yy} \approx \sigma_{xx} - \sigma_{zz} = 170$ ppm, $\alpha = 20°$. $^{13}C'$: $\sigma_{xx} = 249.4$ ppm, $\sigma_{zz} = 87.9$ ppm, $\alpha = 37°$. $\sigma_{yy} = 191.1$ ppm is obtained from the average chemical shift of ubiquitin (BMRB 17769) (Cornilescu et al., 1998), following the suggested calibration (Cisnetti et al., 2004). The main axis z of the diffusion anisotropy tensor is assumed to lie in the peptide plane. Its orientation is encoded by $\beta_{C^\alpha C'}$.

Eq. (10). While local motions could be modeled in more detail to better match the shape of the TCF using, for example, an extended MF approach (Clore et al., 1990), correlation time distributions (Hsu et al., 2018) or dynamic detectors (Smith et al., 2017, 2019), we only intend to divide $J(0)$, i.e., the TCF's enclosed area, into contributions with and without orientational biases in an intuitive and simple manner. Attributed solely to the A_k, Eq. (7), we now consider the effect of these biases from an experimental perspective.

3 Methods

We will assume the canonical peptide plane geometry of Corey et al. (1953) as depicted in Fig. 2, including approximate principal components of the CSA tensors for ^{15}N and $^{13}C'$ adapted from Geoffrey Bodenhausen and coworkers (Cisnetti et al., 2004; Loth et al., 2005).

As demonstrated by Kadeřávek et al. (2014), the spectral densities of IDPs are best mapped by combining the transversal (Γ_{xy}) and the longitudinal (Γ_z) CCR rates between the ^{15}N CSA and the NH^N dipole. Employing the expressions of Bodenhausen and coworkers (Cisnetti et al., 2004), we have

$$\Gamma_{xy}^{N/NH} = k_{N/NH}\Delta_N\left[4J_{NH,xx}(0) + 3J_{NH,xx}(\omega_N)\right], \quad (12)$$

$$\Gamma_z^{N/NH} = k_{N/NH}\Delta_N\left[6J_{NH,xx}(\omega_N)\right] \quad (13)$$

$$k_{N/NH} = \frac{2}{5}\frac{1}{24\pi}\frac{\mu_0\hbar\gamma_n\gamma_h}{r_{NH}^3}B_0\gamma_n,$$

where μ_0 is the vacuum permeability, $\hbar$ is the reduced Planck constant, γ is the gyromagnetic ratio, r is the distance between the nuclei, B_0 is the magnetic field strength and $\Delta_N = (\sigma_{xx} - \sigma_{yy}) = (\sigma_{xx} - \sigma_{zz})$ is the size difference of the ^{15}N CSA principal components (in ppm). Mapping $J_{NH,xx}(0)$ amounts to the simple subtraction $\Gamma_{xy}^{N/NH} - 0.5\Gamma_z^{N/NH}$.

To complement these rates, we consider their counterparts for the $^{13}C'$ CSA and the $C'C^\alpha$ dipole:

$$\begin{aligned}\Gamma_{xy}^{C'/C'C^\alpha} &= k_{C'/C'C^\alpha}\big[(\sigma_{xx} - \sigma_{zz}) \\ &\quad\cdot\left(4J_{C'C^\alpha,xx}(0) + J_{C'C^\alpha,xx}(\omega_C)\right) \\ &\quad + (\sigma_{yy} - \sigma_{zz}) \\ &\quad\cdot\left(4J_{C'C^\alpha,yy}(0) + 3J_{C'C^\alpha,yy}(\omega_C)\right)\big], \end{aligned} \quad (14)$$

$$\begin{aligned}\Gamma_z^{C'/C'C^\alpha} &= k_{C'/C'C^\alpha}\big[(\sigma_{yy} - \sigma_{zz})6J_{C'C^\alpha,xx}(\omega_C) \\ &\quad + (\sigma_{yy} - \sigma_{zz})6J_{C'C^\alpha,yy}(\omega_C)\big], \end{aligned} \quad (15)$$

$$k_{C'/C'C^\alpha} = \frac{2}{5}\frac{1}{24\pi}\frac{\mu_0\hbar\gamma_c^2}{r_{C'C^\alpha}^3}B_0\gamma_c$$

with xx, yy and zz referring to the principal components of the fully anisotropic $^{13}C'$ CSA tensor. Again, high frequency contributions can be eliminated via the linear combination $\Gamma_{xy}^{C'/C'C^\alpha} - 0.5\Gamma_z^{C'/C'C^\alpha}$.

While the measurement of transverse CCR is well established, longitudinal CCR has been studied considerably less. In part this is due to subtleties of the involved relaxation pathways which involve multi-exponential auto- and cross-correlated relaxation effects. Another reason lies in technical limitations as longitudinal relaxation rates are generally smaller due to their Larmor frequency dependence. Notably, this effect is far less pronounced for the smaller correlation times present in IDPs (cf. Fig. 1). While $^{15}N^1H^N$ relaxation is well understood and several sensitive NMR techniques have been proposed to measure $\Gamma_{xy}^{N/NH}$ and $\Gamma_z^{N/NH}$ (Tjandra et al., 1996; Kroenke et al., 1998; Pelupessy et al., 2003, 2007; Kadeřávek et al., 2015), $^{13}C'$ relaxation is generally more problematic (Dayie and Wagner, 1997; Wang et al., 2006). Since we could not find any previous attempts to measure the longitudinal CCR rate $\Gamma_z^{C'/C'C^\alpha}$ in the literature, we see fit to assess its general feasibility.

Aside from the symmetrical reconversion principle of Bodenhausen and coworkers (Pelupessy et al., 2003, 2007), $^{13}C'/^{13}C'^{13}C^\alpha$ CSA-DD CCR can be measured either by monitoring the relaxation asymmetry of the $^{13}C'^{13}C^\alpha$ doublet or by means of a "quantitative gamma" experiment in which the sum and difference of the $^{13}C'$ doublet relax-

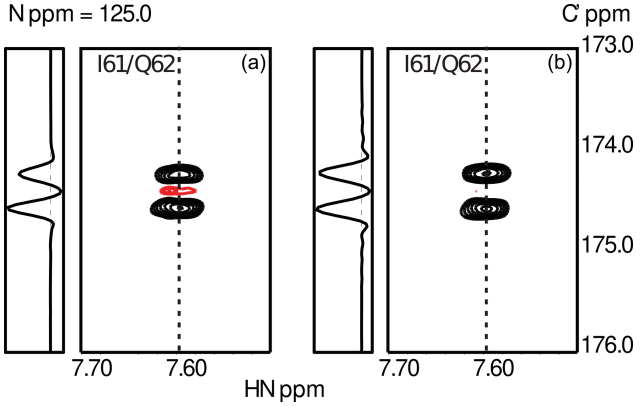

Figure 3. Experimental results from the measurements of transverse **(a)** and longitudinal **(b)** $^{13}C'/^{13}C'^{13}C^{\alpha}$ CSA-DD CCR as described in Sect. 3. Data were obtained using ubiquitin, a small globular protein of 76 residues. The figure shows the spectral region for the peptide plane spanning residues I61/Q62. The asymmetry of the $^{13}C^{\alpha}$ doublet is visible in the cross-sections taken at the positions indicated by dashed lines. As expected, CCR effects are more pronounced in the case of transverse relaxation.

ation are measured independently. In contrast to previous approaches relying on two separate experiments ("reference" and "cross") (Schwalbe et al., 2002), we determine $\Gamma_z^{C'/C'C^{\alpha}}$ by quantifying the different longitudinal relaxation in the $^{13}C'^{13}C^{\alpha}$ doublet recorded in a non-constant-time $^{13}C'$ evolution following the relaxation period. Transverse relaxation $\Gamma_{xy}^{C'/C'C^{\alpha}}$ is measured by more conventional quantification of differential line broadening of the $^{13}C'^{13}C^{\alpha}$ doublet recorded in constant-time mode.

To obtain sufficient spectral resolution, the CCR rates are measured directly from the intensity difference in a $^{13}C^{\alpha}$-coupled 3D HNCO experiment: (i) in the case of transversal CCR by quantification of differential line broadening of the $^{13}C'^{13}C^{\alpha}$ doublet during constant-time $^{13}C'$ evolution and (ii) for longitudinal CCR during real-time $^{13}C^{\alpha}$-coupled $^{13}C'$ evolution preceded by a longitudinal relaxation delay T during which $^{13}C'/^{13}C'^{13}C^{\alpha}$ CSA-DD CCR is active. This approach yields reliable longitudinal CCR rates as long as the mixing time T is short compared to $^{13}C'$ T_1 relaxation. Typical data obtained for the small globular protein ubiquitin are shown in Fig. 3

To suppress $^{13}C'^{13}C^{\alpha}$ cross-relaxation, a $^{13}C'$ is inverted in the middle of the relaxation delay T. Additional unwanted CCR pathways involving the $^{13}C'$ CSA and $^{13}C'^{1}H/^{13}C'^{15}N$ dipoles are suppressed by ^{1}H decoupling and ^{15}N inversion. As the ^{2}J couplings to remote carbons ($^{13}C'^{13}C^{\beta}$ and $^{13}C'_i{}^{13}C^{\alpha}_{i+1}$) are not resolved, CCR effects can be expected to average out for short and intermediate mixing times. While up to 20 % in size of the $^{13}C'^{13}C^{\alpha}$ CCR, the $\pm^{13}C'^{13}C^{\beta}$ CCR components contribute to the same line. The CCR rates are obtained from the $^{13}C'^{13}C^{\alpha}$ doublet as $\log(\frac{I_a}{I_b})/2T$. Details of the pulse sequence and NMR parameters will be given elsewhere. Two exemplary $^{13}C'^{13}C^{\alpha}$ doublets measured for I61/Q62 in human ubiquitin are shown in Fig. 3.

With the general feasibility of the measurements demonstrated, we can now define a ratio Q analogous to Sect. 2, Eq. (9):

$$Q \equiv \frac{\Gamma_{xy}^{C'/C'C^{\alpha}} - 0.5\Gamma_z^{C'/C'C^{\alpha}}}{\Gamma_{xy}^{N/NH} - 0.5\Gamma_z^{N/NH}} = \frac{4k_{C'/C'C^{\alpha}}\left[(\sigma_{xx}-\sigma_{zz})J_{C'C^{\alpha},xx}(0)+(\sigma_{yy}-\sigma_{zz})J_{C'C^{\alpha},yy}(0)\right]}{4k_{N/NH}\Delta_N J_{NH,xx}(0)}. \quad (16)$$

To assess the sensitivity of Q (Eq. 16), it is evaluated according to Eqs. (7), (8), (11), (12)–(15) with $\tau_3^{-1} = \tau_{int}^{-1} + 4D_{\perp} + 2D_{\parallel} = \tau_{int}^{-1} + \tau_{eff}^{-1}$ under the following conditions: as specified in Fig. 2, all CSA tensors have fixed orientation and size. Following Mantsyzov et al. (2014), the main axis, z, of the axially symmetric diffusion tensor is assumed to lie in the peptide plane; hence, Q is a function of the polar angles θ only; see Eq. (7). Defining the $C^{\alpha}C'$ orientation as 0° reference, the main axis is rotated from 0 to 180° towards the NH^N vector assuming anisotropy values $\frac{D_{\parallel}}{D_{\perp}}$ of 1.5 and 2.5, effective tumbling times $\tau_{eff} = (4D_{\perp} + 2D_{\parallel})^{-1}$ of 1 and 2.5 ns, internal correlation times τ_{int} of 100 and 500 ps and order parameters S^2 between 0 an 1. The magnetic field strength B_0 is the same for all rates and thus cancels out. The results are summarized in Fig. 4.

4 Results and discussion

Experimental considerations necessarily result in compromises. The fully anisotropic $^{13}C'$ CSA not only leads to spectral density contributions of two perpendicular components, it is also subject to considerable variations (Markwick et al., 2005; Cisnetti et al., 2004; Loth et al., 2005). One might be tempted to avoid the uncertainties and complications that come with the $^{13}C'$ CSA by considering dipolar relaxation only. However, compared to the NH^N spin pair, the small gyromagnetic ratios and long internuclear distances of other dipoles lead to far smaller and less sensitive rates (Carlomagno et al., 2000). In addition, the $J(0)$ components are generally neither dominant nor easily separated. The $^{13}C'$ CSA both provides effective means of relaxation and allows for a straightforward extraction of $J(0)$ components. With an approximate ratio $(\sigma_{xx}-\sigma_{zz})/(\sigma_{yy}-\sigma_{zz}) \approx 1.5$ and the beneficial orientation of the $C'C^{\alpha}$ vector, the $J_{C'C^{\alpha},xx}(\omega)$ contribution is generally far more pronounced: for $30° \leq \alpha \leq 44°$, the TCF amplitudes would be $0.48 \leq P_2(C'C^{\alpha} \cdot xx) \leq 0.79$ and $0.02 \geq P_2(C'C^{\alpha} \cdot yy) \geq -0.29$ based on the geometry of Fig. 2.

Figure 4 shows the ratio Q (Eq. 16) for different choices of τ_{eff}, τ_{int}, S^2 and $\frac{D_{\parallel}}{D_{\perp}}$ as a function of the diffusion tensor orientation. The main axis is assumed to lie in the peptide plane with the orientation denoted relative to $C'C^{\alpha}$ in terms

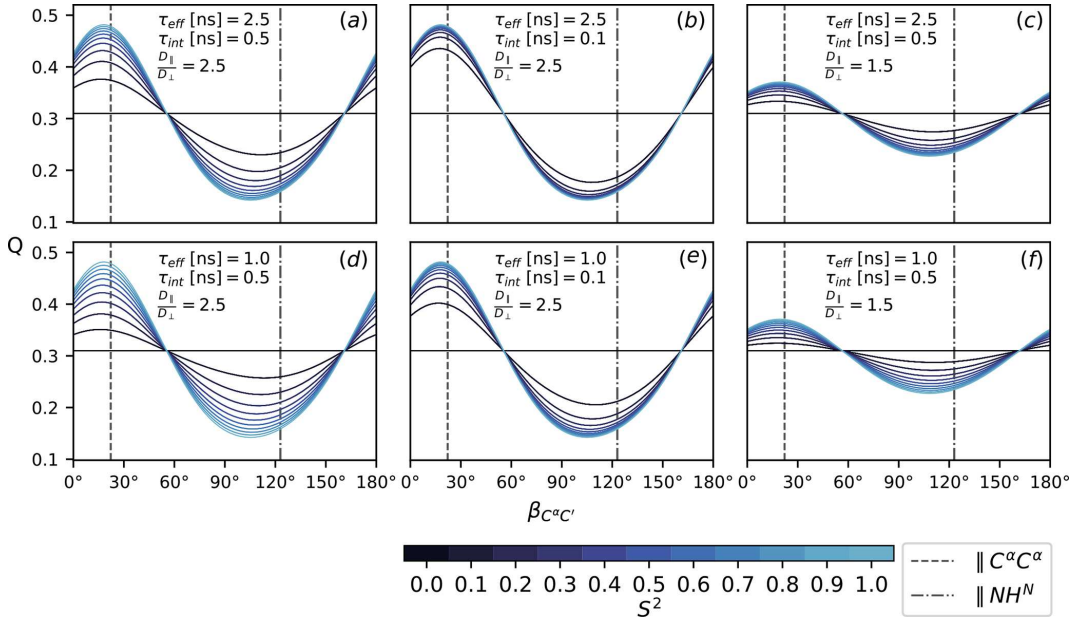

Figure 4. The ratio Q, Eq. (16), as a function of the diffusion tensor orientation denoted by $\beta_{C^\alpha C'}$, Fig. 2. Dashed lines indicate the orientation of the NH^N and the $C^\alpha C^\alpha$ vector. All rates are calculated according to Eqs. (7), (8), (11), (12)–(15) with $\tau_3^{-1} = \tau_{int}^{-1} + \tau_{eff}^{-1}$. Order parameters from 0 and 1 are color-coded. Panels **(a–f)** show Q for different choices of τ_{eff}, τ_{int} and $\frac{D_\parallel}{D_\perp}$. The magnetic field strength, B_0, is the same for all rates.

of the angle $\beta_{C'C^\alpha}$; see Fig. 2. Comparing all panels (a)–(f) at once, it can be seen that the isotropic ($S^2 = 0$) baseline at around 0.3 is independent of the specific correlation times τ_{eff} and τ_{int}; see Eq. (10). The same value is obtained for $\frac{D_\parallel}{D_\perp} = 1$, which is easily assessed from the convergence behavior for different anisotropy values in (c) and (f) and (a), (b), (d) and (e). How strongly Q reports on the asserted presence of diffusion anisotropy depends on the S^2-mediated weight difference between the orientation-dependent $A_k\tau_k$ (7) and the isotropic τ_{eff}. Both higher overall tumbling τ_{eff} and smaller isotropic motions τ_{int} yield a more sensitive Q for increasingly smaller order parameters S^2; see panels (a), (b), (d) and (e). Of course, this interpolation is only approximate and can become more intricate if the local motions are considered in more detail. In this simplified case, the particular choice of τ_{int} and S^2 is to some extent arbitrary as $A_k\tau_k$, τ_{int} and S^2 merely weight the isotropic and anisotropic contributions to the TCF's enclosed area $J(0)$. Still, the range $\tau_{eff} \geq 1\,\text{ns} > \tau_{int}$ was chosen based on timescales recently reported for MD simulations of IDPs (Kämpf et al., 2018).

Besides the obvious influence of $\frac{D_\parallel}{D_\perp}$ itself, Q strongly depends on the orientation of the diffusion tensor. The orientations of the NH^N and the $C^\alpha C^\alpha$ vectors are highlighted in all panels (a)–(f). In an extended chain, $C^\alpha C^\alpha$ is approximately parallel to the main axis, while NH^N stands perpendicular to it or vice versa for an α-helix. Both orientations correspond well to the minimum and maximum of Q. The range of Q depends on the size of the anisotropy $\frac{D_\parallel}{D_\perp}$. For a value of 2.5, as was previously asserted for α-synuclein (Mantsyzov et al., 2014, 2015), the effect on Q can be quite substantial (panels a, b, d, e). For $\frac{D_\parallel}{D_\perp} = 1.5$, it is far less pronounced (panels c and f).

We conclude that, if the concept of anisotropic tumbling of segmental α-helices and extended chains is reasonably applicable and sufficiently pronounced, Q would allow us to detect its signature. Actual quantification of $\frac{D_\parallel}{D_\perp}$ is of course obstructed by the limited validity of the asserted dynamic model. While the presence of relaxation-active tumbling motions does imply a certain degree of local rigidity, the structural heterogeneity of IDPs certainly challenges many of the simplifying assumptions made. Still, the ratio Q might give an indication of how relevant these concepts are for different protein systems, e.g., a partially folded region (Salvi et al., 2017; Marcellini et al., 2020) or a highly disordered segment (Mantsyzov et al., 2014). While particularly sensitive to large correlation times, Q will report on all sources of anisotropy present in $J(0)$. Differences in local mobility, CSA tensor variations, overall structural flexibility and experimental uncertainties will certainly shift and blur the ratio expected for isotropic motions. Still, if we assume a set of consecutive residues to experience shared anisotropic diffusion, the sizes of $J(0)$ should reflect the presence of slower tumbling motions, and Q should exhibit a systematic and sequence-persistent pattern. If Q adheres closely to the isotropic expectation (Eq. 10), it would appear that peptide plane dynamics in IDPs are isotropic and well probed by conven-

tional ^{15}N relaxation alone. If Q and the sizes of $J(0)$ imply systematic and correlated deviations from the isotropic case (Eq. 10), it would hint towards different inherent mobilities in the peptide plane such as the 3D GAF-type (Bremi and Brüschweiler, 1997) dynamics predicted by Salvi et al. (2017). Indeed, the sensitivity of Q along the $C^{\alpha}C^{\alpha}$ direction illustrates the potential of $C'/C'C^{\alpha}$ CCR in investigating this type of motion.

Thus, while introduced and assessed in terms of diffusion anisotropy, we expect the combination of transversal and longitudinal $C'/C^{\alpha}C'$ CCR rates to prove informative even outside this limited scope. For the locally dominated dynamics of IDPs in particular, differences and similarities to the NH^N spectral density can provide valuable structural insights even without invoking specific dynamic models. As the previously highlighted studies demonstrate, MD simulations can be expected to play a key role in rationalizing possible sources of anisotropy for different protein systems ranging from "fully disordered" (Mantsyzov et al., 2014) to partially structured (Salvi et al., 2017; Marcellini et al., 2020). In addition, the spectral densities can also be evaluated directly. While the proposed experiments do not allow us to map $J_{C'C^{\alpha},xx}$ and $J_{C'C^{\alpha},yy}$ individually, the contributions of different Larmor frequencies are fully separated. Graphical representations in particular can provide model-independent intuition about the timescales at play (Idiyatullin et al., 2001; Křížová et al., 2004; Kadeřávek et al., 2014). Expressions such as $J(0) - J(\omega)$ (Idiyatullin et al., 2001), intended to suppress the contribution of faster timescales (cf. Fig. 1), are available as well. More extensive analysis could be realized using general frameworks such as correlation time distributions (Khan et al., 2015; Hsu et al., 2018) or dynamic detectors (Smith et al., 2017, 2019).

5 Conclusions

On the occasion of Geoffrey Bodenhausen's 70th anniversary, we built on his extensive body of work to conceptualize experimental means for the investigation of anisotropic segmental dynamics in IDPs. Spectral density mapping protocols based on transversal and longitudinal CCR of NH^N were translated to the $C^{\alpha}C'$ spin pair of the same peptide plane. By isolating and comparing the zero frequency contributions, we derived an intuitive experimental measure for the presence of anisotropic dynamics in IDPs. Building on the simplified image of a symmetric top, we show that pronounced anisotropic tumbling of extended chain and α-helical segments should be readily detectable. But even outside the context of this simplistic model, contributions of different frequencies can be separated and assessed similarly to spectral density mapping protocols. Interestingly, the required measurement of longitudinal $C'/C^{\alpha}C'$ CCR has not been investigated before. Hence, a simple proof of concept for a possible measurement scheme was provided. To further substantiate and explore the presented concepts in an experimental setting, a systematic evaluation of different pulse sequences is currently under preparation in our lab.

While detecting and quantifying the presence of anisotropy in IDP dynamics might seem like a humble academic endeavor, we believe it to be an important step not only towards a better understanding of this important protein family but also towards immediate applications in biological and biomedical research as well as drug design. We thus take particular delight from the fact that Geoffrey Bodenhausen's *l'art pour l'art* pulse sequence design is also a telling testimony for the unforeseeable impact of non-utilitarian basic research driven by and inspired by scholarly thinking.

Appendix A

Following Ghose et al. (1998, Eq. 3, p. 488), the spectral density of an anisotropically tumbling dynamic molecule can be approximated as

$$J_{\boldsymbol{u},\boldsymbol{v}}(\omega) = \sum_{k=0}^{2} \left[\frac{S_k^2 \tau_k}{1+(\omega\tau_k)^2} + \frac{(A_k(\boldsymbol{u},\boldsymbol{v}) - S_k^2)\tau_3}{1+(\omega\tau_3)^2} \right]. \tag{A1}$$

Following the notation of Vögeli and Yao (2009), the order parameter is defined as

$$S_k^2 \equiv \langle A_k(\boldsymbol{u},\boldsymbol{v}) \rangle, \tag{A2}$$

i.e., as the value A_k decays to fast local motions. As noted by Vögeli and Yao (2009), Eq. (A1) can be written in the form of an auto-correlated TCF by setting A_k as a prefactor:

$$J_{\boldsymbol{u},\boldsymbol{v}}(\omega) = \sum_{k=0}^{2} A_k(\boldsymbol{u},\boldsymbol{v}) \left[\frac{S'^2_k \tau_k}{1+(\omega\tau_k)^2} + \frac{(1-S'^2_k)\tau_3}{1+(\omega\tau_3)^2} \right]. \tag{A3}$$

The order parameters are then defined as ratios:

$$S'^2_k \equiv \frac{\langle A_k(\boldsymbol{u},\boldsymbol{v}) \rangle}{A_k(\boldsymbol{u},\boldsymbol{v})}. \tag{A4}$$

While these generalized order parameters do not adhere to the definitions of Lipari and Szabo (Lipari and Szabo, 1982), they still equate to 1 in the case of a fully rigid molecule. It can be seen from Eq. (A3) that the inclusion of local motions requires one order parameter for each A_k in order to balance the isotropic and anisotropic contributions. The simplified spectral density proposed in the main text, Eq. (11), corresponds to the approximation that all A_k decay about the same relative amount (as in the edge case of isotropic tumbling). Without the index k for the order parameter, $S^2 = S'^2_0 = S'^2_1 = S'^2_2$, Eq. (A3) simplifies to Eq. (11):

$$\begin{aligned} J_{\boldsymbol{u},\boldsymbol{v}}(\omega) &= \sum_{k=0}^{2} A_k(\boldsymbol{u},\boldsymbol{v}) \left[\frac{S^2 \tau_k}{1+(\omega\tau_k)^2} + \frac{(1-S^2)\tau_3}{1+(\omega\tau_3)^2} \right] \\ &= S^2 \sum_{k=0}^{2} A_k(\boldsymbol{u},\boldsymbol{v}) \frac{\tau_k}{1+(\omega\tau_k)^2} \\ &\quad + (1-S^2) P_2(\boldsymbol{u}\cdot\boldsymbol{v}) \frac{\tau_3}{1+(\omega\tau_3)^2}. \end{aligned} \tag{A5}$$

Equation (A5) is similar to the approximation proposed by Ghose et al. (1998, Eq. 7, p. 488) but includes the prefactor $P_2(\boldsymbol{u}\cdot\boldsymbol{v})$ for the internal TCF, preserving the isotropic limit ($\frac{D_\parallel}{D_\perp} = 1$, $\tau_{\mathrm{iso}} = \tau_0 = \tau_1 = \tau_2$) as

$$J_{\boldsymbol{u},\boldsymbol{v}}(\omega) = P_2(\boldsymbol{u}\cdot\boldsymbol{v}) \left[\frac{S^2 \tau_{\mathrm{iso}}}{1+(\omega\tau_{\mathrm{iso}})^2} + \frac{(1-S^2)\tau_3}{1+(\omega\tau_3)^2} \right]. \tag{A6}$$

In this case, S^2 again corresponds to the familiar auto-correlated order parameter of Lipari and Szabo (1982), the auto- and cross-correlated TCF are related by the simple factor $P_2(\boldsymbol{u}\cdot\boldsymbol{v})$. For sufficiently small angles between $\boldsymbol{u}$ and $\boldsymbol{v}$, this relation can be extended to approximate anisotropic tumbling in accordance with the MF rationale of Lipari and Szabo (Tjandra et al., 1996; Kroenke et al., 1998). As noted by Halle (2009) in his foundational study on the MF formalism, this approach can also be contextualized within the MF framework of Halle and Wennerström (1981).

Code availability. The Python code used for simulations and plotting (Figs. 1 and 4) is provided as a Jupyter Notebook in the Supplement.

Data availability. The preliminary NMR data shown for ubiquitin (Fig. 3) are available from the authors upon request.

Supplement. The supplement related to this article is available online at: https://doi.org/10.5194/mr-2-557-2021-supplement.

Author contributions. RK, CK and IC devised the project. CK compiled the theoretical considerations. IC and CK performed the numerical simulations. GK and RK assessed the experimental feasibility. GK designed the pulse sequence. IC and CK illustrated the results. CK wrote the article with contributions from all authors.

Competing interests. The authors declare that they have no conflict of interest.

Disclaimer. Publisher's note: Copernicus Publications remains neutral with regard to jurisdictional claims in published maps and institutional affiliations.

Special issue statement. This article is part of the special issue "Geoffrey Bodenhausen Festschrift". It is not associated with a conference.

Acknowledgements. The authors acknowledge the support from the Austrian Science Fund (FWF).

Financial support. This research has been supported by the Austrian Science Fund (FWF; grant nos. P28359 and P28937).

Review statement. This paper was edited by Daniel Abergel and reviewed by two anonymous referees.

References

Abergel, D. and Bodenhausen, G.: A simple model for NMR relaxation in the presence of internal motions with dynamical coupling, J. Chem. Phys., 121, 761–768, https://doi.org/10.1063/1.1756867, 2004.

Abergel, D. and Bodenhausen, G.: Predicting internal protein dynamics from structures using coupled networks of hindered rotators, J. Chem. Phys., 123, https://doi.org/10.1063/1.2110028, 2005.

Barnes, C. A., Shen, Y., Ying, J., Takagi, Y., Torchia, D. A., Sellers, J. R., and Bax, A.: Remarkable Rigidity of the Single α-Helical Domain of Myosin-VI As Revealed by NMR Spectroscopy, J. Am. Chem. Soc., 141, 9004–9017, https://doi.org/10.1021/jacs.9b03116, 2019.

Bremi, T. and Brüschweiler, R.: Locally Anisotropic Internal Polypeptide Backbone Dynamics by NMR Relaxation, J. Am. Chem. Soc., 119, 6672–6673, https://doi.org/10.1021/ja9708676, 1997.

Bussell, R. and Eliezer, D.: Residual Structure and Dynamics in Parkinson's Disease-associated Mutants of α-Synuclein*, J. Biol. Chem., 276, 45996–46003, https://doi.org/10.1074/jbc.M106777200, 2001.

Carlomagno, T., Maurer, M., Hennig, M., and Griesinger, C.: Ubiquitin Backbone Motion Studied via NHN$-$C$'$C$^{\alpha}$ Dipolar-Dipolar and C$'-$C$'$C$^{\alpha}$/NHN CSA-Dipolar Cross-Correlated Relaxation, J. Am. Chem. Soc., 122, 5105–5113, https://doi.org/10.1021/ja993845n, 2000.

Chang, S.-L. and Tjandra, N.: Temperature dependence of protein backbone motion from carbonyl ^{13}C and amide ^{15}N NMR relaxation, J. Magn. Reson., 174, 43–53, https://doi.org/10.1016/j.jmr.2005.01.008, 2005.

Cisnetti, F., Loth, K., Pelupessy, P., and Bodenhausen, G.: Determination of Chemical Shift Anisotropy Tensors of Carbonyl Nuclei in Proteins through Cross-Correlated Relaxation in NMR, ChemPhysChem, 5, 807–814, https://doi.org/10.1002/cphc.200301041, 2004.

Clore, G. M. and Iwahara, J.: Theory, Practice, and Applications of Paramagnetic Relaxation Enhancement for the Characterization of Transient Low-Population States of Biological Macromolecules and Their Complexes, Chem. Rev., 109, 4108–4139, https://doi.org/10.1021/cr900033p, 2009.

Clore, G. M., Szabo, A., Bax, A., Kay, L. E., Driscoll, P. C., and Gronenborn, A. M.: Deviations from the simple two-parameter model-free approach to the interpretation of nitrogen-15 nuclear magnetic relaxation of proteins, J. Am. Chem. Soc., 112, 4989–4991, https://doi.org/10.1021/ja00168a070, 1990.

Corey, R. B., Pauling, L. C., and Astbury, W. T.: Fundamental dimensions of polypeptide chains, P. Roy. Soc. Lond. B Bio., 141, 10–20, https://doi.org/10.1098/rspb.1953.0011, 1953.

Cornilescu, G., Marquardt, J. L., Ottiger, M., and Bax, A.: Validation of Protein Structure from Anisotropic Carbonyl Chemical Shifts in a Dilute Liquid Crystalline Phase, J. Am. Chem. Soc., 120, 6836–6837, https://doi.org/10.1021/ja9812610, 1998.

Daragan, V. A. and Mayo, K. H.: Using the Model Free Approach to Analyze NMR Relaxation Data in Cases of Anisotropic Molecular Diffusion, J. Phys. Chem. B, 103, 6829–6834, https://doi.org/10.1021/jp9911393, 1999.

Dayie, K. T. and Wagner, G.: Carbonyl Carbon Probe of Local Mobility in ^{13}C,^{15}N-Enriched Proteins Using High-Resolution Nuclear Magnetic Resonance, J. Am. Chem. Soc., 119, 7797–7806, https://doi.org/10.1021/ja9633880, 1997.

Deschamps, M.: Cross-Correlated Relaxation with Anisotropic Reorientation and Small Amplitude Local Motions, J. Phys. Chem. A, 106, 2438–2445, https://doi.org/10.1021/jp013407e, 2002.

Deschamps, M. and Bodenhausen, G.: Anisotropy of Rotational Diffusion, Dipole–Dipole Cross-Correlated NMR Relaxation and Angles between Bond Vectors in Proteins, ChemPhysChem, 2, 539–543, https://doi.org/10.1002/1439-7641(20010917)2:8/9<539::AID-CPHC539>3.0.CO;2-M, 2001.

Eastman, P., Swails, J., Chodera, J. D., McGibbon, R. T., Zhao, Y., Beauchamp, K. A., Wang, L.-P., Simmonett, A. C., Harrigan, M. P., Stern, C. D., Wiewiora, R. P., Brooks, B. R., and Pande, V. S.: OpenMM 7: Rapid development of high performance algorithms for molecular dynamics, PLOS Comput. Biol., 13, 1–17, https://doi.org/10.1371/journal.pcbi.1005659, 2017.

Ferrage, F., Pelupessy, P., Cowburn, D., and Bodenhausen, G.: Protein Backbone Dynamics through $^{13}C'-^{13}C^{\alpha}$ Cross-Relaxation in NMR Spectroscopy, J. Am. Chem. Soc., 128, 11072–11078, https://doi.org/10.1021/ja0600577, 2006.

Ghose, R., Huang, K., and Prestegard, J. H.: Measurement of Cross Correlation between Dipolar Coupling and Chemical Shift Anisotropy in the Spin Relaxation of ^{13}C, ^{15}N-Labeled Proteins, J. Magn. Reson., 135, 487–499, https://doi.org/10.1006/jmre.1998.1602, 1998.

Gopal, S. M., Wingbermühle, S., Schnatwinkel, J., Juber, S., Herrmann, C., and Schäfer, L. V.: Conformational Preferences of an Intrinsically Disordered Protein Domain: A Case Study for Modern Force Fields, J. Phys. Chem. B, 125, 24–35, https://doi.org/10.1021/acs.jpcb.0c08702, 2021.

Grudziąż, K., Zawadzka-Kazimierczuk, A., and Koźmiński, W.: High-dimensional NMR methods for intrinsically disordered proteins studies, nMR Methods of Characterizing Biomolecular Structural Dynamics and Conformational Ensembles, Methods, 148, 81–87, https://doi.org/10.1016/j.ymeth.2018.04.031, 2018.

Halle, B.: The physical basis of model-free analysis of NMR relaxation data from proteins and complex fluids, J. Chem. Phys., 131, 1–224507, https://doi.org/10.1063/1.3269991, 2009.

Halle, B. and Wennerström, H.: Interpretation of magnetic resonance data from water nuclei in heterogeneous systems, J. Chem. Phys., 75, 1928–1943, https://doi.org/10.1063/1.442218, 1981.

Hsu, A., Ferrage, F., and Palmer, A. G.: Analysis of NMR Spin-Relaxation Data Using an Inverse Gaussian Distribution Function, Biophys. J., 115, 2301–2309, https://doi.org/10.1016/j.bpj.2018.10.030, 2018.

Idiyatullin, D., Daragan, V. A., and Mayo, K. H.: A New Approach to Visualizing Spectral Density Functions and Deriving Motional Correlation Time Distributions: Applications to an α-Helix-Forming Peptide and to a Well-Folded Protein, J. Magn. Reson., 152, 132–148, https://doi.org/10.1006/jmre.2001.2372, 2001.

Iwahara, J., Schwieters, C. D., and Clore, G. M.: Ensemble Approach for NMR Structure Refinement against 1H Paramagnetic Relaxation Enhancement Data Arising from a Flexible Paramagnetic Group Attached to a Macromolecule, J. Am. Chem. Soc., 126, 5879–5896, https://doi.org/10.1021/ja031580d, 2004.

Kadeřávek, P., Zapletal, V., Rabatinová, A., Krásný, L., Sklenář, V., and Žídek, L.: Spectral density mapping protocols for analysis of molecular motions in disordered proteins, J. Biomol. NMR, 58, 193–207, https://doi.org/10.1007/s10858-014-9816-4, 2014.

Kadeřávek, P., Grutsch, S., Salvi, N., Tollinger, M., Žídek, L., Bodenhausen, G., and Ferrage, F.: Cross-correlated relaxation measurements under adiabatic sweeps: determination of local order in proteins, J. Biomol. NMR, 63, 353–365, https://doi.org/10.1007/s10858-015-9994-8, 2015.

Kämpf, K., Izmailov, S. A., Rabdano, S. O., Groves, A. T., Podkorytov, I. S., and Skrynnikov, N. R.: What Drives 15N Spin Relaxation in Disordered Proteins? Combined NMR/MD Study of the H4 Histone Tail, Biophys. J., 115, 2348–2367, https://doi.org/10.1016/j.bpj.2018.11.017, 2018.

Kauffmann, C., Zawadzka-Kazimierczuk, A., Kontaxis, G., and Konrat, R.: Using Cross-Correlated Spin Relaxation to Characterize Backbone Dihedral Angle Distributions of Flexible Protein Segments, ChemPhysChem, 22, 18–28, https://doi.org/10.1002/cphc.202000789, 2021.

Khan, S., Charlier, C., Augustyniak, R., Salvi, N., Déjean, V., Bodenhausen, G., Lequin, O., Pelupessy, P., and Ferrage, F.: Distribution of Pico- and Nanosecond Motions in Disordered Proteins from Nuclear Spin Relaxation, Biophys. J., 109, 988–999, https://doi.org/10.1016/j.bpj.2015.06.069, 2015.

Křížová, H., Žídek, L., Stone, M. J., Novotny, M. V., and Sklenář, V.: Temperature-dependent spectral density analysis applied to monitoring backbone dynamics of major urinary protein-I complexed with the pheromone 2-*sec*-butyl-4,5-dihydrothiazole*, J. Biomol. NMR, 28, 369–384, https://doi.org/10.1023/B:JNMR.0000015404.61574.65, 2004.

Kroenke, C. D., Loria, J. P., Lee, L. K., Rance, M., and Palmer, A. G.: Longitudinal and Transverse $^{1}H-^{15}N$ Dipolar/^{15}N Chemical Shift Anisotropy Relaxation Interference: Unambiguous Determination of Rotational Diffusion Tensors and Chemical Exchange Effects in Biological Macromolecules, J. Am. Chem. Soc., 120, 7905–7915, https://doi.org/10.1021/ja980832l, 1998.

Kümmerer, F., Orioli, S., Harding-Larsen, D., Hoffmann, F., Gavrilov, Y., Teilum, K., and Lindorff-Larsen, K.: Fitting side-chain NMR relaxation data using molecular simulations, bioRxiv, https://doi.org/10.1101/2020.08.18.256024, 2020.

Lienin, S. F., Bremi, T., Brutscher, B., Brüschweiler, R., and Ernst, R. R.: Anisotropic Intramolecular Backbone Dynamics of Ubiquitin Characterized by NMR Relaxation and MD Computer Simulation, J. Am. Chem. Soc., 120, 9870–9879, https://doi.org/10.1021/ja9810179, 1998.

Lipari, G. and Szabo, A.: Model-free approach to the interpretation of nuclear magnetic resonance relaxation in macromolecules. 1. Theory and range of validity, J. Am. Chem. Soc., 104, 4546–4559, https://doi.org/10.1021/ja00381a009, 1982.

Loth, K., Pelupessy, P., and Bodenhausen, G.: Chemical Shift Anisotropy Tensors of Carbonyl, Nitrogen, and Amide Proton Nuclei in Proteins through Cross-Correlated Relaxation in NMR Spectroscopy, J. Am. Chem. Soc., 127, 6062–6068, https://doi.org/10.1021/ja042863o, 2005.

Mantsyzov, A. B., Maltsev, A. S., Ying, J., Shen, Y., Hummer, G., and Bax, A.: A maximum entropy approach to the study of residue-specific backbone angle distributions in α-synuclein, an intrinsically disordered protein, Protein Sci., 23, 1275–1290, https://doi.org/10.1002/pro.2511, 2014.

Mantsyzov, A. B., Shen, Y., Lee, J. H., Hummer, G., and Bax, A.: MERA: a webserver for evaluating backbone torsion angle distributions in dynamic and disordered proteins from NMR data, J. Biomol. NMR, 63, 85–95, https://doi.org/10.1007/s10858-015-9971-2, 2015.

Marcellini, M., Nguyen, M.-H., Martin, M., Hologne, M., and Walker, O.: Accurate Prediction of Protein NMR Spin Relaxation by Means of Polarizable Force Fields. Application to Strongly Anisotropic Rotational Diffusion, J. Phys. Chem. B, 124, 5103–5112, https://doi.org/10.1021/acs.jpcb.0c01922, 2020.

Markwick, P. R. L., Sprangers, R., and Sattler, M.: Local Structure and Anisotropic Backbone Dynamics from Cross-Correlated

NMR Relaxation in Proteins, Angew. Chem. Int. Edit., 44, 3232–3237, https://doi.org/10.1002/anie.200462495, 2005.

Meirovitch, E., Shapiro, Y. E., Polimeno, A., and Freed, J. H.: Protein Dynamics from NMR: The Slowly Relaxing Local Structure Analysis Compared with Model-Free Analysis, J. Phys. Chem. A, 110, 8366–8396, https://doi.org/10.1021/jp056975t, 2006.

Modig, K. and Poulsen, F. M.: Model-independent interpretation of NMR relaxation data for unfolded proteins: the acid-denatured state of ACBP, J. Biomol. NMR, 42, 163–177, https://doi.org/10.1007/s10858-008-9280-0, 2008.

Nodet, G., Abergel, D., and Bodenhausen, G.: Predicting NMR Relaxation Rates in Anisotropically Tumbling Proteins through Networks of Coupled Rotators, ChemPhysChem, 9, 625–633, https://doi.org/10.1002/cphc.200700732, 2008.

Ottiger, M. and Bax, A.: Determination of Relative N−HN, N−C′, $C^{\alpha}-C'$, and $C^{\alpha}-H^{\alpha}$ Effective Bond Lengths in a Protein by NMR in a Dilute Liquid Crystalline Phase, J. Am. Chem. Soc., 120, 12334–12341, https://doi.org/10.1021/ja9826791, 1998.

Pelupessy, P., Espallargas, G. M., and Bodenhausen, G.: Symmetrical reconversion: measuring cross-correlation rates with enhanced accuracy, J. Magn. Reson., 161, 258–264, https://doi.org/10.1016/S1090-7807(02)00190-8, 2003.

Pelupessy, P., Ferrage, F., and Bodenhausen, G.: Accurate Measurement of Longitudinal Cross-Relaxation Rates in Nuclear Magnetic Resonance, J. Chem. Phys., 126, 134 508, 1–10, https://doi.org/10.1063/1.2715583, 2007.

Piana, S., Donchev, A. G., Robustelli, P., and Shaw, D. E.: Water Dispersion Interactions Strongly Influence Simulated Structural Properties of Disordered Protein States, J. Phys. Chem. B, 119, 5113–5123, https://doi.org/10.1021/jp508971m, 2015.

Piana, S., Robustelli, P., Tan, D., Chen, S., and Shaw, D. E.: Development of a Force Field for the Simulation of Single-Chain Proteins and Protein–Protein Complexes, J. Chem. Theory Comput., 16, 2494–2507, https://doi.org/10.1021/acs.jctc.9b00251, 2020.

Rauscher, S., Gapsys, V., Gajda, M. J., Zweckstetter, M., de Groot, B. L., and Grubmüller, H.: Structural Ensembles of Intrinsically Disordered Proteins Depend Strongly on Force Field: A Comparison to Experiment, J. Chem. Theory Comput., 11, 5513–5524, https://doi.org/10.1021/acs.jctc.5b00736, 2015.

Richert, R. and Blumen, A. (Eds.): Disorder Effects on Relaxational Processes, Springer, Berlin Heidelberg, https://doi.org/10.1007/978-3-642-78576-4_1, 1994.

Robustelli, P., Piana, S., and Shaw, D. E.: Developing a molecular dynamics force field for both folded and disordered protein states, P. Natl. Acad. Sci. USA, 115, E4758–E4766, https://doi.org/10.1073/pnas.1800690115, 2018.

Salomon-Ferrer, R., Götz, A. W., Poole, D., Le Grand, S., and Walker, R. C.: Routine Microsecond Molecular Dynamics Simulations with AMBER on GPUs. 2. Explicit Solvent Particle Mesh Ewald, J. Chem. Theory Comput., 9, 3878–3888, https://doi.org/10.1021/ct400314y, 2013.

Salvi, N., Abyzov, A., and Blackledge, M.: Multi-Timescale Dynamics in Intrinsically Disordered Proteins from NMR Relaxation and Molecular Simulation, J. Phys. Chem. Lett., 7, 2483–2489, https://doi.org/10.1021/acs.jpclett.6b00885, 2016.

Salvi, N., Abyzov, A., and Blackledge, M.: Analytical Description of NMR Relaxation Highlights Correlated Dynamics in Intrinsically Disordered Proteins, Angew. Chem. Int. Edit., 56, 14020–14024, https://doi.org/10.1002/anie.201706740, 2017.

Schanda, P.: Relaxing with liquids and solids – A perspective on biomolecular dynamics, J. Magn. Reson., 306, 180–186, https://doi.org/10.1016/j.jmr.2019.07.025, 2019.

Schwalbe, H., Carlomagno, T., Hennig, M., Junker, J., Reif, B., Richter, C., and Griesinger, C.: [2] - Cross-Correlated Relaxation for Measurement of Angles between Tensorial Interactions, in: Nuclear Magnetic Resonance of Biological Macromolecules Part A, edited by: James, T. L., Dötsch, V., and Schmitz, U., Academic Press, London and San Diego, Methods in Enzymology, 338, 35–81, https://doi.org/10.1016/S0076-6879(02)38215-6, 2002.

Shea, J.-E., Best, R. B., and Mittal, J.: Physics-based computational and theoretical approaches to intrinsically disordered proteins, Curr. Opin. Struc. Biol., 67, 219–225, https://doi.org/10.1016/j.sbi.2020.12.012, 2021.

Smith, A. A., Ernst, M., and Meier, B. H.: Because the Light is Better Here: Correlation-Time Analysis by NMR Spectroscopy, Angew. Chem. Int. Edit., 56, 13590–13595, https://doi.org/10.1002/anie.201707316, 2017.

Smith, A. A., Ernst, M., Meier, B. H., and Ferrage, F.: Reducing bias in the analysis of solution-state NMR data with dynamics detectors, J. Chem. Phys., 151, 034102, https://doi.org/10.1063/1.5111081, 2019.

Stone, J. E., Phillips, J. C., Freddolino, P. L., Hardy, D. J., Trabuco, L. G., and Schulten, K.: Accelerating molecular modeling applications with graphics processors, J. Comput. Chem., 28, 2618–2640, https://doi.org/10.1002/jcc.20829, 2007.

Stone, J. E., Hardy, D. J., Ufimtsev, I. S., and Schulten, K.: GPU-accelerated molecular modeling coming of age, J. Mol. Graph. Model., 29, 116–125, https://doi.org/10.1016/j.jmgm.2010.06.010, 2010.

Tjandra, N., Szabo, A., and Bax, A.: Protein Backbone Dynamics and ^{15}N Chemical Shift Anisotropy from Quantitative Measurement of Relaxation Interference Effects, J. Am. Chem. Soc., 118, 6986–6991, https://doi.org/10.1021/ja960510m, 1996.

Tugarinov, V., Liang, Z., Shapiro, Y. E., Freed, J. H., and Meirovitch, E.: A Structural Mode-Coupling Approach to ^{15}N NMR Relaxation in Proteins, J. Am. Chem. Soc., 123, 3055–3063, https://doi.org/10.1021/ja003803v, 2001.

Vögeli, B.: Comprehensive description of NMR cross-correlated relaxation under anisotropic molecular tumbling and correlated local dynamics on all time scales, J. Chem. Phys., 133, 014 501, https://doi.org/10.1063/1.3454734, 2010.

Vögeli, B.: The nuclear Overhauser effect from a quantitative perspective, Prog. Nucl. Mag. Res. Sp., 78, 1–46, https://doi.org/10.1016/j.pnmrs.2013.11.001, 2014.

Vögeli, B. and Yao, L.: Correlated Dynamics between Protein HN and HC Bonds Observed by NMR Cross Relaxation, J. Am. Chem. Soc., 131, 3668–3678, https://doi.org/10.1021/ja808616v, 2009.

Vugmeyster, L., Pelupessy, P., Vugmeister, B. E., Abergel, D., and Bodenhausen, G.: Cross-correlated relaxation in NMR of macromolecules in the presence of fast and slow internal dynamics, highly polarized nuclear spin systems and dipolar interactions in NMR, C. R. Phys., 5, 377–386, https://doi.org/10.1016/j.crhy.2004.02.004, 2004.

Wang, T., Weaver, D. S., Cai, S., and Zuiderweg, E. R. P.: Quantifying Lipari–Szabo modelfree parameters from ^{13}CO

NMR relaxation experiments, J. Biomol. NMR, 36, 79–102, https://doi.org/10.1007/s10858-006-9047-4, 2006.

Woessner, D. E.: Spin Relaxation Processes in a Two-Proton System Undergoing Anisotropic Reorientation, J. Chem. Phys., 36, 1–4, https://doi.org/10.1063/1.1732274, 1962.

Xue, Y., Podkorytov, I. S., Rao, D. K., Benjamin, N., Sun, H., and Skrynnikov, N. R.: Paramagnetic relaxation enhancements in unfolded proteins: Theory and application to drkN SH3 domain, Protein Sci., 18, 1401–1424, https://doi.org/10.1002/pro.153, 2009.

Ying, J., Roche, J., and Bax, A.: Homonuclear decoupling for enhancing resolution and sensitivity in NOE and RDC measurements of peptides and proteins, a special "JMR Perspectives" issue: Foresights in Biomolecular Solution-State NMR Spectroscopy – From Spin Gymnastics to Structure and Dynamics, J. Magn. Reson., 241, 97–102, https://doi.org/10.1016/j.jmr.2013.11.006, 2014.

Zerbetto, M., Buck, M., Meirovitch, E., and Polimeno, A.: Integrated Computational Approach to the Analysis of NMR Relaxation in Proteins: Application to ps-ns Main Chain $^{15}N-^{1}H$ and Global Dynamics of the Rho GTPase Binding Domain of Plexin-B1, J. Phys. Chem. B, 115, 376–388, https://doi.org/10.1021/jp108633v, 2011.

Zerze, G. H., Zheng, W., Best, R. B., and Mittal, J.: Evolution of All-Atom Protein Force Fields to Improve Local and Global Properties, J. Phys. Chem. Lett., 10, 2227–2234, https://doi.org/10.1021/acs.jpclett.9b00850, 2019.

4

AN NMR METHOD TO MEASURE LOCAL CORRELATION TIMES IN THE PEPTIDE PLANE

I. Ceccolini, C. Kauffmann, J. Holzinger, R. Konrat, and A. Zawadzka Kazimierczuk, "A set of cross-correlated relaxation experiments to probe the correlation time of two different and complementary spin pairs," *Journal of Magnetic Resonance*, vol. 361, p. 107661, 2024 [72]

DOI: 10.1016/j.jmr.2024.107661

PERSONAL CONTRIBUTION

Conceptualization, methodology, investigation, formal analysis, validation, data curation, writing.

Journal of Magnetic Resonance 361 (2024) 107661

Contents lists available at ScienceDirect

Journal of Magnetic Resonance

journal homepage: www.elsevier.com/locate/jmr

A set of cross-correlated relaxation experiments to probe the correlation time of two different and complementary spin pairs

Irene Ceccolini [a], Clemens Kauffmann [b], Julian Holzinger [a], Robert Konrat [a,*], Anna Zawadzka-Kazimierczuk [c,*]

[a] Department of Structural and Computational Biology, Max Perutz Laboratories, University of Vienna, Vienna Biocenter Campus 5, 1030 Vienna, Austria
[b] Wiener Linien GmbH & Co KG, Erdbergstraße 202, 1030 Vienna, Austria
[c] University of Warsaw, Faculty of Chemistry, Biological and Chemical Research Centre, Żwirki i Wigury 101, 02-089 Warsaw, Poland

ARTICLE INFO

Keywords:
Cross correlated relaxation
Protein dynamics
Intrinsically disordered proteins
Correlation time

ABSTRACT

Intrinsically disordered proteins (IDPs) defy the conventional structure-function paradigm by lacking a well-defined tertiary structure and exhibiting inherent flexibility. This flexibility leads to distinctive spin relaxation modes, reflecting isolated and specific motions within individual peptide planes. In this work, we propose a new pulse sequence to measure the longitudinal $^{13}C'$ CSA-$^{13}C'$-$^{13}C^{\alpha}$ DD CCR rate $\Gamma_z^{C'/C'C^{\alpha}}$ and present a novel 3D version of the transverse $\Gamma_{xy}^{C'/C'C^{\alpha}}$ CCR rate, adopting the symmetrical reconversion approach. We combined these rates with the analogous $\Gamma_{xy}^{N/NH}$ and $\Gamma_z^{N/NH}$ CCR rates to derive residue-specific correlation times for both spin-pairs within the same peptide plane. The presented approach offers a straightforward and intuitive way to compare the correlation times of two different and complementary spin vectors, anticipated to be a valuable aid to determine IDPs backbone dihedral angles distributions. We performed the proposed experiments on two systems: a folded protein ubiquitin and *Coturnix japonica* osteopontin, a prototypical IDP. Comparative analyses of the results show that the correlation times of different residues vary more for IDPs than globular proteins, indicating that the dynamics of IDPs is largely heterogeneous and dominated by local fluctuations.

1. Introduction

Over the past 20 years, it has become apparent that conformational changes and internal local motions are essential for the functioning of biomolecules. This holds particularly true in the context of intrinsically disordered proteins (IDPs), a distinctive class of proteins. IDPs defy the traditional paradigm by lacking well-defined tertiary structures and often secondary elements under physiological conditions. Instead, they exist as an ensemble of rapidly inter-converting heterogeneous fully functional conformations [1–4]. Interestingly, IDPs are present in many cellular pathways playing a crucial role in regulation, recognition, signaling, and control of protein–protein interaction networks. Because of their nature, these proteins are related with many human diseases, such as cancer, amyloidosis, neurodegenerative diseases, cardiovascular disease, and diabetes [5,6].

Despite the substantial research efforts to understand the structural ensemble these biomolecules sample [7–9], the dynamics driving conformational transitions are yet not entirely understood [10–13]. The complex interplay between structure and dynamics in IDPs highlights the necessity to further explore this intricate relationship.

Solution state NMR is the most widely used technique to probe internal motions, conformational changes and interactions in IDPs with atomic resolution [3,14–17]. In particular, NMR spin relaxation provides not only qualitative but also quantitative information about the timescales and amplitudes of proteins molecular motions [18–23]. The dynamic information is obtained by looking at the Fourier transform (FT) of the time correlation function (TCF), namely the spectral density function (SDF). The motional modes timescales are encoded in the correlation time defined in very general terms as the integral of the normalized TCF [24,25]. To get mechanistic insight, relaxation rates are then generally rationalized in terms of motional models, such as model-free (MF [24]), extended MF approach [26], 3D GAF model [18,27], spectral density mapping protocols [28–30] or others [31–34].

NMR spin relaxation studies historically centered on folded proteins, where the ^{15}N-^{1}H vector takes center stage. This vector successfully captures the shared tumbling frame within the protein's 3D structure, involving multiple spin probes [24,35]. The correlated motions of individual ^{15}N-^{1}H spin vectors offer a comprehensive overview of collective dynamics, reflecting the overall tumbling due to Brownian motion.

* Corresponding authors.
E-mail addresses: robert.konrat@univie.ac.at (R. Konrat), anzaw@chem.uw.edu.pl (A. Zawadzka-Kazimierczuk).

https://doi.org/10.1016/j.jmr.2024.107661
Received 11 January 2024; Received in revised form 12 March 2024; Accepted 14 March 2024
Available online 18 March 2024

Accurate probing of residual internal local dynamics is achieved using sensitive and robust methodologies [10,18,29,36].

However, in the case of IDPs, the inherent flexibility and lack of well-defined tertiary structure in IDPs result in distinct spin relaxation modes, reflecting the more isolated and specific motions of the individual peptide planes [37].

Traditional ^{15}N-^{1}H NMR spin relaxation experiments, in the context of IDPs, may not always offer a fully comprehensive understanding of the dynamic behavior of these complex systems. Recent MD studies, have provided insights on the contributions of different motional modes to relaxation in IDPs [23,38–43]. These studies rely on the extensions of well known model for folded proteins to disordered systems, and still have the limitation of being case-dependent and not generalizable, illustrating the inevitable difficulties that come with extending concepts of folded proteins to IDPs [44]. The interpretation of relaxation studies is further complicated by experimental limitations. In particular, extensive conformational exchange leads to inherently averaged data, while significant water exchange introduce an extra relaxation outlet. To address these limitations, alternative experimental and analytical approaches become essential.

We recently identified a set of transverse and longitudinal cross-correlated relaxation (CCR) experiments that effectively isolate the SDF at zero $J(0)$, for ^{15}N-^{1}H and ^{13}C′-^{13}C$^{\alpha}$ spin vectors [44]. This enables a smooth comparison of local dynamics among diverse spin pairs within the same rigid peptide plane, without invoking a particular motional model, providing a way to get valuable structural insights into IDPs realm.

To precisely quantify CCR rates the ideal method is the symmetrical reconversion approach [45,46]. Recently, symmetrical reconversion has also been applied to obtain transverse CCR rates, due to ^{15}N chemical shift anisotropy (CSA) and ^{15}N-^{1}H dipole–dipole (DD) interactions ($\Gamma_{xy}^{N/NH}$), for IDPs [47]. When regarding the measurement of longitudinal ^{15}N (CSA)/^{15}N-^{1}H (DD) CCR rates ($\Gamma_{z}^{N/NH}$), competing H^{N}-H$^{\alpha}$ cross-relaxation mechanisms must be considered, as noted by Kroenke et al. [48]. To account for these mechanisms and ensure reliable measurement of longitudinal rates, a symmetrical reconversion experiment was developed [46]. In contrast, measuring CCR rates in ^{13}C′ nuclei poses challenges due to the inherent relaxation characteristics [49,50]. Despite this challenge, only Loth et al. [51] developed an experiment to detect transverse CCR due to ^{13}C′ (CSA) and ^{13}C′-^{13}C$^{\alpha}$ (DD) ($\Gamma_{xy}^{C'/C'C^{\alpha}}$) interference, and to date, no attempts have been made to measure the longitudinal ones ($\Gamma_{z}^{C'/C'C^{\alpha}}$).

In this study, we introduce a novel pulse sequence designed to measure the longitudinal CCR rate $\Gamma_{z}^{C'/C'C^{\alpha}}$ adopting the symmetrical reconversion approach. Additionally, we present a new 3D version of the transverse $\Gamma_{xy}^{C'/C'C^{\alpha}}$ rate previously introduced in [51]. The study also incorporates the pulse sequences to measure both transverse $\Gamma_{xy}^{N/NH}$ and longitudinal $\Gamma_{z}^{N/NH}$ CCR rates based on the ones proposed in [47]. The proposed set of experiments serves as a powerful method for deriving residue-specific correlation times for both spin vectors ^{15}N-^{1}H and ^{13}C′-^{13}C$^{\alpha}$. The presented approach does not need to account for exchange, and offers a straightforward and intuitive way to compare the correlation times of two different spin vectors within the same peptide plane, without prior assumptions on the nature of the motions driving relaxation. Its application is anticipated to be valuable, especially in determining protein backbone dihedral angles distributions, where proper referencing of local dynamics is crucial, aiding in the distinction between geometric and dynamic contributions.

To demonstrate the applicability and efficacy of the method, we present a comparative analysis of results obtained for the folded protein ubiquitin and *Coturnix japonica* (Japanese quail) osteopontin (qOPN), a prototypical IDP [52–57].

2. Theory

In the following section, we demonstrate how the $J(0)$ component of the SDF is a suitable proxy for the correlation time. We also present how to derive it from experimental transverse and longitudinal CCR rates, due to chemical shift anisotropy (CSA) and dipole–dipole (DD) interactions.

The semiclassical NMR relaxation theory [58–60] shows that relaxation processes can be formally described, for a system in solution, by the time correlation function (TCF)

$$C_{\vec{u},\vec{v}}(t) = \langle P_2(\vec{u}(0)\cdot\vec{v}(t))\rangle, \tag{1}$$

where $P_2(x) = \frac{1}{2}(3x^2-1)$ is the second order Legendre polynomial, $\vec{u}$ and $\vec{v}$ describe the orientation in the reference frame of the unit spin-vectors (either DD or CSA) involved in the relaxation process, at time 0 and t [25,61]. Nevertheless, what we probe in an NMR relaxation experiment is the SDF

$$J_{\vec{u},\vec{v}}(\omega) = \int_0^{\infty} C_{\vec{u},\vec{v}}(t)\cos(\omega t)dt. \tag{2}$$

For most relaxation processes, the TCF can be described by a sum of mono exponential decaying functions:

$$C_{\vec{u},\vec{v}}(t) = \sum_{k=1}^{N} a_k e^{-t/\tau_k}, \tag{3}$$

where τ_k are the effective correlation times, and a_k are weighting coefficients [62]. At $t = 0$ we obtain the following condition on the weights:

$$\sum_{k=1}^{N} a_k = C_{\vec{u},\vec{v}}(0). \tag{4}$$

Evaluating the SDF at zero and inserting Eq. (3) into Eq. (2) yields:

$$J_{\vec{u},\vec{v}}(0) = \sum_{k=1}^{N} a_k \int_0^{\infty} e^{-t/\tau_k}dt = \sum_{k=1}^{N} a_k\tau_k = (\sum_{k=1}^{N} a_k)\frac{\sum_{k=1}^{N} a_k\tau_k}{\sum_{k=1}^{N} a_k}. \tag{5}$$

Employing the weights condition in Eq. (4) we can recast Eq. (5) as

$$J_{\vec{u},\vec{v}}(0) = C_{\vec{u}\vec{v}}(0)\tau_{\vec{u}\vec{v}}, \tag{6}$$

where $\tau_{\vec{u}\vec{v}} = \frac{\sum_{k=1}^{N} a_k\tau_k}{\sum_{k=1}^{N} a_k}$ is the weighted average correlation time. When regarding the case $\vec{u} = \vec{v}$ (auto-correlated relaxation), $C_{\vec{u},\vec{u}}(0) = \langle P_2(\vec{u}(0)\cdot\vec{u}(0))\rangle$ equals 1. Indeed at $t = 0$ the vectors u align with themselves, and $\tau_{\vec{u},\vec{u}}$ simply equals to $J_{\vec{u},\vec{u}}(0)$. This is the one usually considered in ^{15}N-^{1}H auto-relaxation, and in spectral density mappings protocols. For a rigid spherical top, it corresponds to the rotational tumbling time [24,35,63].

The presence of multiple relaxation mechanisms with equal tensor rank (e.g. DD/DD, CSA/DD or CSA/CSA interference) result in a TCF $C_{\vec{u},\vec{v}}(t)$ encoding cross terms [64]. With $\vec{u} \neq \vec{v}$ (cross-correlated relaxation), the TCF describes the interference effects occurring if $\vec{u}$ and $\vec{v}$ do not move independently but in a correlated manner. In this case, $C_{\vec{u},\vec{v}}(t)$ does not start at 1 but at $\langle P_2(\vec{u}(0)\cdot\vec{v}(0))\rangle$. Note that when the angle between the vectors $\vec{u}$ and $\vec{v}$ is known and fixed $\langle P_2(\vec{u}(0)\cdot\vec{v}(0))\rangle$ reduces to $P_2(\cos\theta_{\vec{u},\vec{v}})$,

$$J_{\vec{u},\vec{v}}(0) = P_2(\cos\theta_{\vec{u},\vec{v}})\tau_{\vec{u}\vec{v}}, \tag{7}$$

where $\theta_{\vec{u},\vec{v}}$ is the angle between $\vec{u}$ and $\vec{v}$. For the interactions considered henceforth, these angles can be considered fixed [65]. To summarize, by accounting for the structural component in $C_{\vec{u},\vec{v}}(0)$, we can extract and compare the correlation times derived from different CCR experiments [30]. Exchange-free $J_{\vec{u},\vec{v}}(0)$ values, for the ^{15}N-^{1}H spin-pair are obtained by a linear combination of $\Gamma_{xy}^{N/NH}$ and $\Gamma_{z}^{N/NH}$ CCR rates [30,62]:

$$J_{NH,xx}(0) = \frac{2\Gamma_{xy}^{N/NH} - \Gamma_{z}^{N/NH}}{8k_{N/NH}\Delta_N}, \tag{8}$$

where

$$\Gamma_{xy}^{N/NH} = k_{N/NH}\Delta_N\left[4J_{NH,xx}(0) + 3J_{NH,xx}(\omega_N)\right], \quad (9)$$

$$\Gamma_{z}^{N/NH} = k_{N/NH}\Delta_N\left[6J_{NH,xx}(\omega_N)\right], \quad (10)$$

$$k_{N/NH} = \frac{2}{5}\frac{1}{24\pi}\frac{\mu_0\hbar\gamma_N\gamma_H}{r_{NH}^3}B_0\gamma_N,$$

μ_0 is the vacuum permeability, $\hbar$ is the reduced Planck constant, γ_i is the gyromagnetic ratio of nucleus i, r is the distance between the nuclei, B_0 is the magnetic field strength and $\Delta_N = (\sigma_{xx} - \sigma_{yy}) = (\sigma_{xx} - \sigma_{zz})$ is the size difference of the ^{15}N CSA principal components.

The correlation time τ_{NH} is derived, combining Eqs. (7) and (8) as follows:

$$J(0) = P_2(\cos\alpha)\tau_{NH} = \frac{2\Gamma_{xy}^{N/NH} - \Gamma_z^{N/NH}}{8k_{N/NH}\Delta_N}$$
$$\tau_{NH} = \frac{2\Gamma_{xy}^{N/NH} - \Gamma_z^{N/NH}}{8k_{N/NH}\Delta_N P_2(\cos\alpha)} \quad (11)$$

where α is the projection angle of σ_{xx} onto the NH bond vector (see Supplementary Material Fig. 1).

The exchange-free $J(0)$ values for the ^{13}C′-^{13}C$^\alpha$ pair are derived in full analogy to Eqs. (9) and (10).

$$\Gamma_{xy}^{C'/C'C^\alpha} = k_{C'/C'C^\alpha}\left[(\sigma_{xx} - \sigma_{zz})(4J_{C'C^\alpha,xx}(0) + 3J_{C'C^\alpha,xx}(\omega_C)) + (\sigma_{yy} - \sigma_{zz})(4J_{C'C^\alpha,yy}(0) + 3J_{C'C^\alpha,yy}(\omega_C))\right] \quad (12)$$

$$\Gamma_{z}^{C'/C'C^\alpha} = k_{C'/C'C^\alpha}\left[(\sigma_{xx} - \sigma_{zz})6J_{C'C^\alpha xx}(\omega_C) + (\sigma_{yy} - \sigma_{zz})6J_{C'C^\alpha yy}(\omega_C)\right] \quad (13)$$

$$k_{C'/C'C^\alpha} = \frac{2}{5}\frac{1}{24\pi}\frac{\mu_0\hbar\gamma_c^2}{r_{C'C^\alpha}^3}B_0\gamma_c$$

with xx, yy, zz referring to the principal components of the fully anisotropic ^{13}C′ CSA tensor.

This time, combining equations Eq. (12), (13) and Eq. (7) yields:

$$\left[(\sigma_{xx} - \sigma_{zz})J_{C'C^\alpha,xx}(0) + (\sigma_{yy} - \sigma_{zz})J_{C'C^\alpha,yy}(0)\right] = \frac{2\Gamma_{xy}^{C'/C'C^\alpha} - \Gamma_z^{C'/C'C^\alpha}}{8k_{C'/C'C^\alpha}}$$
$$\left[(\sigma_{xx} - \sigma_{zz})P_2(\cos\alpha_1)\tau_{C'C^\alpha,xx} + (\sigma_{yy} - \sigma_{zz})P_2(\cos\alpha_2)\tau_{C'C^\alpha,yy}\right] = \frac{2\Gamma_{xy}^{C'/C'C^\alpha} - \Gamma_z^{C'/C'C^\alpha}}{8k_{C'/C'C^\alpha}}, \quad (14)$$

where α_1 and α_2 denote the projection angles between the xx and yy principal components of the 13C′ CSA tensor, respectively, and the $C'C^\alpha$ bond (see Supplementary Material Fig. 1).

Because of the anisotropy of the ^{13}C′ CSA tensor, two separate correlation times, $\tau_{C'C^\alpha,xx}$ and $\tau_{C'C^\alpha,yy}$, are present. In principle, we cannot separate them. In practice, however, we can extract an effective tau by formally treating them as equal. Possible differences between $\tau_{C'C^\alpha,xx}$ and $\tau_{C'C^\alpha,yy}$ are far less impactful than their respective weights (see Figure 2 A in the Supplementary Material). Notably, $(\sigma_{xx}-\sigma_{zz})P_2(\cos\alpha_1)$ is almost seven times larger than $(\sigma_{yy} - \sigma_{zz})P_2(\cos\alpha_2)$ (see Section 4.2).

$$\tau_{C'C^\alpha,eff} = \frac{2\Gamma_{xy}^{C'/C'C^\alpha} - \Gamma_z^{C'/C'C^\alpha}}{8k_{C'/C'C^\alpha}[(\sigma_{xx} - \sigma_{zz})P_2(\cos\alpha_1) + (\sigma_{yy} - \sigma_{zz})P_2(\cos\alpha_2)]}. \quad (15)$$

Now consider that we have also assumed the CSA tensors to be known precisely even though they vary with their chemical environment [51,66,67], which in itself can act as a source of relaxation. For folded proteins, the use of a fixed average ^{15}N CSA geometry was shown to be a reasonable approximation [61]. For ^{13}C′ CSA tensors and/or highly flexible protein systems, no such studies have been conducted to this date, which adds some uncertainty to the extracted correlation times (see Figure 2B,C in the Supplementary Material). MD and DFT studies can certainly help to quantify the size of this effect. Here, we will resort to a fixed CSA tensor geometry, in order to interpret the rates in more intuitive terms.

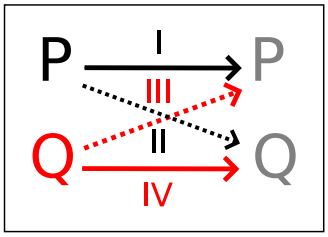

Fig. 1. Illustration outlining the symmetrical reconversion approach for quantifying CCR rates. Auto experiments are represented with continuous lines, while cross experiments are indicated with dashed lines. In red are highlighted the additional experiments III and IV, complementing the conventional auto and cross experiments (I and II) in time-domain techniques.

3. The NMR experiments

The symmetrical reconversion approach, introduced by Pelupessy et al. [45], stands as a unique method for quantifying cross-correlated relaxation (CCR) rates. While it can be classified as a time-domain technique, encompassing the standard auto-experiment (I) to monitor the decay of the initial operator P over time, and the cross-experiment (II) to observe the build-up of a new operator Q created via CCR [68], the symmetrical reconversion surpasses traditional methodologies. It introduces two additional experiments: a Q-to-P cross-experiment (III) and a Q-to-Q auto-experiment (IV) (Fig. 1), providing notable advantages compared to alternative techniques. Firstly, it cancels out errors resulting from pulse miscalibration and uncontrolled attenuation factors associated with relaxation. Secondly, it contributes to the effective averaging of auto-relaxation rates. Finally, the rates obtained with this method do not depend on the efficiency of the initial excitation of P and Q, nor on the efficiency of their detection [45,46]. Given these strengths, we unequivocally chose it as the most accurate method for quantifying CCR rates in our work.

3.1. Transverse Cross-Correlated Relaxation (CCR) $\Gamma_{xy}^{N/NH}$ experiment

Fig. 2 illustrates the pulse sequence used to measure the transverse CCR rates $\Gamma_{xy}^{N/NH}$ due to ^{15}N chemical shift anisotropy (CSA) and ^{15}N and ^{15}N-^{1}H dipole–dipole (DD) interactions. Our implementation closely follows the one outlined in [47]. We introduced only minor modifications: (i) The two consecutive INEPT steps after the CCR block ($2N_zH_z \rightarrow N_z$ and $N_z \rightarrow 2N_zC_z'$) are merged into a single one ($2N_zH_z \rightarrow 2N_zC_z'$), (ii) Sensitivity enhancement [69] is included at the end of the pulse sequence, and (iii) a 6-element composite pulse [70] is used for simultaneous inversion of C′ and C$^\alpha$ nuclei during the CCR block (instead of Q3 pulse).

The sequence begins with an INEPT transfer, generating $2N_zH_z$ two-spin order. A water flip-back is then applied with −x or (−x, x) phases to maintain water along +z, depending on the selected blocks. Now, four distinct pathways can be chosen: auto-experiments I and IV, or cross-experiments II and III.

In experiments I and II, the two-spin order $2N_zH_z$ transforms into N_z magnetization through an INEPT step. In contrast, experiments III and IV preserve the $2N_zH_z$ term by applying a composite pulse alternating between π and 0° phases, followed by an appropriate receiver phase change.

All pathways share a common core: the CCR block. It begins with a $\pi/2$ pulse flipping the ^{15}N magnetization in the y-axis, creating either N_y (I, II) or $2N_yH_z$ (III, IV). A nitrogen π pulse in the middle of the relaxation period T_c refocuses ^{15}N chemical shift evolution, while composite Shaka pulses [70] on ^{13}C refocus unwanted CCR due to interference with ^{13}C′ or ^{13}C$^\alpha$. The relaxation block concludes with a $\pi/2$ pulse flipping back the ^{15}N magnetization to the z-axis, generating $2N_zH_z$ or N_z.

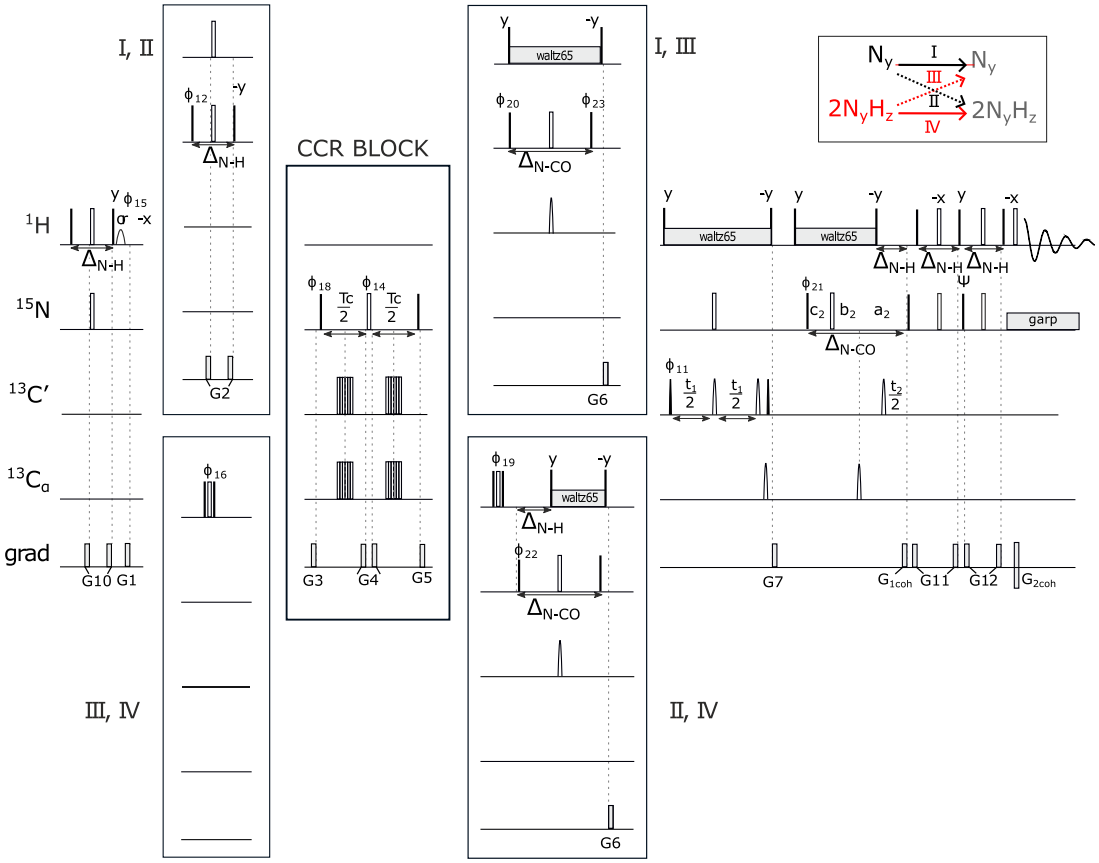

Fig. 2. Pulse sequence for the measurement of the transverse CCR rates for ^{15}N chemical shift anisotropy (CSA) and ^{15}N-^{1}H dipolar-dipolar (DD) interactions denoted as $\Gamma_{xy}^{N/NH}$.^{13}C′ evolution is in real-time (t1) mode and ^{15}N evolution is in constant-time or semi-constant time mode (depending on the maximum evolution time achieved): $a_2 = (t_2 + \Delta_{NCO})/2$; $b_2 = t_2 \cdot (t_2^{max} - \Delta_{NCO})/2t_2^{max}$; $c_2 = \Delta_{NCO} \cdot (t_2^{max} - t_2)/2t_2^{max}$. Narrow filled and wide unfilled bars indicate $\pi/2$ and π pulses, respectively, while the wide filled rectangle stands for ^{1}H decoupling performed with waltz65 [71]. Low unfilled round pulse are for selective $\pi/2$ pulses applied to the water resonance. The narrow unfilled and wide filled round pulses indicate selective $\pi/2$ (Q5 and time-reversed Q5 pulses) and π (Q3 pulse) shaped pulses used for ^{13}C′ and ^{13}C$^\alpha$ excitation and inversion, respectively [72]. Simultaneous inversion of ^{13}C′ and ^{13}C$^\alpha$ spins was achieved using 6-element composite pulse [70]. Unspecified pulse phases are assumed along the x-axis. Phase cycles: $\phi_{15} = (-x, x); \phi_{12} = (x, -x); \phi_{16} = (y, -x); \phi_{18} = 8(x), 8(-x); \phi_{14} = 16(x), 16(y), 16(-x), 16(-y); \phi_{20} = 4(-x), 4(x); \phi_{23} = 64(y), 64(-y); \phi_{19} = 4(y), 4(-x); \phi_{22} = 64(x), 64(-x); \phi_{17} = 4(-y), 4(y); \phi_{11} = 2(x), 2(-x)$. For carbon dimension, quadrature detection was achieved in a States-TPPI manner [73], by incrementing ϕ_{11} phase. For nitrogen dimension, the evolution of individual quadrature components of the signal was achieved by incremental change of ϕ_{21} and Ψ phases as well as G_{2coh} amplitude sign, in echo/anti-echo manner. Receiver phase $\phi_{rec} = \phi_{11} + 2\phi_{14} + \phi_{12} + \phi_{18} + \phi_{20} + \phi_{22}$. 1 ms sine-bell gradient pulses (G10 = 17 G/cm, G1 = 37 G/cm, G2 = 19 G/cm, G3 = 29 G/cm, G4 = 23 G/cm, G5 = 13 G/cm, G6 = 11 G/cm, G7= 41 G/cm, G11 = −5 G/cm, G12 = −2 G/cm) are used. The delay Δ_{NH} = 5.4 ms while the delay Δ_{NCO} = 28 ms. The relaxation delay T$_c$ is varied between 40, and 100 ms. A total of four experiments are performed following a different path as indicated by I, II, III, IV. On the top right, an inset shows the initial and final operators selected before and after the CCR block. Auto experiments are represented with continuous lines, while cross experiments are indicated with dashed lines. In red are highlighted the additional experiments III and IV, typical of the symmetrical reconversion approach.

Following the relaxation block, experiments I and III select and transform the N_z magnetization into $2C'_zN_z$ term via an INEPT step. In experiments II and IV, the $2N_zH_z$ two-spin order is chosen using a composite pulse, and next converted into $2C'_zN_z$ term.

In all schemes, ^{13}C′ evolves in a real-time manner during t_1, while ^{15}N evolves in a constant-time or semi-constant time manner (automatically chosen based on maximum evolution time achieved) during t_2. Sensitivity enhancement is applied at the end. Each experiment has the same detection period t_3, during which the amide proton $^1H^N$ magnetization is observed, similar to a 3D HNCO-type experiment.

3.2. Transverse Cross-Correlated Relaxation (CCR) $\Gamma_{xy}^{C'/C'C^\alpha}$ experiment

After detailing the pulse sequence used to measure $\Gamma_{xy}^{N/NH}$, we now focus on the transverse $\Gamma_{xy}^{C'/C'C^\alpha}$ CCR rate, illustrated in Fig. 3. This sequence shares similarities with the previous one but is tailored for ^{13}C′ CSA and ^{13}C′-^{13}C$^\alpha$ DD interactions. The pulse sequence is based on the idea proposed in [51], which we extended to a 3D version. We also introduced the following changes: (i) The nitrogen component is preserved during the first selection and the CCR evolution, allowing to shorten some blocks of the sequence and remove others, and (ii) The sensitivity-enhancement scheme [69] is employed at the end.

The four distinct pathways start with the operator $2N_zC'_z$ created after the initial INEPT steps. In experiments I and II, an additional INEPT transfer generates the three-spin order $4N_zC'_zC^\alpha_z$. Two C^α $(\pi/2)$ pulses, with the second one phase alternated with the receiver, suppress unwanted $2N_zC'_z$ term. In experiments III and IV, the operator $2N_zC'_z$ is retained, and the relaxation block directly follows the initial INEPT steps.

At the beginning of the relaxation block, a $\pi/2$ pulse on ^{13}C′ generates $2N_zC'_y$ or $4N_zC'_yC^\alpha_z$ magnetization. During the relaxation period T$_c$, a π pulse on ^{13}C′ refocuses its chemical shift evolution. The last $\pi/2$ pulse flips back ^{13}C′ magnetization: we exit the CCR block with $2N_zC'_z$ or $4N_zC'_zC^\alpha_z$ term.

In experiments I and III, two ^{13}C$^\alpha$ $(\pi/2)$ pulses with a proper phase-cycle select $4N_zC'_yC^\alpha_z$ anti-phase magnetization. This term is then converted to $2N_zC'_y$ through an INEPT step combined with proton decoupling during t_1. In experiments II and IV, the $2N_zC'_y$ term is chosen by applying a $\pi/2$ on ^{13}C$^\alpha$ followed by a gradient.

After the selection, ^{13}C′ chemical shift evolves in real-time during t_1. The last $\pi/2$ pulse generates $2N_zC'_z$ two-spin order, subsequently

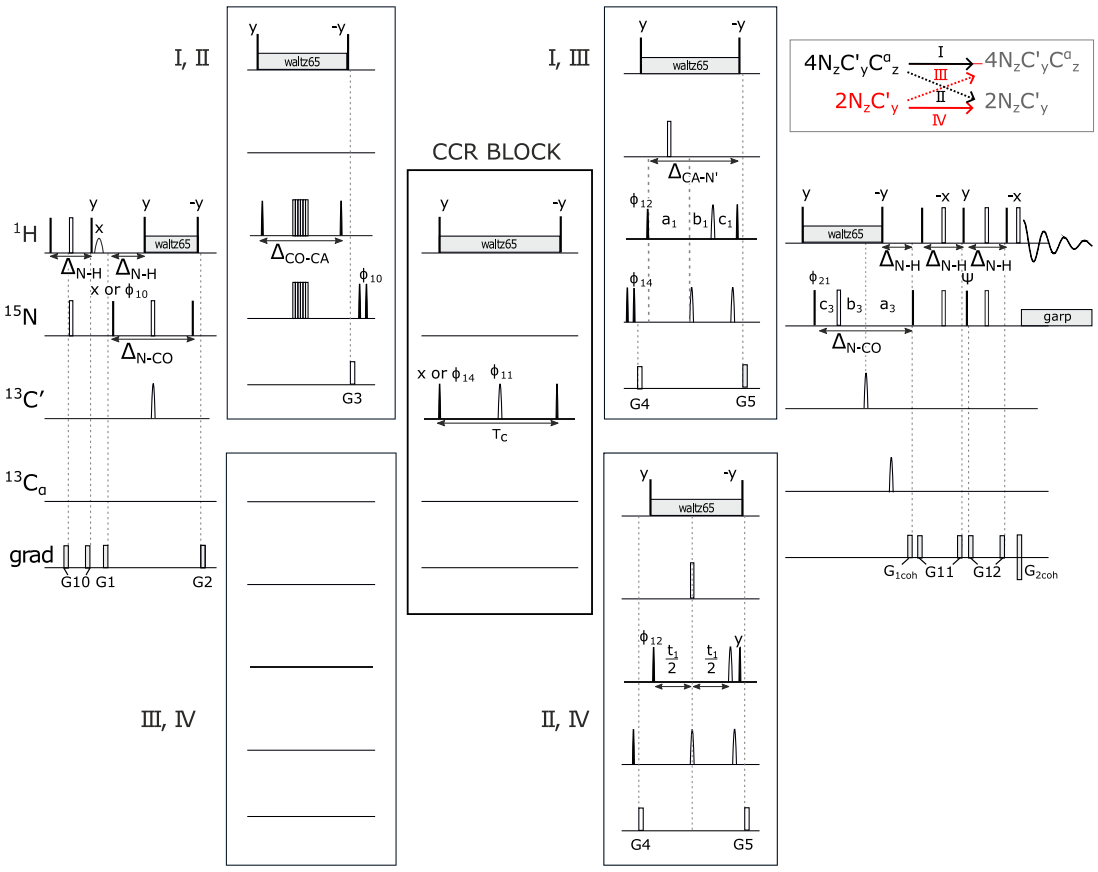

Fig. 3. Pulse sequence for the measurement of the transverse CCR rates for $^{13}C'$ chemical shift anisotropy (CSA) and $^{13}C'$-$^{13}C^{\alpha}$ dipolar-dipolar (DD) interactions denoted as $\Gamma_{xy}^{C'/C'C^{\alpha}}$.$^{13}C'$ evolution is in real-time (t1) mode and ^{15}N evolution is in constant-time or semi-constant time mode (depending on the maximum evolution time achieved): $a_2 = (t_2 + \Delta_{NCO})/2$; $b_2 = t_2 \cdot (t_2^{max} - \Delta_{NCO})/2t_2^{max}$; $c_2 = \Delta_{NCO} \cdot (t_2^{max} - t_2)/2t_2^{max}$. Narrow filled and wide unfilled bars indicate $\pi/2$ and π pulses, respectively, while the wide filled rectangle stands for ^{1}H decoupling performed with waltz65 [71]. Low unfilled round pulse are for selective $\pi/2$ pulses applied to the water resonance. The narrow unfilled and wide filled round pulses indicate selective $\pi/2$ (Q5 and time-reversed Q5 pulses) and π (Q3 pulse) shaped pulses used for $^{13}C'$ and $^{13}C^{\alpha}$ excitation and inversion, respectively [72]. Simultaneous inversion of $^{13}C'$ and $^{13}C^{\alpha}$ spins was achieved using 6-element composite pulse [70]. Unspecified pulse phases are assumed along the x-axis. Phase cycles: $\phi_{10} = (x, -x); \phi_{12} = 2(x), 2(-x); \phi_{14} = 4(x), 4(-x); \phi_{11} = 8(x), 8(y)$. For carbon dimension, quadrature detection was accomplished using States-TPPI [73] approach (phase ϕ_{14} was incremented). For nitrogen dimension, the evolution of individual quadrature components of the signal was achieved by incremental change of ϕ_{21} and Ψ phases and G_{2coh} gradient amplitude sign, in echo/anti-echo manner. Receiver phase $\phi_{rec} = \phi_{11} + 2\phi_{14} + \phi_{12} + \phi_{18} + \phi_{20} + \phi_{22}$. 1 ms sine-bell gradient pulses (G10 = 17 G/cm, G1 = 37 G/cm, G2 = 19 G/cm, G3 = 29 G/cm, G4 = 23 G/cm, G5 = 13 G/cm, G6 = 11 G/cm, G7= 41 G/cm, G11 = −5 G/cm, G12 = −2 G/cm) are used. The following delays are used: Δ_{NH}= 5.4 ms, Δ_{NCO} = 28 ms and Δ_{COCA} = 9.1 ms. The relaxation delay T_c is varied between 80, 100 and 120 ms. A total of four experiments are performed following a different path as indicated by I, II, III, IV. On the top right, an inset shows the initial and final operators selected before and after the CCR block. Auto experiments are represented with continuous lines, while cross experiments are indicated with dashed lines. In red are highlighted the additional experiments III and IV, typical of the symmetrical reconversion approach.

converted into $2N_zH_z$ by an INEPT transfer during t_2. Detectable proton magnetization is observed during t_3 in all experiments.

3.3. Longitudinal Cross-Correlated Relaxation (CCR) experiment

The measurement of longitudinal CCR rates have been historically challenging due to technical limitations arising from smaller cross-relaxation rates compared to auto-relaxation rates.

Furthermore, the relaxation pathways involved in longitudinal CCR are more complex than those observed in transverse CCR, and include multi-exponential cross-correlated and auto-correlated cross-relaxation effects. In cases where competing cross-relaxation mechanisms involving a third operator are present, the first-order averaging is no longer sufficient [48].

When measuring the longitudinal CCR rate $\Gamma_z^{N/NH}$, competing homonuclear cross relaxation mechanisms as H^{α}-H^{N} homonuclear NOEs with the close-by H^{α} protons affect the rates. To address this issue, Pelupessy et al. [46] developed a symmetrical reconversion experiment that involves a swapping block in the middle of the relaxation block, which acts as a unitary matrix that convert the operator P into Q and vice versa. In this way the relaxation matrix can be averaged up to the second-order, effectively suppressing undesired NOE effects.

In contrast, the measurement of the longitudinal CCR rate $\Gamma_z^{C'/C'C^{\alpha}}$ does not necessitate a swapping block, for two main reasons. Firstly, the homonuclear $^{13}C'$-$^{13}C^{\alpha}$ NOE is very small [74]. Secondly, to a good approximation, we can substantially treat the $^{13}C'$-$^{13}C^{\alpha}$ spin-pair as isolated. The CCR arising from $^{13}C'$ CSA and $^{13}C'$-$^{13}C^{\beta}$ DD interactions is negligible due to the large distance between these nuclei. Moreover, the evolution of this rate would not lead to an observable magnetization. Also any interaction with the surrounding protons can be ignored thanks to application of proton decoupling during the CCR block. The only potential threat to rate accuracy arises from contribution of $^{15}N_i$ CSA - $^{15}N_i$-$^{13}C^{\alpha}_{i-1}$ DD interaction, but this can be neglected due to the large distance between $^{15}N_i$ and $^{13}C^{\alpha}_{i-1}$ nuclei, combined with the low gyromagnetic ratio of the ^{15}N isotope.

Now, we turn our attention to the pulse sequence details presented in Fig. 4. For simplicity, this figure exclusively shows the CCR core blocks, denoted as $\Gamma_z^{N/NH}$ and $\Gamma_z^{C'/C'C^{\alpha}}$, which replace the corresponding blocks in Fig. 2 and Fig. 3, respectively. Recalling the experimental design, it consists of four distinct pathways, denoted as I, II, III, and IV.

The implementation of the experiment to measure the $\Gamma_z^{N/NH}$ rate was based on Srb et al. [47], with the same differences as described in Section 3.1. While assessing the longitudinal CCR rate $\Gamma_z^{N/NH}$, we

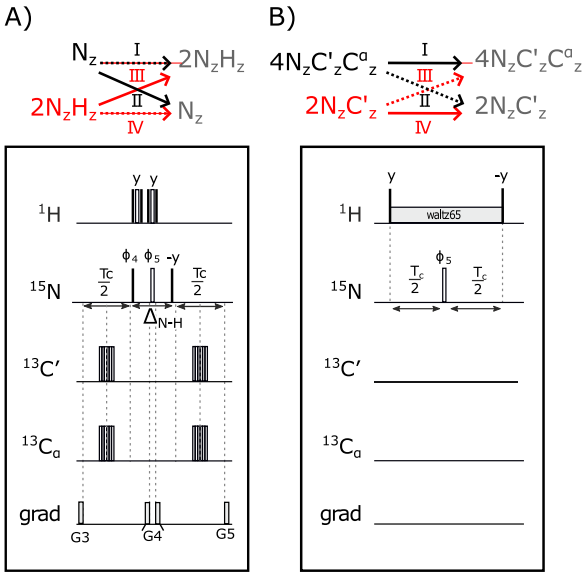

Fig. 4. Pulse sequences relaxation blocks for the measurement of the longitudinal CCR rates $\Gamma_z^{N/NH}$ and $\Gamma_z^{C'/C'C^{\alpha}}$, respectively shown in panel **A** and **B**. Narrow filled and unfilled bars indicate $\pi/2$ and π pulses, respectively, while the wide filled rectangle stands for proton decoupling performed with waltz65 [71]. Composite Shaka pulses [70] are employed to suppress unwanted coupling to ^{13}C. Unspecified pulse phases are assumed along the x-axis. Phase cycles: $\phi_4 = 8(x), 8(-x)$ and $\phi_5 = 16(x), 16(y), 16(-x), 16(-y)$. 1 ms sine-bell gradient pulses (G3 = 19 G/cm, G4 = 23 G/cm, G5 = 11 G/cm) are used. The delay $\Delta_{NH} = 1/2J_{NH}$ is 5.7 ms. The relaxation delay T_c is varied between 80,100 and 120 ms. A total of four experiments are performed as indicated in Figs. 2 and 3. In Panel **A**, the central INEPT block swaps operators P and Q. The composite proton ^{1}H pulses maintain water along +z. On the top of each panels, we highlight the initial and final operators selected before and after the CCR block. Auto experiments are represented with continuous lines, while cross experiments are indicated with dashed lines. In red are highlighted the additional experiments III and IV, typical of the symmetrical reconversion approach.

can enter the relaxation block in Fig. 4A with two different operators. From pathways I and II we start with N_z magnetization, instead from pathways III and IV we begin with the two spin order $2N_zH_z$. Because of the swapping block, facilitated by the INEPT step in the middle of the relaxation delay, pathways I and IV become the cross-experiments while pathways II and III the auto-experiments. Additionally, composite ^{1}H pulses effectively preserves water magnetization along +z, and Shaka pulses suppress undesirable ^{13}C′ and ^{13}C$^{\alpha}$ couplings.

In Fig. 4B, entry into the relaxation block can occur with the three-spin order $4N_zC'_zC^{\alpha}_z$ from pathways I and II, or with the two-spin order $2N_zC'_z$ following experiments III and IV. During the relaxation period T_c, a π pulse on nitrogen is applied to prevent spurious CCR evolution.

The subsequent details remain consistent with those previously described in Sections 3.1 and 3.2.

4. Materials and methods

4.1. Protein preparation

Uniformly ^{15}N /^{13}C labeled ubiquitin was purchased from ASLA Biotech. The NMR sample was dissolved in 10 mM potassium phosphate buffer of pH = 6.5. The final protein concentration was 1 mM.

The following paragraph describes the cloning and expression of the qOPN sequence in a pET11d plasmid. The plasmid is transformed into an E. coli BL21(DE3) strain and incubated at 37 °C for 45 min, followed by plating on an ampicillin agar plate and incubation overnight at 37 °C. A colony from the plate is then used to prepare a preculture in LB medium with ampicillin, which is incubated overnight at 37 °C. The preculture is then used to inoculate 1 liter of LB medium with ampicillin and grown until the optical density at 600 nm wavelength (OD_{600}) reaches 0.8–1.0. The cells are harvested, resuspended in cold 1xPBS buffer [55], sonicated, and heated at 90 °C for 10 min with fresh DTT added. The cell lysate is centrifuged, and the supernatant is subjected to ammonium sulfate precipitation to bring the solution to 50% saturation. The protein is purified using an anion exchange column and concentrated using a 10 kDa cut-off. The protein concentration is measured using a NanoDrop™, and if the A280/260 ratio is higher than 0.7, the anion exchange purification is repeated to remove excess DNA. The final protein concentration was 2.6 mM at pH = 6.5, 10% D_2O.

4.2. NMR measurements

The NMR pulse sequences (for Bruker spectrometers) are available from the authors upon request.

All the NMR experiments acquired on ubiquitin were recorded in a magnetic field B_0 = 18.79 T on Bruker Avance III HD spectrometer (^{1}H Larmor frequency 800 MHz) equipped with a 5 mm TCI-HCN cryogenically-cooled probehead.

The one acquired on qOPN were recorded on Bruker Avance III HD+, equipped with a Bruker RT 5 mm TXI probe, operating at 800 MHz. All the experiments were measured at 298 K. The ^{1}H carrier was placed at 4.7 ppm (water signal), the ^{13}C carrier at 40 ppm, and the ^{15}N carrier at 116 ppm. Band-selective ^{13}C pulses were applied at 174 and 56 ppm to excite or invert ^{13}C′ and ^{13}C$^{\alpha}$ spins, respectively. The following band-selective pulses were used: 240 ms with Q5 and time reversed Q5 shapes for ^{13}C′ and ^{13}C$^{\alpha}$ excitation, 192 ms Q3 shapes for ^{13}C′/^{13}C$^{\alpha}$ inversion/refocusing [72]. Proton decoupling is achieved with waltz65 [71], while decoupling of ^{15}N spins during acquisition was performed with garp [75].

All experiments on ubiquitin were measured as 2D versions (^{15}N and ^{1}H) of the sequences reported in Figs. 2, 3, and 4, using the conventional sampling scheme, while the ones on qOPN were performed in their 3D versions using non-uniform sampling (NUS) scheme [76,77]. To check the accuracy of NUS data reconstruction, we also measured a 3D NUS version of the $\Gamma_{xy}^{N/NH}$ rate for ubiquitin, and compared these results with those obtained conventionally (see Fig. 3 in Supplementary Material). For ubiquitin, the transverse CCR rates (Γ_{xy}^{CCR}) were measured at two different delays T_c = 40 and 100 ms, and the longitudinal ones (Γ_z^{CCR}) were carried at T_c = 80, 100 and 120 ms. The standard deviation is reported as an estimate of the experimental errors. For qOPN, Γ_{xy}^{CCR} were measured at two different delays T_c = 60 and 100* ms, and Γ_z^{CCR} experiments were carried at T_c = 60, 100* and 120. The asterisk denotes the experiments repeated three times to better estimate the experimental errors when using spectra reconstructed from NUS data.

All ubiquitin spectra were processed with NMRPipe [78]. To process qOPN NUS spectra we used the compressed-sensing IST algorithm

[79]. The spectra were analyzed and the peak heights evaluated with Sparky [80]. The resonances were assigned according to BMRB Entries 17769 [81] and 27443 [82], for ubiquitin and qOPN respectively. Detailed information on the acquisition parameters are provided in the Supplementary Material Tables 1 and 2.

The Γ_{xy}^{CCR} are directly extracted as follows:

$$\sqrt{\frac{A_{II}(T)A_{III}(T)}{A_I(T)A_{IV}(T)}} = \tanh\left|(\Gamma_{xy}^{CCR}T)\right| \tag{16}$$

$$|\Gamma_{xy}^{CCR}| = \frac{1}{T}\operatorname{arctanh}\left(\sqrt{\frac{A_{II}(T)A_{III}(T)}{A_I(T)A_{IV}(T)}}\right) \tag{17}$$

where A_i are the amplitudes of the four signals recorded with the experiments $i = I, II, III, IV$ (Figs. 2 and 3) and T is the relaxation delay [45]. Eq. (17), should be modified when the experiments are acquired with different number of scans. In this case, the amplitudes A_i should be first divided by the number of scans.

While the analytical description of Γ_z^{CCR} is more complex, it can be approximated by the rate equation

$$|\Gamma_z^{CCR}| = \frac{1}{T}\operatorname{arctanh}\left(\sqrt{\frac{A_{II}(T)A_{III}(T)}{A_I(T)A_{IV}(T)}}\Big/(1 - \Delta T + O(T^3))\right), \tag{18}$$

where T is the relaxation delay, Δ is the difference of the autorelaxation rates ρ_P and ρ_Q, and $O(T^3)$ represents higher orders of the Taylor expansion in T (see Appendix A). Eq. (18) reduces to Eq. (17) when ΔT is negligible compared to 1, namely when $\rho_P \approx \rho_Q$, or for short relaxation times T. For longer delays, an estimate of Δ, can be obtained by taking the approximation up to second order in T of the ratio of the signal amplitudes of the auto-experiments IV and I (Fig. 4B, cite):

$$\frac{A_{IV}(T)}{A_I(T)} = k(1 - 2\Delta T + 2\Delta^2T^2 + O(T^3)) = k(\exp(-2\Delta T) + O(T^3)). \tag{19}$$

where the constant k accounts for the unequal efficiencies of initial excitation and detection of the operators P and Q in the two auto-experiments. The Γ_z^{CCR} rate and the Δ are derived by fitting simultaneously the experimental intensities of Eqs. (18) and (19).

In cases where competing cross-relaxation mechanisms involving a third operator are present, such as the H^α-H^N NOE, a swapping block has to be added (see Section 3.3, Fig. 4A) [46]. This time, the density matrix of the system becomes more complex and the rates can be approximated by Eq. (20). The correction is extracted from the dependence on T of ratio of the amplitudes of experiments III and II, and $\Gamma_{z,swap}^{CCR}$ is obtain by fitting simultaneously the experimental intensities of Eqs. (20) and (21).

$$|\Gamma_{z,swap}^{CCR}| = \frac{1}{T}\operatorname{arctanh}\left(\sqrt{\frac{A_I(T)\ A_{IV}(T)}{A_{II}(T)A_{III}(T)}}\Big/(1 + \frac{1}{24}\Delta^2T^2 + O(T^5))\right), \tag{20}$$

$$\frac{A_{III}(T)}{A_{II}(T)} = k\frac{B}{A} = k\exp(-\Delta T)/(1 + \frac{1}{12}\Gamma_z^2\Delta T^3 + O(T^5)), \tag{21}$$

where Γ_z stands for $\Gamma_{z,swap}^{CCR}$ (see Appendix B).

It is usually a good practice to acquire cross versions of the experiments with higher number of scans due to their significantly lower sensitivity. The obtained rates are shown in the Supplementary Material Tables 3 and 4.

Once the rates are obtained, the correlation times for the spin vectors ^{15}N-^{1}H and ^{13}C′-^{13}C$^\alpha$ are derived using Eqs. (11) and (15), respectively (see Section 2). The prefactors k and the amplitudes $P_2(\cos\alpha)$, $P_2(\cos\alpha_1)$ and $P_2(\cos\alpha_2)$ are here calculated considering the peptide plane geometry of Corey and Pauling [83] and the approximate principal components of the CSA tensors for ^{15}N and ^{13}C′ presented in [67].

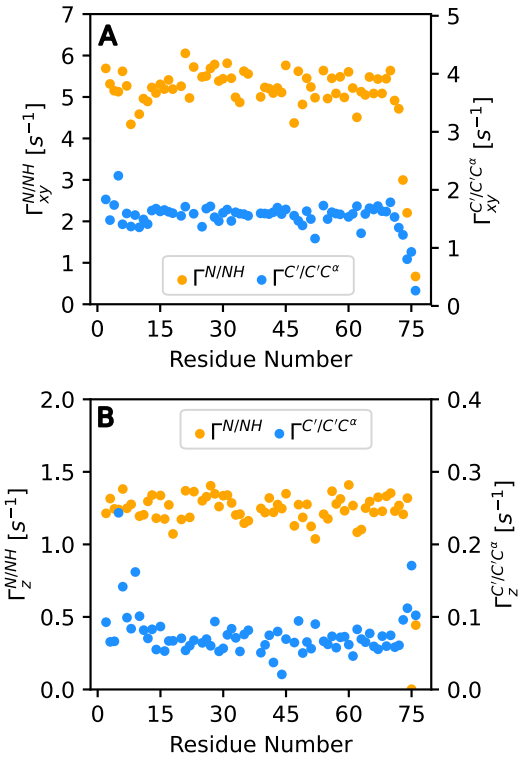

Fig. 5. Obtained CCR rates in uniformly labeled ^{15}N/^{13}C ubiquitin Sample: Panel **A** presents the transverse CCR rates for ^{15}N chemical shift anisotropy (CSA) and ^{15}N-^{1}H dipolar-dipolar (DD) interactions denoted as $\Gamma_{xy}^{N/NH}$ (orange), as well as for ^{13}C′ CSA and ^{13}C′-^{13}C$^\alpha$ DD interactions denoted as $\Gamma_z^{C'/C'C^\alpha}$ (sky blue). These rates are obtained by mapping the amplitudes A_i of the four signals from experiments $i = I, II, III, IV$ in Figs. 2 and 3 into Eq. (17). In Panel **B**, longitudinal CCR rates $\Gamma_z^{N/NH}$ (orange) and $\Gamma_z^{C'/C'C^\alpha}$ (sky blue) are displayed. These rates are measured by substituting the CCR blocks in Figs. 2 and 3 with the blocks depicted in Fig. 4. The $\Gamma_z^{N/NH}$ values are extracted by simultaneous fitting of experimental intensities A_i using Eqs. (18) and (19), while the $\Gamma_z^{C'/C'C^\alpha}$ values are obtained by jointly fitting experimental intensities A_i following Eqs. (20) and (21).

5. Results and discussion

5.1. Pulse sequence benchmark and application to a folded protein

To assess the efficacy of the proposed pulse sequences and study a folded system, we first applied them to a uniformly ^{15}N /^{13}C labeled ubiquitin sample. We recorded 2D versions (^{15}N and ^{1}H dimensions) of the experiments (Fig. 2, Fig. 3, and Fig. 4) using conventional sampling scheme. All the rates were acquired with a minimum of two relaxation delays (T_c) to ensure the correct implementation of the symmetrical reconversion scheme (see Supplementary Material Figure 4).

Fig. 5 displays the obtained results. In particular, Fig. 5A shows the transverse CCR rates $\Gamma_{xy}^{N/NH}$ (orange) and $\Gamma_{xy}^{C'/C'C^\alpha}$ (light blue), while Fig. 5B displays the experimental longitudinal CCR rates $\Gamma_z^{N/NH}$ (orange) and $\Gamma_z^{C'/C'C^\alpha}$ (light blue). The results align consistently with prior studies on ubiquitin [42,74,84–86]. We have also directly compared our rates with the ones derived adopting the symmetrical reconversion approach [47,51] and obtained a good agreement (see Supplementary Material Figure 5).

All CCR rates are largely uniform across residues with only minor variations observed. The larger transverse rates are in agreement with the well-established notion that relaxation in folded proteins is predominantly governed by motions in the nanosecond timescale. As motion slows down, the longitudinal rates, sensitive to fast local motions, become less pronounced. Instead, the sampling of zero-frequency $J(0)$ terms encoded in transverse rates becomes increasingly pronounced.

5.2. Unraveling dynamics in disorder: Pulse sequence insights into an intrinsically disordered protein

Having established the robustness of our pulse sequences, we extended our study to the IDP qOPN.

The pulse sequences were acquired in their 3D versions using non-uniform sampling (NUS) scheme, which is particularly suitable for more crowed IDPs spectra [87]. However, regions with overlapping signals were still evident, leading us to choose not to calculate rates for 60 unresolved residues. Nonetheless, this still accounts for a significant coverage (68%), considering the extensively repetitive sequence and the constrained chemical shift dispersion intrinsic to the system.

Fig. 6 presents the results obtained for a uniformly $^{15}N/^{13}C$ labeled sample of qOPN.

In contrast to the uniformity observed in ubiquitin, qOPN rates present a distinctive profile. This is particularly noticeable in the transverse rates (Fig. 6A), where three regions encompassing residues 120–132, 140–175 and 176–190 are less flexible (higher rates) [82,88].

What draws attention is that qOPN $\Gamma_{xy}^{N/NH}$ values are considerably smaller than the corresponding ubiquitin rates, indicating a higher mobility of the ^{15}N-^{1}H vector in qOPN.

Regarding the longitudinal rates, qOPN $\Gamma_{z}^{N/NH}$ rates are smaller than ubiquitin ones, whereas the $\Gamma_{z}^{C'/C'C^{\alpha}}$ values are larger. Essentially, qOPN longitudinal rates are actually closer in size, possibly reflecting inherent mobility, either the nature of motions or the timescales involved.

It is worth noting that the difference between transverse and longitudinal rates in qOPN is less pronounced than in ubiquitin. The transverse rates in qOPN are clearly smaller but the longitudinal rates are comparable in actual size to ubiquitin. With less slower motions contributing to the $J(0)$, the transverse rates get smaller and closer in size to the longitudinal ones. However, discerning the precise factors responsible remains challenging without accounting for field dependency [89,90]. An accurate quantification and description of the different motions leading to a specific relaxation profile strictly depends on the chosen dynamical model. However, it is still hard to directly relate the TCF with the nature of the motional modes IDPs undergo, and to correctly determine their impact on the resulting relaxation rates. It has been shown that the potential dynamic modes influencing spin relaxation in disordered systems include [37]: (i) Sub-picosecond librations of the NH bonds; (ii) harmonic fluctuations of torsional angles (ϕ, ψ) along the peptide chain (10–100 ps); (iii) ϕ, ψ jumps involving barrier crossing (0.01–1 ns); (iv) concerted tumbling, encompassing the entire protein chain or its more structured segments (relevant for transient structured elements with a sufficient long lifespan). Recently, Salvi et al. [39,40] have rephrased the 3D GAF model [18] to essentially parametrized the NH TCFs in: (1) the reorientation of the peptide plane, influenced by variations in the flanking dihedral angles ϕ, ψ along with NH librations; and (2) the 'tumbling of the peptide plane', described by the rotational correlation function of the $C_{i-1}^{\alpha}C_{i}^{\alpha}$ vector. According to this model, we can infer that variations of the dihedral angles and libration of the NH vectors tune down the $\Gamma^{C'/C'C^{\alpha}}$ rates (see Fig. 6). This applies quite well along the sequence except for the first twenty residues (see Fig. 6A) where the model breaks down: on average we obtain higher transverse NH rates than expected. It is reasonable to speculate about the presence of a more 'structured' segment within qOPN, where the two spin vectors undergo some kind of shared segmental motion (refer to Fig. 7B in the next Section). Noticeable deviations in the transverse ^{15}N relaxation rates were also observed for the residual α-helix in [39]. This adjusted 3D GAF model, in the case of disordered systems can become rather formal. As rationalized by Kämpf: '[...] the peptide plane in an IDP senses not only the fluctuations/jumps of the adjacent torsional angles ϕ_{i-1} and ψ_{i}, but also the conformational transitions involving more remote torsional angles ϕ_{i-k}, ψ_{i-k} and ϕ_{i+k}, ψ_{i+k}' [37], p. 2350). In this way, the 'tumbling of the peptide plane' ignores the existence of several motional modes, wrongly implying less complexity. It is worth noting that Salvi's approach might not be universally applicable. We also like to stress that addressing the presented question is not the major scope of this paper. We recognize that a mechanistic understanding of the underlying motions can be intricate and is often oversimplified, and believe that J(0), i.e. the TCF's enclosed area, may not encode the underlying motions in a clear cut manner [44]. Here, we only intend to compare what we observed in two systems with different structural attributes.

5.3. Correlation time extraction and analysis

The different dynamic behavior and the timescales probed by the two system under analysis, become apparent when calculating the correlation time (tau, τ) for both ^{15}N-^{1}H and $^{13}C'$-$^{13}C^{\alpha}$ vectors. As discussed in Section 2 the correlation time is defined as the normalized $J(0)$ (see Eq. (5)), which is simply the integral of the TCF.

Panels A and C in Fig. 7 display the obtained results for ubiquitin. Here, the two spin vectors exhibit comparable tau values (Fig. 7A). Remarkably, upon evaluating the ratio between $\tau_{C'C^{\alpha}}$ and τ_{NH} (Fig. 7C), it consistently converge around one, implying that both vectors exhibit similar dynamics. The observed deviations from one, implying a higher mobility of the ^{15}N-^{1}H vector, are in agreement with previous works [30,74,86]. One can notice that the residues in the tail emerge as outliers. The inherent flexibility of the end of the backbone chain mirrors the dynamics observed in some residues of qOPN, suggesting, as expected [91], a similar behavior.

Upon analyzing the extracted correlation times for qOPN (Fig. 7B), we observe a greater diversity throughout the sequence. The local correlation times vary for neighboring residues along the backbone thus pointing to decoupling of peptide plane motions. Moreover, for many residues the difference between $\tau_{C'C^{\alpha}}$ and τ_{NH} is more pronounced compared to the one observed in ubiquitin. Indeed, the average value of the ratio $\tau_{C'C^{\alpha}}/\tau_{NH}$ is consistently above one (Fig. 7D).

The found differences between the correlation times of NH and $C'C^{\alpha}$ vectors are certainly related to the different contributions to relaxation of various motional tendencies. Now consider that the extracted tau values are influenced by the choice of model that can be adjusted, it is really about assessing the underlying motions [51]. To circumvent these concerns, one can opt for an alternative approach by simply examining the difference $2\Gamma_{xy} - \Gamma_{z}$ (see Supplementary Material Figure 6). This method allows for a straightforward separation of the terms proportional to $J(0)$, facilitating a cleaner comparison of the mapped SDF without making any assumptions on the motions driving relaxation [44]. In this regards, other graphical representations can provide model-independent intuition about motions timescales [30,33]. A more in-depth analysis is possible using correlation time distributions [21,34] or dynamic detectors [92].

6. Conclusions

The presented work provides a highly sensitive set of experiments that enables the probing of correlation times for two different yet complementary spin vectors within the same peptide plane.

Our study on ubiquitin, a folded protein, confirmed that both ^{15}N-^{1}H and $^{13}C'$-$^{13}C^{\alpha}$ vectors exhibit predominantly similar dynamics, dominated by nanoseconds timescales. This translates into a greater influence of the $J(0)$ terms due to the shared isotropic tumbling motion, rather than $J(\omega)$ high frequency contributions, as evidenced by the relatively small values of the longitudinal CCR rates Γ_{z}. The observed deviation from 1 in the $\tau_{C'C^{\alpha}}/\tau_{NH}$ ratio are in agreement whit previous findings.

In the case of an IDP, such as qOPN, we observed correlation times which were smaller in size and largely varied across the sequence compared to ubiquitin extracted values. Indicating that in more flexible and complex systems, which lack a defined 3D structure, diversity in

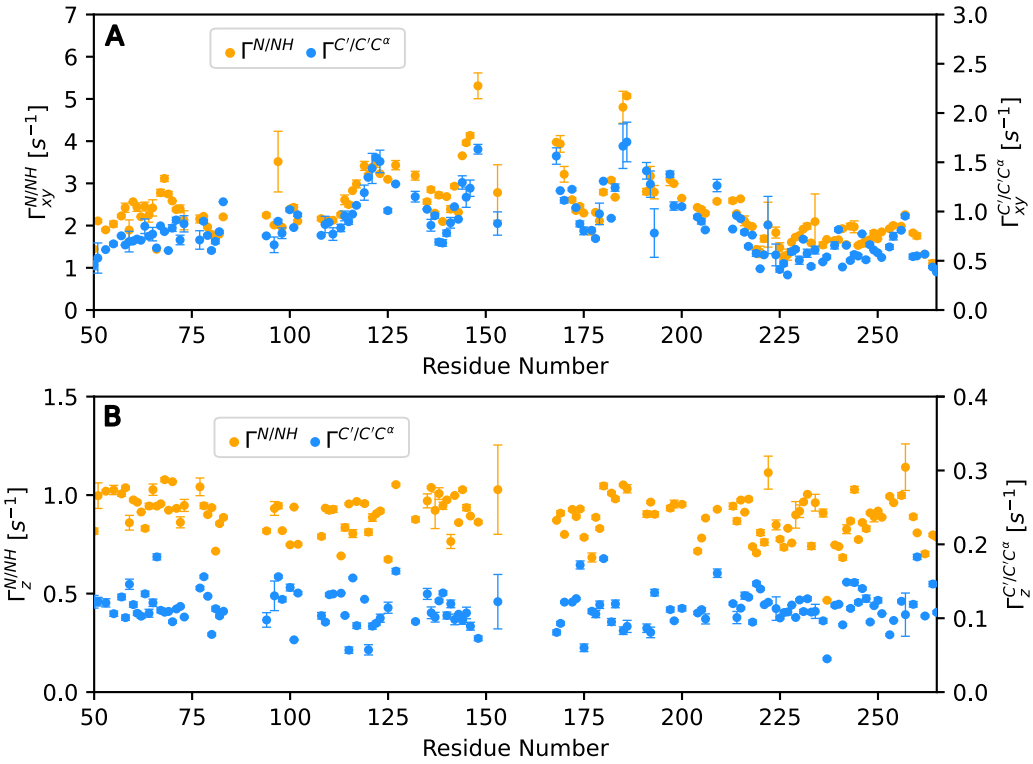

Fig. 6. Obtained CCR rates in uniformly labeled $^{15}N/^{13}C$ qOPN Sample: Panel **A** presents the transverse CCR rates for ^{15}N chemical shift anisotropy (CSA) and ^{15}N-^{1}H dipolar-dipolar (DD) interactions denoted as $\Gamma_{xy}^{N/NH}$ (orange), as well as for $^{13}C'$ CSA and $^{13}C'$-$^{13}C^\alpha$ DD interactions denoted as $\Gamma_z^{C'/C'C^\alpha}$ (sky blue). These rates are obtained by mapping the amplitudes A_i of the four signals from experiments $i = \mathrm{I}, \mathrm{II}, \mathrm{III}, \mathrm{IV}$ in Figs. 2 and 3 into Eq. (17). In Panel **B**, longitudinal CCR rates $\Gamma_z^{N/NH}$ (orange) and $\Gamma_z^{C'/C'C^\alpha}$ (sky blue) are displayed. These rates are measured by substituting the CCR blocks in Figs. 2 and 3 with the blocks depicted in Fig. 4. The $\Gamma_z^{N/NH}$ values are extracted by simultaneous fitting of experimental intensities A_i using Eqs. (18) and (19), while the $\Gamma_z^{C'/C'C^\alpha}$ values are obtained by jointly fitting experimental intensities A_i following Eqs. (20) and (21).

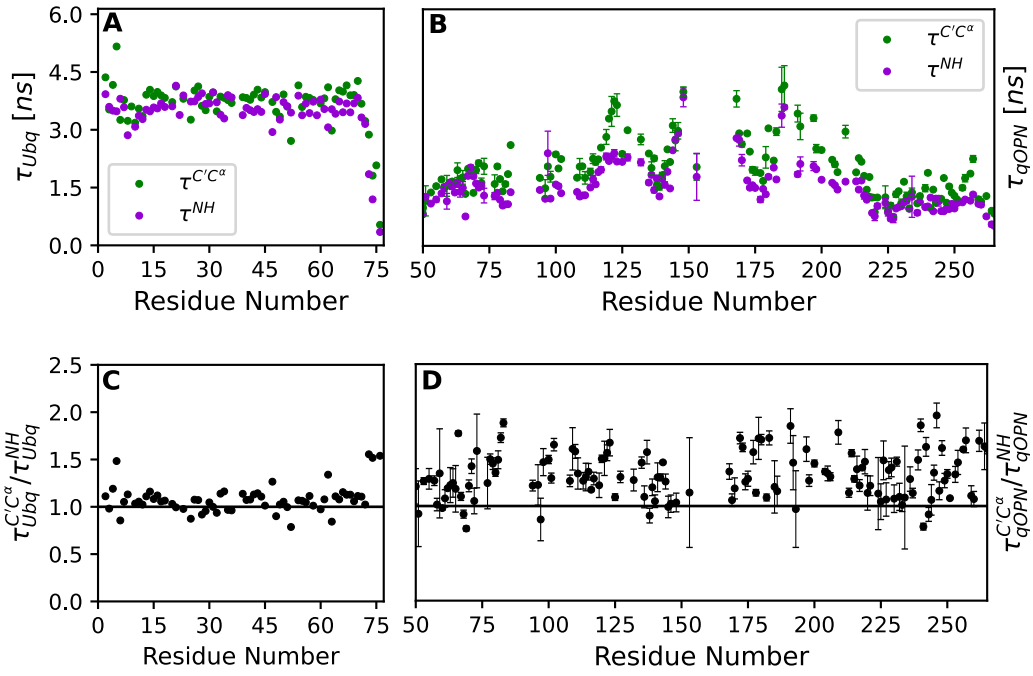

Fig. 7. Correlation times of the Two Spin-Pairs ^{15}N-^{1}H and $^{13}C'$-$^{13}C^\alpha$ in ubiquitin and qOpn: Correlation times (τ) for spin-pairs ^{15}N-^{1}H (purple) and $^{13}C'$-$^{13}C^\alpha$ (green) are depicted in panels **A** and **B** respectively, showcasing results for the well folded ubiquitin, and the intrinsically disordered qOPN. The correlation times $\tau^{N/NH}$ are determined using Eq. (11), and $\tau^{C'/C'C^\alpha}$ are derived from Eq. (15). Panels **C** and **D** present the ratio of $\tau^{C'/C'C^\alpha}$ to $\tau^{N/NH}$ for ubiquitin and qOPN, respectively.

dynamics across the sequence becomes more pronounced, and local dynamics seems to drive relaxation. Because NMR spin relaxation experiments ultimately probe the SDF at few selected frequencies, too little information is available and generally different dynamical models at once would fit the limited set of data [24]. In this study, we only intend to map the spectral density function (SDF) at zero frequency $J(0)$, i.e. the weighted averaged correlation time, and report the noticeable differences and variations observed in two structurally different

systems, without accounting for any particular motional model [28,44]. A possible solution to the limited amount of SDF values we can map is high-resolution relaxometry [89,90].

To conclude, we were able to show that while ^{15}N-based spin relaxation measurements are sufficient to probe conformational dynamics in folded proteins, IDPs are far more heterogeneous and require the determination of additional and complementary spin probes. The proposed experimental scheme serves this purpose and we anticipate valuable applications particularly for the quantification of CCR rates aiming at the determination of protein backbone dihedral angles for which a proper referencing of local dynamics is crucial to disentangle geometric and dynamic contributions.

CRediT authorship contribution statement

Irene Ceccolini: Writing – review & editing, Writing – original draft, Visualization, Validation, Software, Methodology, Investigation, Formal analysis, Data curation, Conceptualization. **Clemens Kauffmann:** Writing – review & editing, Methodology. **Julian Holzinger:** Resources. **Robert Konrat:** Writing – review & editing, Supervision, Project administration, Methodology, Funding acquisition, Conceptualization. **Anna Zawadzka-Kazimierczuk:** Writing – review & editing, Supervision, Software, Methodology, Investigation, Conceptualization.

Declaration of competing interest

The authors declare that they have no known competing financial interests or personal relationships that could have appeared to influence the work reported in this paper.

Data availability

Data will be made available on request.

Acknowledgments

We thank P.Pelupessy and P.Kadeřávek for fruitful discussions and valuable support. This work was supported by the Austrian Science Fund FWF P 35098-B.

Appendix

Within the forthcoming appendix sections, we will derive the equations used to compute the longitudinal cross-correlated relaxation (CCR) rates $\Gamma_z^{C'/C'C^\alpha}$ and $\Gamma_z^{N/NH}$ presented in Section 4.2. Our derivation closely follows the one outlined in [46,74]. This comprehensive derivation aims to provide a robust understanding of the performed analyses.

Appendix A. Derivation of longitudinal cross-correlated relaxation rates

The evolution of the spin density is described using the Liouville formalism, as presented in [93]. Within this framework, the spin system at a given time point T is determined by solving the homogeneous master equation

$$\frac{d\sigma(t)}{dt} = -\hat{\mathbf{L}}(t)\sigma(t), \tag{A.1}$$

where, $\hat{\mathbf{L}}$ is the Liouvillan superoperator, represented in the following by an effective relaxation matrix. We now focus on the sequence shown in Fig. 4B for the measurement of the longitudinal CCR rate $\Gamma_{xy}^{C'/C'C^\alpha}$. At the onset of the relaxation delay, the density operator exists in either P = $2N_zC'_z$ or Q = $4N_zC'_zC^\alpha_z$ states. Cross-correlated relaxation, stemming from the interference of the ^{13}C′ CSA and the ^{13}C′-^{13}C$^\alpha$ dipolar coupling, leads to the partial conversion of P into Q and vice versa. To a reasonable approximation, the spin pair ^{13}C′-^{13}C$^\alpha$ can be considered isolated, as already discussed in Section 3.3.

The Liouvillan space is therefore spanned only by P and Q. Assuming the ^{1}H magnetization is locked and that the π pair refocuses the ^{15}N undesired couplings, Eq. (A.1) reads:

$$\frac{d}{dt}\begin{Bmatrix}\langle P(t)\rangle\\ \langle Q(t)\rangle\end{Bmatrix} = -\begin{bmatrix}\rho_P & \Gamma_z\\ \Gamma_z & \rho_Q\end{bmatrix}\begin{Bmatrix}\langle P(t)\rangle\\ \langle Q(t)\rangle\end{Bmatrix}, \tag{A.2}$$

where ρ_P and ρ_Q are the autorelaxation rates of P and Q, and Γ_z the longitudinal cross-correlated relaxation rates. Eq. (A.2), can be solved analytically:

$$\begin{Bmatrix}\langle P(T)\rangle\\ \langle Q(T)\rangle\end{Bmatrix} = \exp(-\bar{\rho}T)\begin{bmatrix}A & C\\ C & B\end{bmatrix}\begin{Bmatrix}\langle P(0)\rangle\\ \langle Q(0)\rangle\end{Bmatrix}, \tag{A.3}$$

where:

$$A = \cosh\left(T\sqrt{\Delta^2+\Gamma_z^2}\right) + \frac{\Delta}{\sqrt{\Delta^2+\Gamma_z^2}}\sinh\left(T\sqrt{\Delta^2+\Gamma_z^2}\right), \tag{A.4}$$

$$B = \cosh\left(T\sqrt{\Delta^2+\Gamma_z^2}\right) - \frac{\Delta}{\sqrt{\Delta^2+\Gamma_z^2}}\sinh\left(T\sqrt{\Delta^2+\Gamma_z^2}\right), \tag{A.5}$$

$$C = -\frac{\Gamma_z}{\sqrt{\Delta^2+\Gamma_z^2}}\sinh\left(T\sqrt{\Delta^2+\Gamma_z^2}\right), \tag{A.6}$$

and

$$\bar{\rho} = (\rho_P+\rho_Q)/2 \tag{A.7}$$

$$\Delta = (\rho_Q-\rho_P)/2. \tag{A.8}$$

The ratio of the four amplitudes in Eq. (16), in this case becomes:

$$\sqrt{\frac{\mathrm{A_{II}}(T)\mathrm{A_{III}}(T)}{\mathrm{A_I}(T)\mathrm{A_{IV}}(T)}} = \sqrt{\frac{C^2}{AB}}. \tag{A.9}$$

A good approximation of the CCR rates can be obtained by expanding up to the second order in T the ratio in (A.9) [46], as follows:

$$\sqrt{\frac{\mathrm{A_{II}}(T)\mathrm{A_{III}}(T)}{\mathrm{A_I}(T)\mathrm{A_{IV}}(T)}} = \Gamma_z^{CCR}T - \Gamma_z^{CCR}\Delta T^2 + O(T^3). \tag{A.10}$$

Now, we can recognize the first term of the Taylor expansion of the hyperbolic tangent and collect it (Eq. (A.11)). In this way it is easier to see that Eq. (A.12) reduces to the equation used to calculate the transverse rates (see Eq. (17)) when ΔT is negligible compared to 1, namely when $\rho_P \approx \rho_Q$, or when $\Sigma T \ll 1$ (for short relaxation times T) [74]

$$\Gamma_z^{CCR}T - \Gamma_z^{CCR}\Delta T^2 + O(T^3) = \tanh(\Gamma_z^{CCR}T)(1-\Delta T + O(T^3)), \tag{A.11}$$

$$|\Gamma_z^{CCR}| = \frac{1}{T}\operatorname{arctanh}\left(\sqrt{\frac{\mathrm{A_{II}}(T)\mathrm{A_{III}}(T)}{\mathrm{A_I}(T)\mathrm{A_{IV}}(T)}}\Big/(1-\Delta T + O(T^3))\right). \tag{A.12}$$

For longer delays, an estimate of the difference of the autorelaxation rates Δ, can be obtained by taking the approximation up to second order in T of the ratio of the signal amplitudes of auto-experiments IV and I:

$$\frac{\mathrm{A_{IV}}(T)}{\mathrm{A_I}(T)} = k\frac{B}{A} = k(1-2\Delta T + 2\Delta^2T^2 + O(T^3)) = k(\exp(-2\Delta T) + O(T^3)). \tag{A.13}$$

where the constant k accounts for the unequal efficiencies of initial excitation and detection of the operators P and Q in the two experiments (I and IV) [46,74].

Appendix B. Derivation of longitudinal cross-correlated relaxation rates in the presence of competing relaxation mechanism

When a spin system is not isolated, it is necessary to account for competing cross-relaxation mechanisms, such as H$^\alpha$-H^N cross relaxation. An effective strategy is to introduce a swapping block in the

middle of the relaxation block (cite, Fig. 4A). The swapping block acts as a unitary matrix that converts the operator P into Q and vice versa. When the swapping block is introduced, the density matrix of the system becomes more complex:

$$\begin{Bmatrix} \langle P(T)\rangle \\ \langle Q(T)\rangle \end{Bmatrix} = \exp(-\bar{\rho}T) \begin{bmatrix} 2AC & C^2+AB \\ C^2+AB & 2BC \end{bmatrix} \begin{Bmatrix} \langle P(0)\rangle \\ \langle Q(0)\rangle \end{Bmatrix}, \tag{B.1}$$

where this time A, B and C are defined for half the time evolution T:

$$A = \cosh\left(\frac{T}{2}\sqrt{\Delta^2+\Gamma_z^2}\right) + \frac{\Delta}{\sqrt{\Delta^2+\Gamma_z^2}}\sinh\left(\frac{T}{2}\sqrt{\Delta^2+\Gamma_z^2}\right) \tag{B.2}$$

$$B = \cosh\left(\frac{T}{2}\sqrt{\Delta^2+\Gamma_z^2}\right) - \frac{\Delta}{\sqrt{\Delta^2+\Gamma_z^2}}\sinh\left(\frac{T}{2}\sqrt{\Delta^2+\Gamma_z^2}\right) \tag{B.3}$$

$$C = -\frac{\Gamma_z}{\sqrt{\Delta^2+\Gamma_z^2}}\sinh\left(\frac{T}{2}\sqrt{\Delta^2+\Gamma_z^2}\right) \tag{B.4}$$

and

$$\bar{\rho} = (\rho_P + \rho_Q)/2 \tag{B.5}$$

$$\Delta = (\rho_Q - \rho_P)/2. \tag{B.6}$$

In this case the ratio becomes:

$$\sqrt{\frac{A_I(T)A_{IV}(T)}{A_{II}(T)A_{III}(T)}} = \sqrt{\frac{4ABC^2}{C^4+2C^2AB+A^2B^2}}. \tag{B.7}$$

An estimate of the longitudinal CCR rates when the swapping block is introduced ($\Gamma^{CCR}_{z,swapp}$) can be derived by expanding in Taylor series the ratio in Eq. (B.7) up to the fourth order in T. Again, we can collect the terms of the expansion of the hyperbolic tangent, to get:

$$\begin{aligned}\sqrt{\frac{A_I(T)A_{IV}(T)}{A_{II}(T)A_{III}(T)}} &= \Gamma_z T(1+\frac{1}{24}\Delta^2T^2 - \frac{1}{3}\Gamma_z^2T^2) + O(T^5) \\ &= \tanh(\Gamma_z T)(1+\frac{1}{24}\Delta^2T^2 + O(T^5))\end{aligned} \tag{B.8}$$

$$|\Gamma_z| = \frac{1}{T}\operatorname{arctanh}\left(\sqrt{\frac{A_I(T)\ A_{IV}(T)}{A_{II}(T)A_{III}(T)}}\Big/(1+\frac{1}{24}\Delta^2T^2+O(T^5))\right) \tag{B.9}$$

where Γ_z is an abbreviation for $\Gamma^{z,swapp}_{CCR}$. Again Eq. (B.9) reduces to Eq. (17) when the delay T is short or when Δ is zero. This time, the correction can be extracted from the dependence on T of ratio of the amplitudes of the auto-experiments III and II,

$$\frac{A_{III}(T)}{A_{II}(T)} = k\frac{B}{A} = k\exp(-\Delta T)/(1+\frac{1}{12}\Gamma_z^2\Delta T^3 + O(T^5)). \tag{B.10}$$

The constant k accounts for the unequal efficiencies of initial excitation and detection of the operators P and Q in the two auto experiments.

Appendix C. Supplementary data

Supplementary material related to this article can be found online at https://doi.org/10.1016/j.jmr.2024.107661.

References

[1] P.E. Wright, H.J. Dyson, Intrinsically unstructured proteins: re-assessing the protein structure-function paradigm, J. Mol. Biol. 2 (293) (1999) 321–331, URL https://www.infona.pl/resource/bwmeta1.element.elsevier-0e9303e0-d1ff-3f43-a687-4baca36bb644.

[2] A.K. Dunker, J.D. Lawson, C.J. Brown, R.M. Williams, P. Romero, J.S. Oh, C.J. Oldfield, A.M. Campen, C.M. Ratliff, K.W. Hipps, Intrinsically disordered protein, J. Mol. Graph. Modell. 19 (1) (2001) 26–59, http://dx.doi.org/10.1016/s1093-3263(00)00138-8.

[3] H.J. Dyson, P.E. Wright, Intrinsically unstructured proteins and their functions, Nat. Rev. Mol. Cell Biol. 6 (3) (2005) 197–208, http://dx.doi.org/10.1038/nrm1589.

[4] P. Tompa, Intrinsically disordered proteins: a 10-year recap, Trends Biochem. Sci. 37 (12) (2012) 509–516, URL https://www.cell.com/trends/biochemical-sciences/fulltext/S0968-0004(12)00125-9.

[5] V.N. Uversky, C.J. Oldfield, A.K. Dunker, Intrinsically disordered proteins in human diseases: Introducing the D ^{2} Concept, Annu. Rev. Biophys. 37 (1) (2008) 215–246, http://dx.doi.org/10.1146/annurev.biophys.37.032807.125924.

[6] M.M. Babu, R. van der Lee, N.S. de Groot, J. Gsponer, Intrinsically disordered proteins: regulation and disease, Curr. Opin. Struct. Biol. 21 (3) (2011) 432–440, http://dx.doi.org/10.1016/j.sbi.2011.03.011.

[7] M. Habeck, Statistical mechanics analysis of sparse data, J. Struct. Biol. 3 (173) (2011) 541–548, URL https://www.infona.pl/resource/bwmeta1.element.elsevier-7ce37711-088d-3998-ab8b-339584ed9f06.

[8] M. Bonomi, G.T. Heller, C. Camilloni, M. Vendruscolo, Principles of protein structural ensemble determination, Curr. Opin. Struct. Biol. 100 (42) (2017) 106–116, URL https://www.infona.pl/resource/bwmeta1.element.elsevier-a1bb35ae-64dc-3407-a895-fcecdae6e90f.

[9] C. Kauffmann, A. Zawadzka-Kazimierczuk, G. Kontaxis, R. Konrat, Using cross-correlated spin relaxation to characterize backbone dihedral angle distributions of flexible protein segments, ChemPhysChem 22 (1) (2021) 18–28, http://dx.doi.org/10.1002/cphc.202000789.

[10] S.-L. Chang, N. Tjandra, Temperature dependence of protein backbone motion from carbonyl 13 C and amide 15 N NMR relaxation, J. Magn. Reson. 174 (1) (2005) 43–53, URL https://ui.adsabs.harvard.edu/abs/2005JMagR.174...43C/abstract.

[11] C.K. Fisher, C.M. Stultz, Constructing ensembles for intrinsically disordered proteins, Curr. Opin. Struct. Biol. 21 (3) (2011) 426–431, http://dx.doi.org/10.1016/j.sbi.2011.04.001.

[12] J.D. Forman-Kay, T. Mittag, From sequence and forces to structure, function, and evolution of intrinsically disordered proteins, Structure 21 (9) (2013) 1492–1499, http://dx.doi.org/10.1016/j.str.2013.08.001.

[13] N. Bolik-Coulon, G. Bouvignies, L. Carlier, F. Ferrage, Experimental characterization of the dynamics of IDPs and IDRs by NMR, in: Intrinsically Disordered Proteins, Elsevier, 2019, pp. 65–92, URL https://www.sciencedirect.com/science/article/pii/B978012816348100003X.

[14] H.J. Dyson, P.E. Wright, Unfolded proteins and protein folding studied by NMR, Chem. Rev. 104 (8) (2004) 3607–3622, http://dx.doi.org/10.1021/cr030403s.

[15] M.R. Jensen, M. Zweckstetter, J.-r. Huang, M. Blackledge, Exploring free-energy landscapes of intrinsically disordered proteins at atomic resolution using NMR spectroscopy, Chem. Rev. 114 (13) (2014) 6632–6660, http://dx.doi.org/10.1021/cr400688u, URL https://pubs.acs.org/doi/10.1021/cr400688u.

[16] R. Konrat, NMR contributions to structural dynamics studies of intrinsically disordered proteins, J. Magn. Reson. 241 (2014) 74–85, URL https://ui.adsabs.harvard.edu/abs/2014JMagR.241...74K/abstract.

[17] G. Nodet, L. Salmon, V. Ozenne, S. Meier, M.R. Jensen, M. Blackledge, Quantitative description of backbone conformational sampling of unfolded proteins at amino acid resolution from NMR residual dipolar couplings, J. Am. Chem. Soc. 131 (49) (2009) 17908–17918, http://dx.doi.org/10.1021/ja9069024, Publisher: American Chemical Society.

[18] T. Bremi, R. Brüschweiler, Locally anisotropic internal polypeptide backbone dynamics by NMR relaxation, J. Am. Chem. Soc. 119 (28) (1997) 6672–6673, http://dx.doi.org/10.1021/ja9708676.

[19] A.G.I. Palmer, NMR characterization of the dynamics of biomacromolecules, Chem. Rev. 104 (8) (2004) 3623–3640, http://dx.doi.org/10.1021/cr030413t.

[20] A. Mittermaier, L.E. Kay, New tools provide new insights in NMR studies of protein dynamics, Science 312 (5771) (2006) 224–228, http://dx.doi.org/10.1126/science.1124964.

[21] S.N. Khan, C. Charlier, R. Augustyniak, N. Salvi, V. Déjean, G. Bodenhausen, O. Lequin, P. Pelupessy, F. Ferrage, Distribution of pico-and nanosecond motions in disordered proteins from nuclear spin relaxation, Biophys. J. 109 (5) (2015) 988–999, URL https://hal.sorbonne-universite.fr/hal-01191810/.

[22] M.L. Gill, R.A. Byrd, A.G. Palmer, Dynamics of GCN4 facilitate DNA interaction: a model-free analysis of an intrinsically disordered region, Phys. Chem. Chem. Phys.: PCCP 18 (8) (2016) 5839–5849, http://dx.doi.org/10.1039/c5cp06197k.

[23] N. Salvi, A. Abyzov, M. Blackledge, Atomic resolution conformational dynamics of intrinsically disordered proteins from NMR spin relaxation, Progr. Nucl. Magn. Reson. Spectr. 102 (2017) 43–60, URL https://inis.iaea.org/search/search.aspx?orig_q=RN:52084366.

[24] G. Lipari, A. Szabo, Model-free approach to the interpretation of nuclear magnetic resonance relaxation in macromolecules. 1. Theory and range of validity, J. Am. Chem. Soc. 104 (17) (1982) 4546–4559, http://dx.doi.org/10.1021/ja00381a009.

[25] V.A. Daragan, K.H. Mayo, Motional model analyses of protein and peptide dynamics using 13C and 15N NMR relaxation, Progr. Nucl. Magn. Reson. Spectr. 31 (1) (1997) 63–105, http://dx.doi.org/10.1016/S0079-6565(97)00006-X.

[26] G.M. Clore, A. Szabo, A. Bax, L.E. Kay, P.C. Driscoll, A.M. Gronenborn, Deviations from the simple two-parameter model-free approach to the interpretation of nitrogen-15 nuclear magnetic relaxation of proteins, J. Am. Chem. Soc. 112 (12) (1990) 4989–4991, http://dx.doi.org/10.1021/ja00168a070.

[27] S.F. Lienin, T. Bremi, B. Brutscher, R. Brüschweiler, R.R. Ernst, Anisotropic intramolecular backbone dynamics of ubiquitin characterized by NMR relaxation and MD computer simulation, J. Am. Chem. Soc. 120 (38) (1998) 9870–9879, http://dx.doi.org/10.1021/ja9810179.

[28] J.W. Peng, G. Wagner, Mapping of spectral density functions using heteronuclear NMR relaxation measurements, J. Magn. Reson. (1969) 98 (2) (1992) 308–332, URL https://www.sciencedirect.com/science/article/pii/002223649290135T, Publisher: Elsevier.

[29] N.A. Farrow, O. Zhang, A. Szabo, D.A. Torchia, L.E. Kay, Spectral density function mapping using 15N relaxation data exclusively, J. Biomol. NMR 6 (2) (1995) 153–162, http://dx.doi.org/10.1007/BF00211779.

[30] P. Kadeřávek, V. Zapletal, A. Rabatinová, L. Krásný, V. Sklenář, L. Žídek, Spectral density mapping protocols for analysis of molecular motions in disordered proteins, J. Biomol. NMR 58 (3) (2014) 193—207, http://dx.doi.org/10.1007/s10858-014-9816-4.

[31] R. Ghose, K. Huang, J.H. Prestegard, Measurement of cross correlation between dipolar coupling and chemical shift anisotropy in the spin relaxation of13C,15N-labeled proteins, J. Magn. Reson. 135 (2) (1998) 487–499, http://dx.doi.org/10.1006/jmre.1998.1602.

[32] V. Tugarinov, Z. Liang, Y.E. Shapiro, J.H. Freed, E. Meirovitch, A structural mode-coupling approach to 15N NMR relaxation in proteins, J. Am. Chem. Soc. 123 (13) (2001) 3055–3063, http://dx.doi.org/10.1021/ja003803v, PMID: 11457016.

[33] D. Idiyatullin, V.A. Daragan, K.H. Mayo, A new approach to visualizing spectral density functions and deriving motional correlation time distributions: Applications to an α-helix-forming peptide and to a well-folded protein, J. Magn. Reson. 152 (1) (2001) 132–148, http://dx.doi.org/10.1006/jmre.2001.2372.

[34] A. Hsu, F. Ferrage, A.G. Palmer 3rd, Analysis of NMR spin-relaxation data using an inverse Gaussian distribution function., Biophys. J. 115 (12) (2018) 2301–2309, URL https://europepmc.org/article/med/30503534.

[35] B. Halle, The physical basis of model-free analysis of NMR relaxation data from proteins and complex fluids, J. Chem. Phys. 131 (22) (2009) 224507, http://dx.doi.org/10.1063/1.3269991.

[36] P. Pelupessy, S. Ravindranathan, G. Bodenhausen, Correlated motions of successive amide N-H bonds in proteins, J. Biomol. NMR 25 (4) (2003) 265–280, http://dx.doi.org/10.1023/A:1023076212536.

[37] K. Kämpf, S.A. Izmailov, S.O. Rabdano, A.T. Groves, I.S. Podkorytov, N.R. Skrynnikov, What drives 15N spin relaxation in disordered proteins? Combined NMR/MD study of the H4 histone tail, Biophys. J. 115 (12) (2018) 2348–2367, http://dx.doi.org/10.1016/j.bpj.2018.11.017.

[38] N. Salvi, A. Abyzov, M. Blackledge, Solvent-dependent segmental dynamics in intrinsically disordered proteins, Sci. Adv. 5 (6) (2019) eaax2348, http://dx.doi.org/10.1126/sciadv.aax2348, Publisher: American Association for the Advancement of Science.

[39] N. Salvi, A. Abyzov, M. Blackledge, Analytical description of NMR relaxation highlights correlated dynamics in intrinsically disordered proteins, Angew. Chem. Int. Ed. 56 (45) (2017) 14020–14024, http://dx.doi.org/10.1002/anie.201706740, _eprint: https://onlinelibrary.wiley.com/doi/pdf/10.1002/anie.201706740.

[40] N. Salvi, A. Abyzov, M. Blackledge, Multi-timescale dynamics in intrinsically disordered proteins from NMR relaxation and molecular simulation, J. Phys. Chem. Lett. 7 (13) (2016) 2483–2489, http://dx.doi.org/10.1021/acs.jpclett.6b00885, PMID: 27300592.

[41] A. Abyzov, N. Salvi, R. Schneider, D. Maurin, R.W. Ruigrok, M.R. Jensen, M. Blackledge, Identification of dynamic modes in an intrinsically disordered protein using temperature-dependent NMR relaxation, J. Am. Chem. Soc. 138 (19) (2016) 6240–6251, http://dx.doi.org/10.1021/jacs.6b02424.

[42] A.B. Mantsyzov, A.S. Maltsev, J. Ying, Y. Shen, G. Hummer, A. Bax, A maximum entropy approach to the study of residue-specific backbone angle distributions in α-synuclein, an intrinsically disordered protein, Prot. Sci. 23 (9) (2014) 1275–1290, http://dx.doi.org/10.1002/pro.2511.

[43] A.B. Mantsyzov, Y. Shen, J.H. Lee, G. Hummer, A. Bax, MERA: a webserver for evaluating backbone torsion angle distributions in dynamic and disordered proteins from NMR data, J. Biomol. NMR 63 (1) (2015) 85–95, http://dx.doi.org/10.1007/s10858-015-9971-2.

[44] C. Kauffmann, I. Ceccolini, G. Kontaxis, R. Konrat, Detecting anisotropic segmental dynamics in disordered proteins by cross-correlated spin relaxation, Magn. Reson. 2 (2) (2021) 557–569, http://dx.doi.org/10.5194/mr-2-557-2021.

[45] P. Pelupessy, G.M. Espallargas, G. Bodenhausen, Symmetrical reconversion: measuring cross-correlation rates with enhanced accuracy, J. Magn. Reson. 161 (2) (2003) 258–264, http://dx.doi.org/10.1016/S1090-7807(02)00190-8.

[46] P. Pelupessy, F. Ferrage, G. Bodenhausen, Accurate measurement of longitudinal cross-relaxation rates in nuclear magnetic resonance, J. Chem. Phys. 126 (13) (2007) 134508, 1–10, http://dx.doi.org/10.1063/1.2715583.

[47] P. Srb, J. Nováček, P. Kadeřávek, A. Rabatinová, L. Krásný, J. Žídková, J. Bobálová, V. Sklenář, L. Žídek, Triple resonance 15N NMR relaxation experiments for studies of intrinsically disordered proteins, J. Biomol. NMR 69 (2017) 133–146, URL https://api.semanticscholar.org/CorpusID:254655632.

[48] C.D. Kroenke, J.P. Loria, L.K. Lee, M. Rance, A.G. Palmer, Longitudinal and transverse 1H-15N dipolar/15N chemical shift anisotropy relaxation interference: Unambiguous determination of rotational diffusion tensors and chemical exchange effects in biological macromolecules, J. Am. Chem. Soc. 120 (31) (1998) 7905–7915, http://dx.doi.org/10.1021/ja980832l.

[49] K.T. Dayie, G. Wagner, Carbonyl carbon probe of local mobility in 13C,15N-enriched proteins using high-resolution nuclear magnetic resonance, J. Am. Chem. Soc. 119 (33) (1997) 7797–7806, http://dx.doi.org/10.1021/ja9633880.

[50] T. Wang, D.S. Weaver, S. Cai, E.R.P. Zuiderweg, Quantifying Lipari–Szabo modelfree parameters from 13CO NMR relaxation experiments, J. Biomol. NMR 36 (2) (2006) 79–102, http://dx.doi.org/10.1007/s10858-006-9047-4.

[51] K. Loth, P. Pelupessy, G. Bodenhausen, Chemical shift anisotropy tensors of carbonyl, nitrogen, and amide proton nuclei in proteins through cross-correlated relaxation in NMR spectroscopy, J. Am. Chem. Soc. 127 (16) (2005) 6062–6068, http://dx.doi.org/10.1021/ja042863o, PMID: 15839707.

[52] J. Sodek, B. Ganss, M. McKee, Osteopontin, Crit. Rev. Oral Biol. Med. 11 (3) (2000) 279–303, http://dx.doi.org/10.1177/10454411000110030101.

[53] H. Rangaswami, A. Bulbule, G.C. Kundu, Expression profile and pathophysiological role of osteopontin, Trends Cell Biol. 2 (16) (2006) 79–87, URL https://www.infona.pl/resource/bwmeta1.element.elsevier-05cecc3a-0598-35ee-9c63-855fc4f51bee.

[54] G. Platzer, A. Schedlbauer, A. Chemelli, P. Ozdowy, N. Coudevylle, R. Auer, G. Kontaxis, M. Hartl, A.J. Miles, B.A. Wallace, O. Glatter, K. Bister, R. Konrat, The metastasis-associated extracellular matrix protein osteopontin forms transient structure in ligand interaction sites, Biochemistry 50 (27) (2011) 6113–6124, http://dx.doi.org/10.1021/bi200291e, URL https://pubs.acs.org/doi/10.1021/bi200291e.

[55] D. Kurzbach, G. Platzer, T.C. Schwarz, M.A. Henen, R. Konrat, D. Hinderberger, Cooperative unfolding of compact conformations of the intrinsically disordered protein osteopontin, Biochemistry 52 (31) (2013) 5167–5175, http://dx.doi.org/10.1021/bi400502c, URL https://pubs.acs.org/doi/10.1021/bi400502c.

[56] D. Kurzbach, T.C. Schwarz, G. Platzer, S. Höfler, D. Hinderberger, R. Konrat, Compensatory adaptations of structural dynamics in an intrinsically disordered protein complex, Angew. Chem. Int. Ed. 53 (15) (2014) 3840–3843, http://dx.doi.org/10.1002/anie.201308389.

[57] A. Beier, T.C. Schwarz, D. Kurzbach, G. Platzer, F. Tribuzio, R. Konrat, Modulation of correlated segment fluctuations in IDPs upon complex formation as an allosteric regulatory mechanism, J. Mol. Biol. 430 (16) (2018) 2439–2452, http://dx.doi.org/10.1016/j.jmb.2018.04.035.

[58] A.G. Redfield, On the theory of relaxation processes, IBM J. Res. Dev. 1 (1) (1957) 19–31, URL https://ieeexplore.ieee.org/abstract/document/5392713/, Publisher: IBM.

[59] A.G. Redfield, The theory of relaxation processes, in: Advances in Magnetic and Optical Resonance, Vol. 1, Elsevier, 1965, pp. 1–32, URL https://www.sciencedirect.com/science/article/pii/B9781483231143500076.

[60] R.K. Wangsness, F. Bloch, The dynamical theory of nuclear induction, Phys. Rev. 89 (4) (1953) 728–739, http://dx.doi.org/10.1103/PhysRev.89.728.

[61] R. Brüschweiler, R.R. Ernst, Molecular dynamics monitored by cross-correlated cross relaxation of spins quantized along orthogonal axes, J. Chem. Phys. 96 (3) (1992) 1758–1766, URL https://pubs.aip.org/aip/jcp/article-abstract/96/3/1758/802090, Publisher: American Institute of Physics.

[62] P. Kadeřávek, S. Grutsch, N. Salvi, M. Tollinger, L. Žídek, G. Bodenhausen, F. Ferrage, Cross-correlated relaxation measurements under adiabatic sweeps: determination of local order in proteins, J. Biomol. NMR 63 (4) (2015) 353–365, http://dx.doi.org/10.1007/s10858-015-9994-8.

[63] B. Halle, H. Wennerström, Interpretation of magnetic resonance data from water nuclei in heterogeneous systems, J. Chem. Phys. 75 (4) (1981) 1928–1943, URL https://pubs.aip.org/aip/jcp/article-abstract/75/4/1928/438499, Publisher: American Institute of Physics.

[64] M. Goldman, Interference effects in the relaxation of a pair of unlike spin-12 nuclei, J. Magn. Reson. (1969) 60 (3) (1984) 437–452, URL https://www.sciencedirect.com/science/article/pii/0022236484900556, Publisher: Elsevier.

[65] C. Scheurer, N.R. Skrynnikov, S.F. Lienin, S.K. Straus, R. Brüschweiler, R.R. Ernst, Effects of dynamics and environment on ^{15} N chemical shielding anisotropy in proteins. a combination of density functional theory, molecular dynamics simulation, and NMR relaxation, J. Am. Chem. Soc. 121 (17) (1999) 4242–4251, http://dx.doi.org/10.1021/ja984159b.

[66] P.R.L. Markwick, R. Sprangers, M. Sattler, Local structure and anisotropic backbone dynamics from cross-correlated NMR relaxation in proteins, Angew. Chem. Int. Ed. 44 (21) (2005) 3232–3237, http://dx.doi.org/10.1002/anie.200462495.

[67] F. Cisnetti, K. Loth, P. Pelupessy, G. Bodenhausen, Determination of chemical shift anisotropy tensors of carbonyl nuclei in proteins through cross-correlated relaxation in NMR, ChemPhysChem 5 (6) (2004) 807–814, http://dx.doi.org/10.1002/cphc.200301041.

[68] N. Tjandra, A. Szabo, A. Bax, Protein backbone dynamics and 15N chemical shift anisotropy from quantitative measurement of relaxation interference effects, J. Am. Chem. Soc. 118 (29) (1996) 6986–6991, http://dx.doi.org/10.1021/ja960510m.

[69] J. Cavanagh, A.G. Palmer, P.E. Wright, M. Rance, Sensitivity improvement in proton-detected two-dimensional heteronuclear relay spectroscopy, J. Magn. Reson. (1969) 91 (2) (1991) 429–436, http://dx.doi.org/10.1016/0022-2364(91)90209-C.

[70] A. Shaka, Composite pulses for ultra-broadband spin inversion, Chem. Phys. Lett. 120 (2) (1985) 201–205, http://dx.doi.org/10.1016/0009-2614(85)87040-8.

[71] Z. Zhou, R. Kümmerle, X. Qiu, D. Redwine, R. Cong, A. Taha, D. Baugh, B. Winniford, A new decoupling method for accurate quantification of polyethylene copolymer composition and triad sequence distribution with 13C NMR, J. Magn. Reson. 187 (2) (2007) 225–233, http://dx.doi.org/10.1016/j.jmr.2007.05.005.

[72] L. Emsley, G. Bodenhausen, Optimization of shaped selective pulses for NMR using a quaternion description of their overall propagators, J. Magn. Reson. (1969) 97 (1) (1992) 135–148, http://dx.doi.org/10.1016/0022-2364(92)90242-Y.

[73] D. Marion, M. Ikura, R. Tschudin, A. Bax, Rapid recording of 2D NMR spectra without phase cycling. Application to the study of hydrogen exchange in proteins, J. Magn. Reson. (1969) 85 (2) (1989) 393–399, http://dx.doi.org/10.1016/0022-2364(89)90152-2.

[74] F. Ferrage, P. Pelupessy, D. Cowburn, G. Bodenhausen, Protein backbone dynamics through 13C‘-13Cα cross-relaxation in NMR spectroscopy, J. Am. Chem. Soc. 128 (34) (2006) 11072–11078, http://dx.doi.org/10.1021/ja0600577, PMID: 16925424.

[75] A. Shaka, P. Barker, R. Freeman, Computer-optimized decoupling scheme for wideband applications and low-level operation, J. Magn. Reson. (1969) 64 (3) (1985) 547–552, http://dx.doi.org/10.1016/0022-2364(85)90122-2.

[76] V.Y. Orekhov, I. Ibraghimov, M. Billeter, Optimizing resolution in multidimensional NMR by three-way decomposition., J. Biomol. NMR 27 (2) (2003) URL https://search.ebscohost.com/login.aspx?direct=true&profile=ehost&scope=site&authtype=crawler&jrnl=09252738&AN=16906484&h=f2d0loJ13ICMhgagkM6u2acG03ZuxcDjzFCmxi%2FwIB%2B8hl7YSPulzZXZWsotQCJ1pd7Umca1hfe%2BDPH2qBmxfw%3D%3D&crl=c.

[77] M. Mayzel, K. Kazimierczuk, V.Y. Orekhov, The causality principle in the reconstruction of sparse NMR spectra, Chem. Commun. (Cambridge, England) 50 (64) (2014) 8947–8950, http://dx.doi.org/10.1039/c4cc03047h.

[78] F. Delaglio, S. Grzesiek, G.W. Vuister, G. Zhu, J. Pfeifer, A.D. Bax, NMRPipe: a multidimensional spectral processing system based on UNIX pipes, J. Biomol. NMR 6 (1995) 277–293, URL https://idp.springer.com/authorize/casa?redirect_uri=https://link.springer.com/article/10.1007/bf00197809&casa_token=RdDPd81U_GYAAAAA:sASg-cBDwMLX0nobv3BFIwTZh490Gnb_j0N6nkAviFPAVWqyZuMDR08inbBxmgnD_GP84NhEJY5A5DU, Publisher: Springer.

[79] K. Kazimierczuk, V.Y. Orekhov, Accelerated NMR spectroscopy by using compressed sensing, Angew. Chem. Int. Ed. 50 (24) (2011) 5556–5559, http://dx.doi.org/10.1002/anie.201100370, Publisher: Wiley Online Library.

[80] W. Lee, M. Tonelli, J.L. Markley, NMRFAM-SPARKY: enhanced software for biomolecular NMR spectroscopy, Bioinformatics 31 (8) (2015) 1325–1327, URL https://academic.oup.com/bioinformatics/article-abstract/31/8/1325/213209, Publisher: Oxford University Press.

[81] G. Cornilescu, J.L. Marquardt, M. Ottiger, A. Bax, Validation of protein structure from anisotropic carbonyl chemical shifts in a dilute liquid crystalline phase, J. Am. Chem. Soc. 118 (1996) 4001–4008, URL https://spin.niddk.nih.gov/bax/lit/508/263.pdf.

[82] B. Mateos, R. Konrat, R. Pierattelli, I.C. Felli, NMR characterization of long-range contacts in intrinsically disordered proteins from paramagnetic relaxation enhancement in ^{13} C direct-detection experiments, ChemBioChem 20 (3) (2019) 335–339, http://dx.doi.org/10.1002/cbic.201800539.

[83] R.B. Corey, L.C. Pauling, W.T. Astbury, Fundamental dimensions of polypeptide chains, Proc. R. Soc. Lond. Ser. B - Biol. Sci. 141 (902) (1953) 10–20, http://dx.doi.org/10.1098/rspb.1953.0011.

[84] N. Tjandra, S.E. Feller, R.W. Pastor, A. Bax, Rotational diffusion anisotropy of human ubiquitin from 15N NMR relaxation, J. Am. Chem. Soc. 117 (50) (1995) 12562–12566, http://dx.doi.org/10.1021/ja00155a020.

[85] D. Yang, R. Konrat, L.E. Kay, A multidimensional NMR experiment for measurement of the protein dihedral angle ψ based on cross-correlated relaxation between 1Hα-13Cα dipolar and 13C‘ (carbonyl) chemical shift anisotropy mechanisms, J. Am. Chem. Soc. 119 (49) (1997) 11938–11940, http://dx.doi.org/10.1021/ja972329z.

[86] T. Carlomagno, M. Maurer, M. Hennig, C. Griesinger, Ubiquitin backbone motion studied via NH ^{N} -C‘C $_{\alpha}$ dipolar-dipolar and C‘-C‘C $_{\alpha}$ /NH ^{N} CSA-dipolar cross-correlated relaxation, J. Am. Chem. Soc. 122 (21) (2000) 5105–5113, http://dx.doi.org/10.1021/ja993845n, URL https://pubs.acs.org/doi/10.1021/ja993845n.

[87] K. Grudziąż, A. Zawadzka-Kazimierczuk, W. Koźmiński, High-dimensional NMR methods for intrinsically disordered proteins studies, Methods 148 (2018) 81–87, http://dx.doi.org/10.1016/j.ymeth.2018.04.031, NMR Methods of Characterizing Biomolecular Structural Dynamics and Conformational Ensembles.

[88] B. Mateos, C. Conrad-Billroth, M. Schiavina, A. Beier, G. Kontaxis, R. Konrat, I.C. Felli, R. Pierattelli, The ambivalent role of proline residues in an intrinsically disordered protein: From disorder promoters to compaction facilitators, J. Mol. Biol. 432 (9) (2020) 3093–3111, http://dx.doi.org/10.1016/j.jmb.2019.11.015.

[89] C. Charlier, S.N. Khan, T. Marquardsen, P. Pelupessy, V. Reiss, D. Sakellariou, G. Bodenhausen, F. Engelke, F. Ferrage, Nanosecond time scale motions in proteins revealed by high-resolution NMR relaxometry, J. Am. Chem. Soc. 135 (49) (2013) 18665–18672, http://dx.doi.org/10.1021/ja409820g.

[90] S.F. Cousin, P. Kadeřávek, N. Bolik-Coulon, Y. Gu, C. Charlier, L. Carlier, L. Bruschweiler-Li, T. Marquardsen, J.-M. Tyburn, R. Brüschweiler, F. Ferrage, Time-resolved protein side-chain motions unraveled by high-resolution relaxometry and molecular dynamics simulations, J. Am. Chem. Soc. 140 (41) (2018) 13456–13465, http://dx.doi.org/10.1021/jacs.8b09107, Publisher: American Chemical Society.

[91] H. Schwalbe, K.M. Fiebig, M. Buck, J.A. Jones, S.B. Grimshaw, A. Spencer, S.J. Glaser, L.J. Smith, C.M. Dobson, Structural and dynamical properties of a denatured protein. heteronuclear 3D NMR experiments and theoretical simulations of lysozyme in 8 M urea, Biochemistry 36 (29) (1997) 8977–8991, http://dx.doi.org/10.1021/bi970049q, Publisher: American Chemical Society.

[92] A.A. Smith, M. Ernst, B.H. Meier, Because the light is better here: Correlation-time analysis by NMR spectroscopy, Angew. Chem. Int. Ed. 56 (44) (2017) 13590–13595, http://dx.doi.org/10.1002/anie.201707316.

[93] R. Ghose, Average liouvillian theory in nuclear magnetic resonance—principles, properties, and applications, Concepts in Magnetic Resonance 12 (3) (2000) 152–172, http://dx.doi.org/10.1002/(SICI)1099-0534(2000)12:3<152::AID-CMR4>3.0.CO;2-P.

A set of cross-correlated relaxation experiments to probe the correlation time of two different and complementary spin pairs

Irene Ceccolini[1], Clemens Kauffmann[2], Julian Holzinger[1], Robert Konrat ✉ [1], and Anna Zawadzka-Kazimierczuk ✉ [3]

[1]Department of Structural and Computational Biology, Max Perutz Laboratories, University of Vienna, Vienna Biocenter Campus 5, 1030 Vienna, Austria
[2]Wiener Linien GmbH & Co KG, Erdbergstraße 202, 1030 Vienna, Austria
[3]University of Warsaw, Faculty of Chemistry, Biological and Chemical Research Centre, Żwirki i Wigury 101, 02-089 Warsaw, Poland

Correspondence: Robert Konrat: robert.konrat@univie.ac.at, Anna Zawadzka-Kazimierczuk: anzaw@chem.uw.edu.pl

Supplementary Material

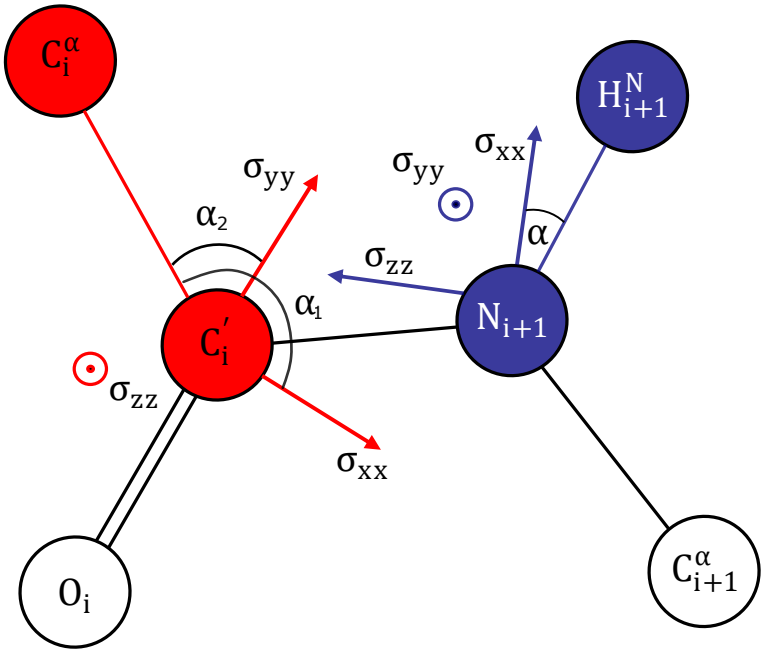

Figure 1. Schematic illustration of the peptide plane as defined by Corey and Pauling (Corey et al. (1953)) adapted from (Kauffmann et al. (2021)). C^α–C' = 1.53 Å, C'–O = 1.24 Å, C'–N = 1.32 Å, N–C^α = 1.47 Å. C^α-C'-O = 121°, C^α-C'-N = 114°, O-C'-N = 125°, C'-N-H = 123°, C'-N-C^α = 123°, H-N-C^α = 114°. N–H = 1.04 Å(Ottiger and Bax (1998)). The ^{15}N and ^{13}C' CSA principal components are adapted from Bodenhausen and coworkers(Cisnetti et al., 2004; Loth et al., 2005). ^{15}N: $\Delta_N \approx \sigma_{xx} - \sigma_{yy} \approx \sigma_{xx} - \sigma_{zz}$ = 170 e^{-6} ppm, α_1 = 20°. ^{13}C': σ_{xx} = 249.4 ppm, σ_{zz} = 87.9 ppm, α_2 = 37°. σ_{yy} = 191.1 ppm (Kauffmann et al. (2021))

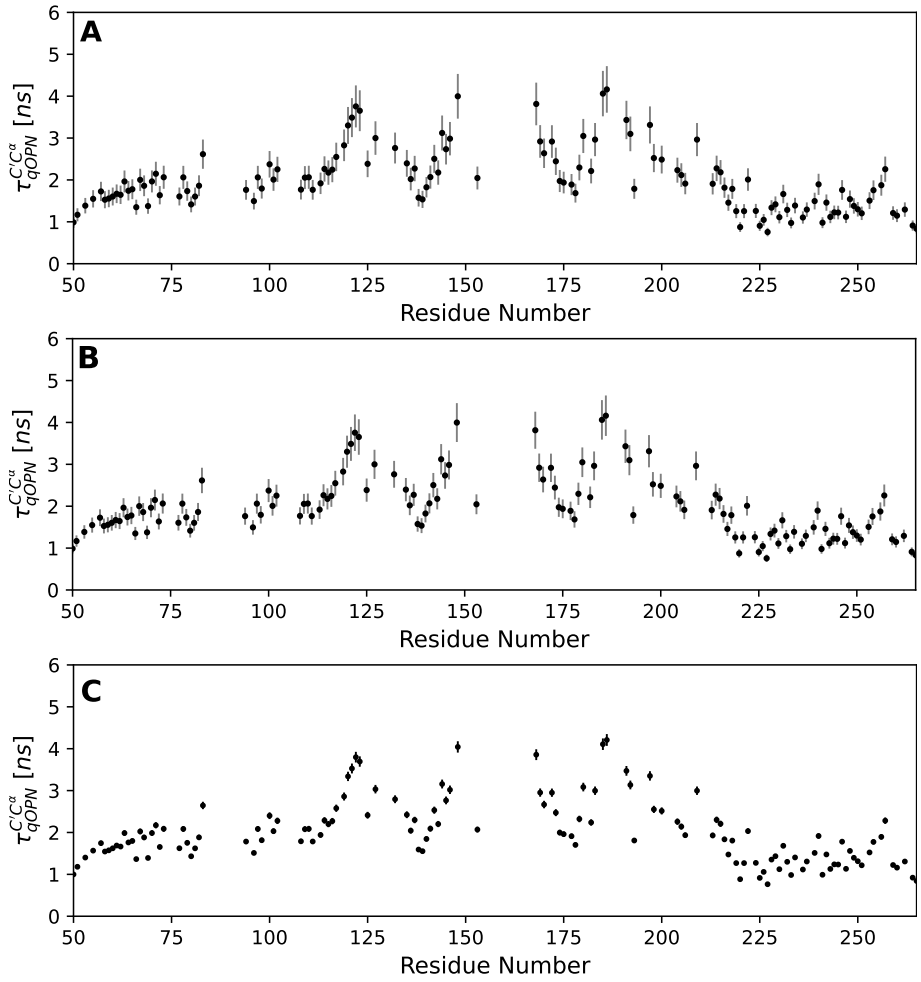

Figure 2. Deviations in the $C'C^\alpha$ correlation time $\tau_{qOPN}^{C'C^\alpha}$ depending on: Panel A) fluctuations in the ratio $\tau_{xx}^{C'C^\alpha}$ / $\tau_{yy}^{C'C^\alpha}$ (see Eq. 16 in the Main Text) with a 20% anisotropy range ($\tau_{xx}^{C'C^\alpha}$ / $\tau_{yy}^{C'C^\alpha}$ = 0.8 to $\tau_{xx}^{C'C^\alpha}$ / $\tau_{yy}^{/'C^\alpha}$ = 1.2). Panel B) changes in the angles α_1 and α_2 (see Figure 5) within the range of 30° to 47° (Loth et al. (2005)). Panel C) changes in the size of the σ_{yy} component of the C′ CSA tensor, spanning from 180 ppm to 220 ppm (Loth et al. (2005)), with the reported value representing the mean.

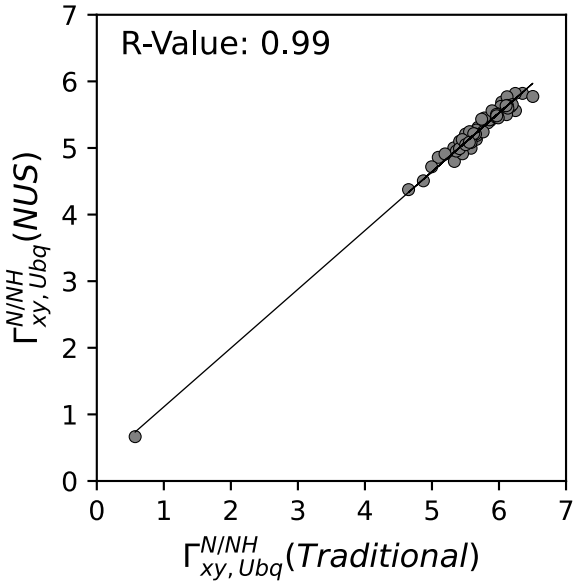

Figure 3. Correlation plot and linear fitting illustrate the transversal N/NH CCR Γ^{NH}_{xy} rates for ubiquitin, comparing values derived from traditionally sampled spectra with those obtained from Non-Uniform Sampling (NUS) reconstructed spectra. The R-Value is reported. The agreement between the two data sets indicate the reliability of both acquisition approaches.

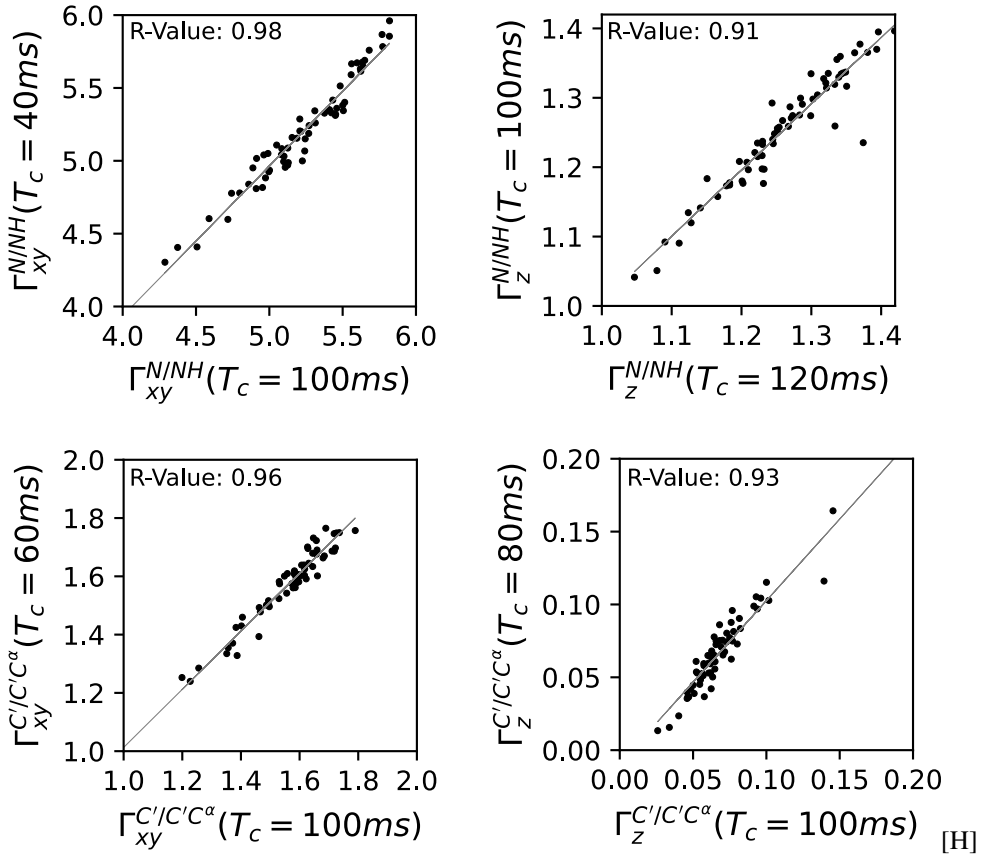

Figure 4. Correlation plots and linear fitting showing the consistency and reliability of the implementation of the symmetrical reconversion approach under varied relaxation delays for ubiquitin. The R-Value are reported.

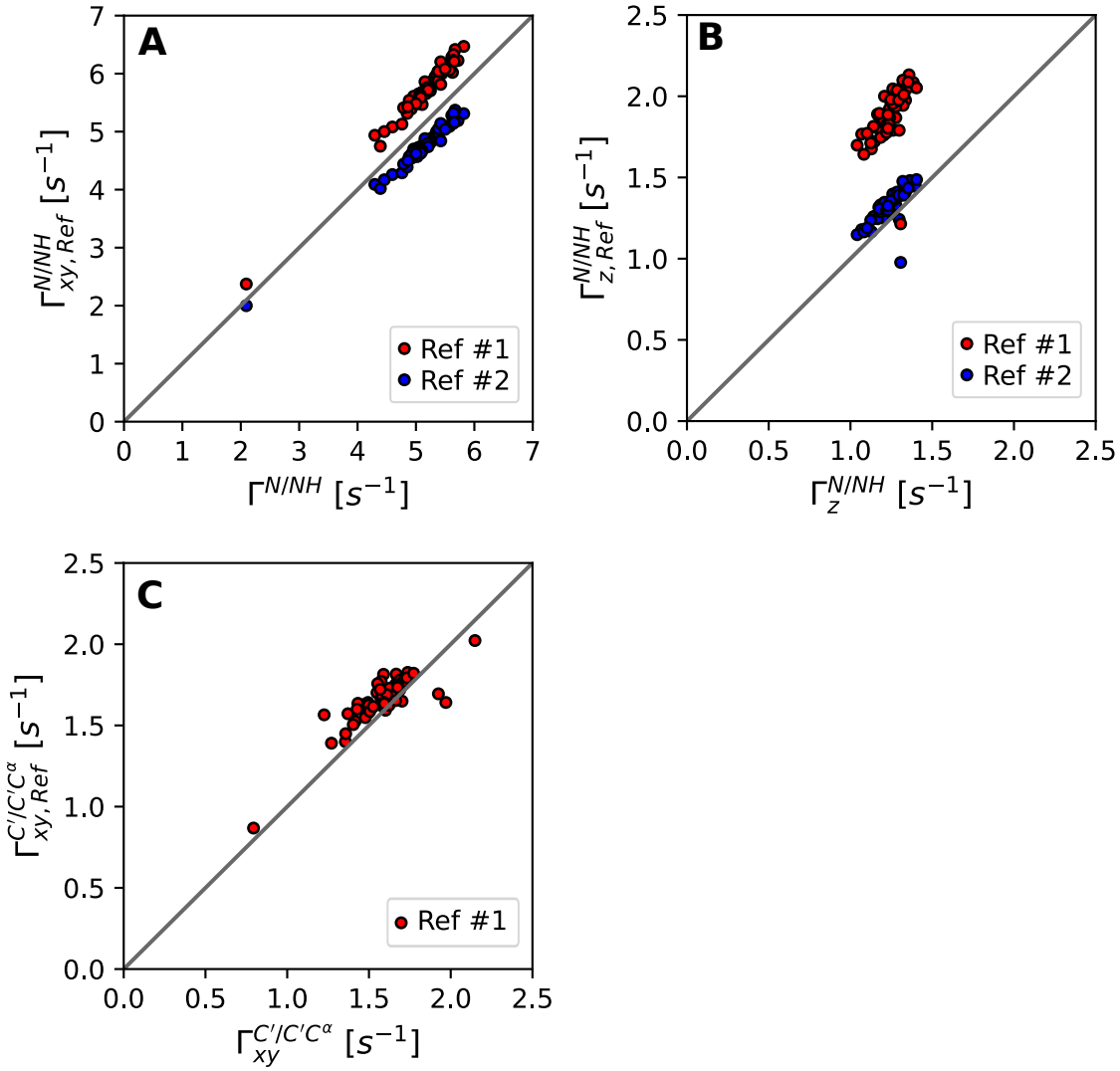

Figure 5. Comparison of the rates derived from the sequences presented in this paper and references. Reference #1 (Loth et al. (2005)) (red) and Reference #2 (Srb et al. (2017)) (blue) are included in the analysis. Panel **A** illustrates transversal $\Gamma^{N/NH}_{xy}$ rates, Panel **B** presents longitudinal $\Gamma^{N/NH}_{z}$ rates, and Panel **C** showcases transversal $\Gamma^{C'/C'C^\alpha}_{xy}$ rates. The observed offsets can be rationalized by considering the variations in experimental conditions (magnetic field: e.g. Ref #1 values are at 600MHz, see the larger offset in the $\Gamma^{N/NH}_{z} \propto J(\omega)$, sample concentration, temperature, and pH).

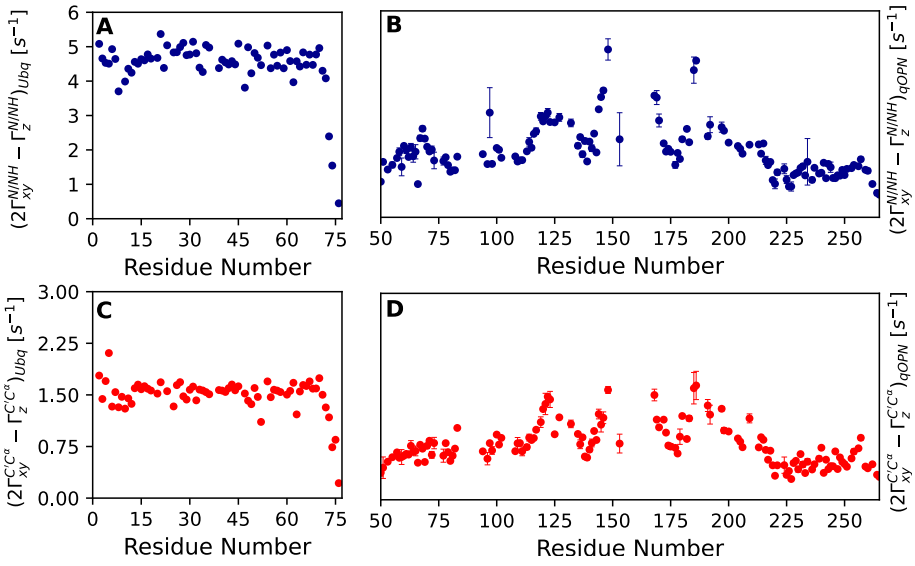

Figure 6. $2\Gamma_{xy}^{CCR} - \Gamma_{z}^{CCR}$ values for ^{15}N-^{1}H and ^{13}C′-^{13}C$^{\alpha}$ spin vectors in human ubiquitin (Ubq) and *Coturnix japonica* osteopontin (qOPN): ubiquitin values of spin-pairs ^{15}N-^{1}H (dark blue) and ^{13}C′-^{13}C$^{\alpha}$ (red) are depicted in panels **A** and **C** respectively, while qOPN ones in panels **B** and **D**.

Table 1. Acquisition parameters of the recorded NMR CCR experiments acquired at 298K on a human ubiquitin sample of 1 mM, at pH = 6.5. 2D ^{15}N-^{1}H data were acquired with conventional sampling. Spectral width of N dimension was 2300 Hz, 150 complex points were acquired along this dimension.

Experiment	Relaxation	N scans per exp version				Total
	delay (ms)	I	II	III	IV	measurement time
$\Gamma_{xy}^{N/NH}$	40	16	32	32	32	12:00 h
	100	16	32	32	32	12:30 h
$\Gamma_{z}^{N/NH}$	80	32	32	16	32	12:20 h
	100	32	32	16	32	12:30 h
	120	32	32	16	32	12:40 h
$\Gamma_{xy}^{C'/C'C^{\alpha}}$	60	16	32	32	16	12:00 h
	100	16	32	32	16	12:20 h
$\Gamma_{z}^{C'/C'C^{\alpha}}$	80	16	160	160	16	43:00 h
	100	16	160	160	16	43:30 h
	120	32	192	192	32	51:00 h

Table 2. Acquisition parameters of the recorded NMR CCR experiments acquired at 298K on a qOPN sample of 2.6mM, at pH = 6.5. 3D data were acquired with non-uniform sampling, 300 indirect-domains points were acquired. Spectral width was set to 3000 Hz and 2300 Hz in C' and N dimensions, respectively. Sampling grid size was 60 and 64 points along C' and N dimensions, respectively.

Experiment	Relaxation	N scans per exp version				Total
	delay (ms)	I	II	III	IV	measurement time
$\Gamma_{xy}^{N/NH}$	60	4	8	8	8	11:50 h
	100	4	8	8	8	12:30 h
$\Gamma_{z}^{N/NH}$	40	8	8	4	8	11:50 h
	100	8	8	4	8	12:30 h
	120	8	8	4	8	12:40 h
$\Gamma_{xy}^{C'/C'C^{\alpha}}$	60	8	8	8	4	12:00 h
	100	8	8	8	4	12:30 h
$\Gamma_{z}^{C'/C'C^{\alpha}}$	60	8	32	32	8	34:30 h
	100	8	32	32	8	35:40 h
	120	8	32	32	8	36:10 h

Table 3: CCR rates obtained for ubiquitin.

Residue	N/NH xy	N/NH z	CCa xy	CCa z
2	5.689	1.214	1.835	0.108
3	5.315	1.316	1.479	0.076
4	5.152	1.245	1.739	0.076
5	5.127	1.24	2.243	0.27
6	5.62	1.382	1.407	0.154
7	5.268	1.249	1.593	0.106
8	4.34	1.276	1.368	0.096
10	4.585	1.195	1.354	0.108
11	4.96	1.204	1.491	0.082
12	4.893	1.297	1.41	0.079
13	5.229	1.34	1.643	0.093
14	5.096	1.181	1.676	0.053
15	5.305	1.337	1.629	0.093
16	5.191	1.175	1.653	0.054
17	5.412	1.272	1.622	0.064
18	5.19	1.072	1.598	0.07
20	5.26	1.172	1.552	0.067
21	6.053	1.37	1.71	0.053
22	4.976	1.186	2.429	0.066
23	5.722	1.364	1.589	0.07
25	5.484	1.301	1.365	0.065
26	5.505	1.328	1.677	0.071
27	5.69	1.404	1.716	0.062
28	5.785	1.348	1.529	0.099
29	5.385	1.261	1.461	0.058
30	5.439	1.336	1.604	0.059
31	5.814	1.34	1.661	0.08
32	5.453	1.285	1.464	0.086
33	4.993	1.203	1.614	0.074
34	4.87	1.209	1.589	0.051
35	5.622	1.146	1.582	0.082

Residue	N/NH xy	N/NH z	CCa xy	CCa z
39	5.002	1.248	1.596	0.051
40	5.231	1.22	1.592	0.059
41	5.204	1.32	1.583	0.079
42	5.095	1.221	1.614	0.032
43	5.216	1.275	1.694	0.088
44	5.11	1.247	1.582	0.031
45	5.762	1.349	1.663	0.077
47	4.373	1.128	1.556	0.073
48	5.621	1.274	1.466	0.101
49	4.82	1.186	1.387	0.044
50	5.453	1.276	1.633	0.066
51	5.241	1.124	1.497	0.053
52	4.982	1.038	1.161	0.107
54	5.637	1.208	1.729	0.066
55	4.962	1.176	1.496	0.059
56	5.451	1.366	1.615	0.081
57	5.086	1.279	1.591	0.057
58	5.486	1.313	1.578	0.074
59	4.989	1.232	2.142	0.079
60	5.605	1.41	1.534	0.061
61	5.216	1.267	1.586	0.055
62	4.509	1.084	1.719	0.086
63	5.127	1.102	1.252	0.071
64	5.05	1.25	1.584	0.069
65	5.482	1.295	1.684	0.082
66	5.084	1.221	1.662	0.065
67	5.433	1.325	1.72	0.048
68	5.086	1.228	1.633	0.085

Residue	N/NH xy	N/NH z	CCa xy	CCa z
70	5.637	1.353	1.786	0.086
71	4.915	1.229	1.532	0.062
72	4.715	1.268	1.349	0.062
73	2.997	1.207	1.224	0.101
74	2.204	1.319	0.805	0.131
76	0.67	0.443	0.263	0.091

Table 4: CCR rates obtained for qOPN.

residue	N/NH xy	err N/NH xy	N/NH z	err N/NH z	CCa xy	err CCa xy	CCa z	err CCa z
50	0.019	0.019	0.817	0.015	0.455	0.047	0.122	0.009
51	0.036	0.036	0.997	0.065	0.528	0.153	0.122	0.006
53	0.025	0.025	1.02	0.006	0.614	0.002	0.121	0.006
55	0.07	0.07	1.026	0.024	0.672	0.018	0.106	0.004
57	0.036	0.036	1.006	0.012	0.753	0.009	0.129	0.004
58	0.108	0.108	1.037	0.009	0.66	0.002	0.101	0.004
59	0.239	0.239	0.86	0.037	0.694	0.105	0.146	0.007
60	0.0	0.0	0.976	0.007	0.7	0.011	0.118	0.004
61	0.1	0.1	0.964	0.005	0.72	0.02	0.107	0.003
62	0.01	0.01	0.914	0.002	0.708	0.003	0.103	0.003
63	0.105	0.105	0.831	0.012	0.851	0.074	0.133	0.004
64	0.165	0.165	0.945	0.014	0.749	0.014	0.107	0.005
65	0.192	0.192	1.028	0.029	0.77	0.068	0.121	0.005
66	0.001	0.001	0.944	0.007	0.63	0.003	0.183	0.004
67	0.08	0.08	0.956	0.005	0.855	0.0	0.111	0.003
68	0.07	0.07	1.078	0.01	0.797	0.012	0.108	0.002
69	0.06	0.06	0.923	0.003	0.604	0.003	0.109	0.001
70	0.012	0.012	1.068	0.004	0.832	0.034	0.095	0.002
71	0.037	0.037	0.933	0.008	0.914	0.027	0.113	0.002
72	0.09	0.09	0.862	0.028	0.711	0.049	0.116	0.001
73	0.226	0.226	0.948	0.031	0.875	0.082	0.102	0.001
77	0.094	0.094	1.042	0.045	0.711	0.094	0.141	0.002
78	0.016	0.016	0.946	0.014	0.901	0.018	0.156	0.002
79	0.029	0.029	0.901	0.006	0.757	0.014	0.13	0.001
80	0.001	0.001	0.937	0.007	0.604	0.014	0.078	0.002
81	0.033	0.033	0.716	0.003	0.697	0.023	0.113	0.003
82	0.013	0.013	0.855	0.007	0.795	0.012	0.103	0.002
83	0.029	0.029	0.887	0.007	1.099	0.003	0.109	0.001
94	0.045	0.045	0.818	0.01	0.753	0.009	0.098	0.01
96	0.022	0.022	0.932	0.035	0.662	0.079	0.13	0.02
97	0.719	0.719	0.946	0.014	0.901	0.018	0.156	0.002

residue	N/NH xy	err N/NH xy	N/NH z	err N/NH z	CCa xy	err CCa xy	CCa z	err CCa z
100	0.01	0.01	0.748	0.004	1.018	0.02	0.142	0.005
101	0.064	0.064	0.939	0.002	0.837	0.006	0.071	0.001
102	0.032	0.032	0.75	0.006	0.966	0.017	0.134	0.002
108	0.048	0.048	0.79	0.012	0.758	0.01	0.103	0.004
109	0.058	0.058	0.934	0.002	0.868	0.083	0.095	0.002
110	0.051	0.051	0.923	0.015	0.89	0.008	0.132	0.002
111	0.044	0.044	0.928	0.016	0.771	0.064	0.133	0.001
113	0.037	0.037	0.691	0.004	0.833	0.037	0.134	0.0
114	0.114	0.114	0.835	0.017	0.955	0.049	0.104	0.001
115	0.058	0.058	0.955	0.005	0.897	0.027	0.057	0.004
116	0.008	0.008	0.805	0.02	0.974	0.007	0.155	0.001
117	0.093	0.093	0.967	0.005	1.063	0.012	0.09	0.004
119	0.107	0.107	0.957	0.009	1.191	0.077	0.126	0.0
120	0.038	0.038	0.812	0.015	1.347	0.009	0.057	0.007
121	0.018	0.018	0.886	0.019	1.437	0.153	0.089	0.004
122	0.117	0.117	0.906	0.004	1.546	0.02	0.093	0.003
123	0.006	0.006	0.919	0.008	1.508	0.114	0.1	0.005
125	0.01	0.01	0.674	0.011	1.009	0.021	0.114	0.008
127	0.11	0.11	1.053	0.007	1.28	0.007	0.164	0.004
132	0.105	0.105	0.877	0.012	1.15	0.054	0.096	0.002
135	0.058	0.058	0.971	0.036	1.023	0.001	0.133	0.007
136	0.059	0.059	1.039	0.006	0.86	0.06	0.107	0.008
137	0.043	0.043	0.923	0.093	0.958	0.025	0.101	0.007
138	0.067	0.067	1.008	0.03	0.691	0.03	0.123	0.002
139	0.019	0.019	0.946	0.018	0.68	0.033	0.134	0.003
140	0.037	0.037	0.975	0.008	0.781	0.03	0.104	0.005
141	0.078	0.078	0.765	0.036	0.885	0.054	0.119	0.005
142	0.051	0.051	0.998	0.004	1.049	0.002	0.098	0.007

residue	N/NH xy	err N/NH xy	N/NH z	err N/NH z	CCa xy	err CCa xy	CCa z	err CCa z
144	0.016	0.016	1.028	0.009	1.295	0.068	0.097	0.005
145	0.052	0.052	0.936	0.016	1.145	0.103	0.107	0.008
146	0.062	0.062	0.894	0.003	1.236	0.083	0.089	0.005
148	0.305	0.305	0.863	0.008	1.632	0.049	0.073	0.003
153	0.658	0.658	1.028	0.227	0.878	0.118	0.122	0.037
168	0.014	0.014	0.872	0.005	1.563	0.083	0.081	0.003
169	0.197	0.197	0.908	0.012	1.212	0.004	0.093	0.003
170	0.186	0.186	0.801	0.003	1.114	0.028	0.122	0.001
172	0.044	0.044	0.927	0.008	1.225	0.015	0.122	0.001
173	0.037	0.037	0.891	0.007	1.039	0.006	0.127	0.001
174	0.047	0.047	0.93	0.009	0.874	0.03	0.172	0.005
175	0.011	0.011	0.786	0.008	0.804	0.039	0.06	0.005
177	0.086	0.086	0.683	0.023	0.809	0.01	0.109	0.003
178	0.009	0.009	0.887	0.01	0.726	0.013	0.106	0.005
179	0.009	0.009	0.83	0.009	0.976	0.109	0.118	0.005
180	0.06	0.06	1.046	0.014	1.308	0.002	0.181	0.002
182	0.045	0.045	1.01	0.008	0.931	0.01	0.095	0.005
183	0.017	0.017	0.981	0.01	1.243	0.037	0.119	0.005
185	0.378	0.378	1.052	0.006	1.663	0.226	0.083	0.005
186	0.051	0.051	1.032	0.021	1.706	0.201	0.089	0.008
191	0.075	0.075	0.904	0.016	1.413	0.084	0.086	0.006
192	0.227	0.227	0.964	0.007	1.278	0.133	0.081	0.007
193	0.159	0.159	0.903	0.013	0.781	0.246	0.135	0.004
197	0.14	0.14	0.934	0.014	1.379	0.031	0.112	0.003
198	0.006	0.006	0.955	0.02	1.055	0.042	0.096	0.002
200	0.014	0.014	0.953	0.01	1.049	0.014	0.113	0.003
204	0.001	0.001	0.715	0.01	0.945	0.016	0.107	0.002
205	0.045	0.045	0.782	0.001	0.901	0.028	0.112	0.002
206	0.028	0.028	0.883	0.006	0.813	0.008	0.099	0.007

residue	N/NH xy	err N/NH xy	N/NH z	err N/NH z	CCa xy	err CCa xy	CCa z	err CCa z
213	0.056	0.056	0.944	0.016	0.822	0.008	0.12	0.002
214	0.027	0.027	0.868	0.015	0.959	0.0	0.101	0.008
215	0.026	0.026	0.975	0.007	0.928	0.01	0.114	0.002
216	0.116	0.116	0.913	0.002	0.79	0.019	0.131	0.005
217	0.03	0.03	0.979	0.01	0.646	0.016	0.128	0.002
218	0.007	0.007	0.738	0.007	0.761	0.001	0.095	0.003
219	0.025	0.025	0.706	0.008	0.574	0.029	0.147	0.003
220	0.134	0.134	0.81	0.015	0.419	0.004	0.14	0.002
221	0.077	0.077	0.761	0.016	0.56	0.01	0.118	0.001
222	0.531	0.531	1.114	0.084	0.863	0.29	0.122	0.002
224	0.13	0.13	0.849	0.025	0.56	0.11	0.113	0.016
225	0.109	0.109	0.776	0.011	0.412	0.027	0.1	0.002
226	0.061	0.061	0.735	0.013	0.472	0.025	0.108	0.003
227	0.131	0.131	0.832	0.004	0.356	0.003	0.109	0.004
228	0.008	0.008	0.757	0.002	0.593	0.031	0.118	0.001
229	0.022	0.022	0.9	0.067	0.616	0.015	0.101	0.001
230	0.038	0.038	0.918	0.032	0.506	0.041	0.125	0.002
231	0.007	0.007	0.965	0.006	0.719	0.015	0.109	0.003
232	0.069	0.069	1.004	0.005	0.576	0.041	0.126	0.003
233	0.016	0.016	0.741	0.016	0.443	0.017	0.108	0.003
234	0.655	0.655	0.961	0.042	0.609	0.04	0.109	0.01
236	0.067	0.067	0.909	0.02	0.489	0.011	0.096	0.003
237	0.007	0.007	0.466	0.005	0.538	0.019	0.045	0.002
239	0.011	0.011	0.747	0.004	0.656	0.035	0.118	0.002
240	0.013	0.013	0.739	0.001	0.816	0.019	0.119	0.001
241	0.043	0.043	0.683	0.013	0.437	0.005	0.091	0.002
242	0.044	0.044	0.827	0.022	0.657	0.007	0.149	0.001
243	0.068	0.068	0.869	0.01	0.503	0.014	0.113	0.002
244	0.141	0.141	1.028	0.016	0.563	0.022	0.148	0.004

residue	N/NH xy	err N/NH xy	N/NH z	err N/NH z	CCa xy	err CCa xy	CCa z	err CCa z
246	0.069	0.069	0.861	0.007	0.773	0.001	0.14	0.002
247	0.044	0.044	0.83	0.013	0.51	0.016	0.127	0.005
248	0.013	0.013	0.91	0.006	0.663	0.021	0.095	0.002
249	0.059	0.059	0.89	0.026	0.609	0.003	0.117	0.001
250	0.009	0.009	0.919	0.005	0.581	0.011	0.124	0.003
251	0.004	0.004	0.887	0.005	0.533	0.002	0.106	0.001
253	0.027	0.027	0.993	0.007	0.64	0.024	0.078	0.001
254	0.049	0.049	0.961	0.003	0.749	0.038	0.097	0.001
256	0.004	0.004	0.998	0.015	0.81	0.003	0.123	0.002
257	0.006	0.006	1.142	0.118	0.953	0.02	0.105	0.029
259	0.047	0.047	0.89	0.011	0.542	0.025	0.119	0.004
260	0.069	0.069	0.808	0.005	0.549	0.008	0.183	0.004
262	0.042	0.042	0.702	0.012	0.567	0.008	0.103	0.002
264	0.072	0.072	0.798	0.008	0.437	0.014	0.146	0.003
265	0.013	0.013	0.787	0.009	0.387	0.001	0.108	0.002

References

Cisnetti, F., Loth, K., Pelupessy, P., and Bodenhausen, G.: Determination of Chemical Shift Anisotropy Tensors of Carbonyl Nuclei in Proteins through Cross-Correlated Relaxation in NMR, ChemPhysChem, 5, 807–814, https://doi.org/https://doi.org/10.1002/cphc.200301041, 2004.

Corey, R. B., Pauling, L. C., and Astbury, W. T.: Fundamental dimensions of polypeptide chains, Proceedings of the Royal Society of London. Series B - Biological Sciences, 141, 10–20, https://doi.org/10.1098/rspb.1953.0011, 1953.

Kauffmann, C., Ceccolini, I., Kontaxis, G., and Konrat, R.: Detecting anisotropic segmental dynamics in disordered proteins by cross-correlated spin relaxation, Magnetic Resonance, 2, 557–569, https://doi.org/10.5194/mr-2-557-2021, 2021.

Loth, K., Pelupessy, P., and Bodenhausen, G.: Chemical Shift Anisotropy Tensors of Carbonyl, Nitrogen, and Amide Proton Nuclei in Proteins through Cross-Correlated Relaxation in NMR Spectroscopy, Journal of the American Chemical Society, 127, 6062–6068, https://doi.org/10.1021/ja042863o, pMID: 15839707, 2005.

Ottiger, M. and Bax, A.: Determination of Relative N-HN, N-C‘, Cα-C‘, and Cα-Hα Effective Bond Lengths in a Protein by NMR in a Dilute Liquid Crystalline Phase, Journal of the American Chemical Society, 120, 12 334–12 341, https://doi.org/10.1021/ja9826791, 1998.

Srb, P., Nováček, J., Kadeřávek, P., Rabatinová, A., Krásný, L., Žídková, J., Bobálová, J., Sklenář, V., and Žídek, L.: Triple resonance 15N NMR relaxation experiments for studies of intrinsically disordered proteins, Journal of Biomolecular NMR, 69, 133 – 146, https://api.semanticscholar.org/CorpusID:254655632, 2017.

Part III

DISCUSSION AND OUTLOOK

5 DISCUSSION AND OUTLOOK

In the past two decades, extensive research has focused on IDPs. The primary aims were to probe residual structure, folding-upon binding events, and understand their dynamic behavior. In this context, NMR spin relaxation experiments have emerged as a powerful tool to investigate the intricate relationship of structure and dynamics in IDPs. However, the experimental information we can obtain for IDPs is more ambiguous to understand compared to folded proteins. The broad conformational space they sample is reflected in averaged NMR observables, which are difficult to deconvolute[70]. For this reason, CCR-based methods, in particular, have long remained limited to folded proteins. This thesis offers a method to disentangle the complexities of CCR rates within the realm of structural disorder.

5.1 AN ADDITIONAL SPIN PAIR TO INVESTIGATE THE STRUCTURAL IMPLICATIONS OF DIFFUSION ANISOTROPY

Chapter 3 presents a conceptual study on the possibility to experimentally detect segmental anisotropic diffusion in IDPs, offering a simple model to describe the spectral density function (SDF) for a rigid rotor tumbling in an isotropic solution. In the latter, the diffusion of an asymmetric top is considered[40], in which the fast local motions are assumed isotropic and modeled as an additional Lorentzian in the SDF. In order to identify any orientational biases, the focus is directed towards the SDF at zero frequency, denoted as $J(0)$, and an additional interaction to the N/NH CSA/DD must be considered. Embedded in the same tumbling frame but with a different and favorable orientation, the $C'/C'C^{\alpha}$ CSA/DD interference is chosen as the best spin pair to detect the diffusion of extended chains or α-helical structural arrangements.

We investigated experimental methods to clearly define and compare these two interactions. By taking advantage of the rigidity of the peptide plane, we demonstrated that mapping $J(0)$ of both $C'C^{\alpha}$ and NH vectors, through the application of CCR effects, enables the potential detection of anisotropic segmental tumbling. Given that both CCR interactions share a common spin, the rapid frequency contributions to the transverse CCR rate (namely $J(\omega_N)$ and $J(\omega_C)$ for the rates considered here), necessitate individual quantification through the measurement of their longitudinal counterparts. Notably, so far, there haven't been any documented experiments focusing on the measurement of longitudinal $C'/C'C^{\alpha}$ CSA/DD CCR.

The latter might seem worthless in the context of folded proteins due to the poor efficiency of the relaxation mechanisms; indeed, the transversal $C'/C'C^{\alpha}$ CCR rates are already rather small compared to the N/NH one[73]. Considering that slow tumbling motions drive spin relaxation in folded proteins, the impact of $J(\omega_C)$ is indeed expected to be tiny. However, in the context of rapidly fluctuating systems such as IDPs, the situation changes. What might have been considered negligible in folded proteins can still be sizeable in disordered systems.

5.2 DETERMINING TWO CORRELATION TIMES IN THE PEPTIDE PLANE

The paper presented in Chapter 4 was initially motivated by the goal of experimentally realizing the CCR-based method outlined in the first manuscript.

The development of CCR pulse sequences reached its peak productivity around 1997 with the introduction of the TROSY experiment[74]. By 2003, the first reviews[75], [76] and book chapters were written, and attention shifted to practical applications[73], [77], [78] and methodology improvements[79]–[83]. Subsequently, there was a notable decline in the popularity of detailed spin-relaxation measurements[23], and imagining the development of new useful CCR pulse sequences became challenging. However, there are still interactions to discover [84]. As already discussed above, this thesis introduces a novel CCR experiment to measure longitudinal $C'/C'C^{\alpha}$ CSA/DD interference.

The aim to precisely quantify segmental diffusion encouraged the author to consider the symmetrical reconversion approach[79] and incorporate it in the novel pulse sequence.

During the development of the CCR rates set, the initial goal started to shift toward the determination of the correlation times for the two spin pairs considered. An adequate estimate for the correlation time τ_{uv} is indeed a necessary prerequisite to extract structural information contained in the TCF at zero $J(0)$ when employing the simple separation of structure and dynamic presented in section 2.2.1. Because $C_{uv}(0)$ is known for the interactions here regarded, a precise quantification of τ_{uv}, defined as the integral under the normalized TCF, would allow for the first time to deconvolute geometrical and dynamics contributions in IDPs without the need to invoke any particular model or assume any particular motion.

To summarize and conclude, this study demonstrates that: (i) additional spin pairs are essential for characterizing anisotropic dynamics in complex and heterogeneous systems, (ii) mapping $J(0)$ and relying on a sans-model factorization of structure and dynamics allow for obtaining precise local correlation times in IDPs and for separat-

ing these two contributions. These findings will aid in determining protein backbone dihedral angles and characterizing IDPs motions.

BIBLIOGRAPHY

[1] P. E. Wright and H. Dyson, "Intrinsically unstructured proteins: Re-assessing the protein structure-function paradigm," *Journal of Molecular Biology*, vol. 293, no. 2, pp. 321–331, 1999.

[2] C. Boesch, A. Bundi, M. Oppliger, and K. Wuthrich, "1h nuclear-magnetic-resonance studies of the molecular conformation of monomeric glucagon in aqueous solution," *European Journal of Biochemistry*, vol. 91, no. 1, pp. 209–214, Nov. 1978.

[3] X. Li, P. Romero, M. Rani, A. K. Dunker, and Z. Obradovic, "Predicting protein disorder for n-, c-and internal regions," *Genome informatics*, vol. 10, pp. 30–40, 1999.

[4] P. Tompa, "Intrinsically unstructured proteins," *Trends in Biochemical Sciences*, vol. 27, no. 10, pp. 527–533, 2002.

[5] V. N. Uversky, J. R. Gillespie, and A. L. Fink, "Why are "natively unfolded" proteins unstructured under physiologic conditions?" *Proteins: Structure, Function, and Bioinformatics*, vol. 41, no. 3, pp. 415–427, 2000.

[6] V. N. Uversky, "Natively unfolded proteins: A point where biology waits for physics," *Protein Science*, vol. 11, no. 4, pp. 739–756, 2002.

[7] V. N. Uversky and A. K. Dunker, "Understanding protein nonfolding," *Biochimica et Biophysica Acta (BBA)-Proteins and Proteomics*, vol. 1804, no. 6, pp. 1231–1264, 2010.

[8] H. J. Dyson and P. E. Wright, "Intrinsically unstructured proteins and their functions," *Nature reviews Molecular cell biology*, vol. 6, no. 3, pp. 197–208, 2005.

[9] C. B. Anfinsen, "Principles that govern the folding of protein chains," *Science*, vol. 181, no. 4096, pp. 223–230, 1973-07-20.

[10] C. Levinthal, "Are there pathways for protein folding?" *Journal de chimie physique*, vol. 65, pp. 44–45, 1968.

[11] N. Rezaei-Ghaleh, M. Blackledge, and M. Zweckstetter, "Intrinsically disordered proteins: From sequence and conformational properties toward drug discovery," *ChemBioChem*, vol. 13, no. 7, pp. 930–950, 2012-05-07.

[12] G. A. Papoian, "Proteins with weakly funneled energy landscapes challenge the classical structure–function paradigm," *Proceedings of the National Academy of Sciences*, vol. 105, no. 38, pp. 14 237–14 238, 2008-09-23.

[13] P. Csermely, R. Palotai, and R. Nussinov, "Induced fit, conformational selection and independent dynamic segments: An extended view of binding events," *Trends in biochemical sciences*, vol. 35, no. 10, pp. 539–546, 2010.

[14] M. R. Jensen, M. Zweckstetter, J.-r. Huang, and M. Blackledge, "Exploring free-energy landscapes of intrinsically disordered proteins at atomic resolution using NMR spectroscopy," *Chemical Reviews*, vol. 114, no. 13, pp. 6632–6660, 2014-07-09.

[15] J. Habchi, P. Tompa, S. Longhi, and V. N. Uversky, "Introducing protein intrinsic disorder," *Chemical Reviews*, vol. 114, no. 13, pp. 6561–6588, 2014-07-09.

[16] J. D. Forman-Kay and T. Mittag, "From sequence and forces to structure, function, and evolution of intrinsically disordered proteins," *Structure*, vol. 21, no. 9, pp. 1492–1499, 2013.

[17] R. Van Der Lee, M. Buljan, B. Lang, R. J. Weatheritt, G. W. Daughdrill, A. K. Dunker, M. Fuxreiter, J. Gough, J. Gsponer, D. T. Jones, P. M. Kim, R. W. Kriwacki, C. J. Oldfield, R. V. Pappu, P. Tompa, V. N. Uversky, P. E. Wright, and M. M. Babu, "Classification of intrinsically disordered regions and proteins," *Chemical Reviews*, vol. 114, no. 13, pp. 6589–6631, 2014-07-09.

[18] K. Sugase, H. J. Dyson, and P. E. Wright, "Mechanism of coupled folding and binding of an intrinsically disordered protein," *Nature*, vol. 447, no. 7147, pp. 1021–1025, 2007.

[19] P. E. Wright and H. J. Dyson, "Linking folding and binding," *Current opinion in structural biology*, vol. 19, no. 1, pp. 31–38, 2009.

[20] V. N. Uversky, C. J. Oldfield, and A. K. Dunker, "Intrinsically disordered proteins in human diseases: Introducing the d ^{2} concept," *Annual Review of Biophysics*, vol. 37, no. 1, pp. 215–246, 2008-06-01.

[21] R. Konrat, "NMR contributions to structural dynamics studies of intrinsically disordered proteins," *Journal of Magnetic Resonance*, vol. 241, pp. 74–85, 2014.

[22] G. Nodet, L. Salmon, V. Ozenne, S. Meier, M. R. Jensen, and M. Blackledge, "Quantitative description of backbone conformational sampling of unfolded proteins at amino acid resolution from NMR residual dipolar couplings," *Journal of the American Chemical Society*, vol. 131, no. 49, pp. 17 908–17 918, 2009.

[23] P. Schanda, "Relaxing with liquids and solids – a perspective on biomolecular dynamics," *Journal of Magnetic Resonance*, vol. 306, pp. 180 –186, 2019.

[24] A. G. Palmer, "NMR characterization of the dynamics of biomacromolecules," *Chemical Reviews*, vol. 104, no. 8, pp. 3623–3640, 2004-08-01.

[25] A. J. Baldwin and L. E. Kay, "NMR spectroscopy brings invisible protein states into focus," *Nature chemical biology*, vol. 5, no. 11, pp. 808–814, 2009.

[26] D. Khago, I. Fucci, and R. A. Byrd, "The role of conformational dynamics in the recognition and regulation of ubiquitination," *Molecules*, vol. 25, p. 5933, 2020.

[27] J. Keeler, *Understanding NMR spectroscopy*. John Wiley & Sons, 2010.

[28] A. G. Palmer, "Nmr probes of molecular dynamics: Overview and comparison with other techniques," *Annual Review of Biophysics and Biomolecular Structure*, vol. 30, pp. 129–155, 2001.

[29] M. H. Levitt, *Spin dynamics: basics of nuclear magnetic resonance*. John Wiley & Sons, 2013.

[30] G. S. Rule and T. K. Hitchens, "Fundamentals of protein NMR spectroscopy," *Focus on structural biology (*, vol. 5, 2006.

[31] M. Akke and A. G. Palmer, "Monitoring macromolecular motions on microsecond to millisecond time scales by r1ρ-r1 constant relaxation time NMR spectroscopy," *Journal of the American Chemical Society*, vol. 118, no. 4, pp. 911–912, 1996-01-01.

[32] M. L. Gill, R. A. Byrd, and A. G. Palmer, "Dynamics of GCN4 facilitate DNA interaction: A model-free analysis of an intrinsically disordered region," *Physical chemistry chemical physics: PCCP*, vol. 18, no. 8, pp. 5839–5849, 2016.

[33] I. Alkorta, J. Elguero, and G. S. Denisov, "A review with comprehensive data on experimental indirect scalar NMR spin–spin coupling constants across hydrogen bonds," *Magnetic Resonance in Chemistry*, vol. 46, no. 7, pp. 599–624, 2008-07.

[34] A. Mittermaier and L. E. Kay, "New tools provide new insights in NMR studies of protein dynamics," *Science*, vol. 312, no. 5771, pp. 224–228, 2006.

[35] T. Bremi and R. Brüschweiler, "Locally anisotropic internal polypeptide backbone dynamics by nmr relaxation," *Journal of the American Chemical Society*, vol. 119, no. 28, pp. 6672–6673, 1997.

[36] S. N. Khan, C. Charlier, R. Augustyniak, N. Salvi, V. Déjean, G. Bodenhausen, O. Lequin, P. Pelupessy, and F. Ferrage, "Distribution of pico- and nanosecond motions in disordered proteins from nuclear spin relaxation," *Biophysical Journal*, vol. 109, no. 5, pp. 988–999, 2015.

[37] G. Lipari and A. Szabo, "Model-free approach to the interpretation of nuclear magnetic resonance relaxation in macromolecules. 1. theory and range of validity," *Journal of the American Chemical Society*, vol. 104, no. 17, pp. 4546–4559, 1982.

[38] B. Halle, "The physical basis of model-free analysis of NMR relaxation data from proteins and complex fluids," *The Journal of Chemical Physics*, vol. 131, no. 22, p. 224 507, 2009.

[39] G. M. Clore, A. Szabo, A. Bax, L. E. Kay, P. C. Driscoll, and A. M. Gronenborn, "Deviations from the simple two-parameter model-free approach to the interpretation of nitrogen-15 nuclear magnetic relaxation of proteins," *Journal of the American Chemical Society*, vol. 112, no. 12, pp. 4989–4991, 1990.

[40] D. E. Woessner, "Spin relaxation processes in a two-proton system undergoing anisotropic reorientation," *The Journal of Chemical Physics*, vol. 36, no. 1, pp. 1–4, 1962.

[41] V. A. Daragan and K. H. Mayo, "Motional model analyses of protein and peptide dynamics using 13C and 15N NMR relaxation," *Progress in Nuclear Magnetic Resonance Spectroscopy*, vol. 31, no. 1, pp. 63–105, 1997.

[42] B. Halle and H. Wennerström, "Interpretation of magnetic resonance data from water nuclei in heterogeneous systems," *The Journal of Chemical Physics*, vol. 75, no. 4, pp. 1928–1943, 1981.

[43] N. Salvi, A. Abyzov, and M. Blackledge, "Multi-timescale dynamics in intrinsically disordered proteins from NMR relaxation and molecular simulation," *The Journal of Physical Chemistry Letters*, vol. 7, no. 13, pp. 2483–2489, 2016.

[44] N. Salvi, A. Abyzov, and M. Blackledge, "Solvent-dependent segmental dynamics in intrinsically disordered proteins," *Science Advances*, vol. 5, no. 6, eaax2348, 2019.

[45] M. Marcellini, M.-H. Nguyen, M. Martin, M. Hologne, and O. Walker, "Accurate prediction of protein NMR spin relaxation by means of polarizable force fields. application to strongly anisotropic rotational diffusion," *The Journal of Physical Chemistry B*, vol. 124, no. 25, pp. 5103–5112, 2020-06-25.

[46] E. Meirovitch, Y. E. Shapiro, A. Polimeno, and J. H. Freed, "Protein dynamics from NMR:the slowly relaxing local structure analysis compared with model-free analysis," *The Journal of Physical Chemistry A*, vol. 110, no. 27, pp. 8366–8396, 2006.

[47] M. Zerbetto, M. Buck, E. Meirovitch, and A. Polimeno, "Integrated computational approach to the analysis of NMR relaxation in proteins: Application to ps-ns main chain ^{15} n- ^{1} h and global dynamics of the rho GTPase binding domain of plexin-b1," *The Journal of Physical Chemistry B*, vol. 115, no. 2, pp. 376–388, 2011.

[48] K. Kämpf, S. A. Izmailov, S. O. Rabdano, A. T. Groves, I. S. Podkorytov, and N. R. Skrynnikov, "What drives 15N spin relaxation in disordered proteins? Combined NMR/MD study of the H4 histone tail," *Biophysical Journal*, vol. 115, no. 12, pp. 2348–2367, 2018.

[49] A. Abyzov, N. Salvi, R. Schneider, D. Maurin, R. W. Ruigrok, M. R. Jensen, and M. Blackledge, "Identification of dynamic modes in an intrinsically disordered protein using temperature-dependent NMR relaxation," *Journal of the American Chemical Society*, vol. 138, no. 19, pp. 6240–6251, 2016-05-18.

[50] A. B. Mantsyzov, A. S. Maltsev, J. Ying, Y. Shen, G. Hummer, and A. Bax, "A maximum entropy approach to the study of residue-specific backbone angle distributions in α-synuclein, an intrinsically disordered protein," *Protein Science*, vol. 23, no. 9, pp. 1275–1290, 2014.

[51] A. B. Mantsyzov, Y. Shen, J. H. Lee, G. Hummer, and A. Bax, "Mera: A webserver for evaluating backbone torsion angle distributions in dynamic and disordered proteins from NMR data," *Journal of biomolecular NMR*, vol. 63, no. 1, pp. 85–95, 2015.

[52] I. Kuprov, *Spin: From Basic Symmetries to Quantum Optimal Control*. Springer Nature, 2023.

[53] J. Cavanagh, *Protein NMR spectroscopy: principles and practice*. Academic press, 1996.

[54] A. G. Redfield, "On the theory of relaxation processes," *IBM Journal of Research and Development*, vol. 1, no. 1, pp. 19–31, 1957.

[55] A. Redfield, "The theory of relaxation processes," in *Advances in Magnetic Resonance*, J. S. Waugh, Ed., vol. 1, Academic Press, 1965, pp. 1–32.

[56] N. Bloembergen, E. M. Purcell, and R. V. Pound, "Relaxation effects in nuclear magnetic resonance absorption," *Phys. Rev.*, vol. 73, pp. 679–712, 7 1948.

[57] R. K. Wangsness and F. Bloch, "The dynamical theory of nuclear induction," *Phys. Rev.*, vol. 89, pp. 728–739, 4 1953.

[58] M. H. Levitt and L. Di Bari, "The homogeneous master equation and the manipulation of relaxation networks," *Bulletin of Magnetic Resonance*, vol. 16, no. 1, pp. 94–114, 1994.

[59] E. Wigner, "On the quantum correction for thermodynamic equilibrium," *Physical Review*, vol. 40, no. 5, pp. 749–759, 1932.

[60] T. O. Levante and R. R. Ernst, "Homogeneous versus inhomogeneous quantum-mechanical master equations," *Chemical physics letters*, vol. 241, no. 1, pp. 73–78, 1995.

[61] B. Vögeli, "The nuclear overhauser effect from a quantitative perspective," *Progress in nuclear magnetic resonance spectroscopy*, vol. 78, pp. 1–46, 2014.

[62] M. Goldman, "Formal theory of spin–lattice relaxation," *Journal of Magnetic Resonance*, vol. 149, no. 2, pp. 160–187, 2001.

[63] R. Brüschweiler and D. A. Case, "Characterization of biomolecular structure and dynamics by NMR cross relaxation," *Progress in nuclear magnetic resonance spectroscopy*, vol. 26, pp. 27–58, 1994.

[64] D. M. Brink and G. R. Satchler, *Angular momentum*. Oxford university press, 1994.

[65] P. S. Hubbard, "Nuclear magnetic resonance and relaxation of four spin molecules in a liquid," *Physical Review*, vol. 128, no. 2, pp. 650–658, 1962-10-15.

[66] A. Abragam, *The principles of nuclear magnetism*. Oxford university press, 1961.

[67] D. A. Case, "Molecular dynamics and NMR spin relaxation in proteins," *Accounts of Chemical Research*, vol. 35, no. 6, pp. 325–331, 2002.

[68] J. S. Blicharski and D. Kruk, "NMR relaxation spectroscopy: Interference effects," *Applied Magnetic Resonance*, vol. 17, no. 2, pp. 367–374, 1999-06-01.

[69] C. Kauffmann, A. Zawadzka-Kazimierczuk, G. Kontaxis, and R. Konrat, "Using cross-correlated spin relaxation to characterize backbone dihedral angle distributions of flexible protein segments," *ChemPhysChem*, vol. 22, no. 1, pp. 18–28, 2021-01-07.

[70] N. Bolik-Coulon, G. Bouvignies, L. Carlier, and F. Ferrage, "Chapter 3 - Experimental characterization of the dynamics of IDPs and IDRs by NMR," in *Intrinsically Disordered Proteins*, N. Salvi, Ed., Academic Press, 2019, pp. 65–92.

[71] C. Kauffmann, I. Ceccolini, G. Kontaxis, and R. Konrat, "Detecting anisotropic segmental dynamics in disordered proteins by cross-correlated spin relaxation," *Magnetic Resonance*, vol. 2, no. 2, pp. 557–569, 2021.

[72] I. Ceccolini, C. Kauffmann, J. Holzinger, R. Konrat, and A. Zawadzka Kazimierczuk, "A set of cross-correlated relaxation experiments to probe the correlation time of two different and complementary spin pairs," *Journal of Magnetic Resonance*, vol. 361, p. 107 661, 2024.

[73] K. Loth, P. Pelupessy, and G. Bodenhausen, "Chemical shift anisotropy tensors of carbonyl, nitrogen, and amide proton nuclei in proteins through cross-correlated relaxation in NMR spectroscopy," *Journal of the American Chemical Society*, vol. 127, no. 16, pp. 6062–6068, 2005.

[74] K. Pervushin, R. Riek, G. Wider, and K. Wüthrich, "Attenuated T_2 relaxation by mutual cancellation of dipole–dipole coupling and chemical shift anisotropy indicates an avenue to NMR structures of very large biological macromolecules in solution," *Proceedings of the National Academy of Sciences*, vol. 94, no. 23, pp. 12 366–12 371, 1997.

[75] A. Kumar, R. C. R. Grace, and P. Madhu, "Cross-correlations in NMR," *Progress in Nuclear Magnetic Resonance Spectroscopy*, vol. 37, no. 3, pp. 191–319, 2000.

[76] H. Schwalbe, T. Carlomagno, M. Hennig, J. Junker, B. Reif, C. Richter, and C. Griesinger, "[2] - Cross-correlated relaxation for measurement of angles between tensorial interactions," in *Nuclear Magnetic Resonance of Biological Macromolecules Part A*, T. L. James, V. Dötsch, and U. Schmitz, Eds., vol. 338, Academic Press, 2002, pp. 35–81.

[77] K. Loth, D. Abergel, P. Pelupessy, M. Delarue, P. Lopes, J. Ouazzani, N. Duclert-Savatier, M. Nilges, G. Bodenhausen, and V. Stoven, "Determination of dihedral Ψ angles in large proteins by combining NHn/CαHα dipole/dipole cross-correlation and chemical shifts," *Proteins: Structure, Function, and Bioinformatics*, vol. 64, no. 4, pp. 931–939, 2006.

[78] L. Vugmeyster and C. J. McKnight, "Slow motions in chicken villin headpiece subdomain probed by cross-correlated NMR relaxation of amide NH bonds in successive residues," *Biophysical Journal*, vol. 95, no. 12, pp. 5941–5950, 2008.

[79] P. Pelupessy, S. Ravindranathan, and G. Bodenhausen, "Correlated motions of successive amide NH bonds in proteins," *Journal of biomolecular NMR*, vol. 25, no. 4, pp. 265–280, 2003.

[80] P. Pelupessy, F. Ferrage, and G. Bodenhausen, "Accurate measurement of longitudinal cross-relaxation rates in nuclear magnetic resonance," *The Journal of Chemical Physics*, vol. 126, no. 13, p. 134 508, 2007.

[81] B. Vögeli and L. Yao, "Correlated dynamics between protein HN and HC bonds observed by NMR cross relaxation," *Journal of the American Chemical Society*, vol. 131, no. 10, pp. 3668–3678, 2009.

[82] B. Vögeli, "How uniform is the peptide plane geometry? A high-accuracy NMR study of dipolar Cα–C′/H N–N cross-correlated relaxation," *Journal of biomolecular NMR*, vol. 50, no. 4, pp. 315–329, 2011.

[83] P. Kadeřávek, S. Grutsch, N. Salvi, M. Tollinger, L. Žídek, G. Bodenhausen, and F. Ferrage, "Cross-correlated relaxation measurements under adiabatic sweeps: Determination of local order in proteins," *Journal of biomolecular NMR*, vol. 63, no. 4, pp. 353–365, 2015.

[84] K. Clemens, K. Krzysztof, T. C. Schwarz, R. Konrat, and Z.-K. Anna, "A novel high-dimensional NMR experiment for resolving protein backbone dihedral angle ambiguities," *Journal of Biomolecular NMR*, vol. 74, no. 4, pp. 257–265, 2020.